

DAY-AHEAD MULTI-OBJECTIVE REACTIVE POWER OPTIMIZATION

A THESIS SUBMITTED TO
THE GRADUATE SCHOOL OF NATURAL AND APPLIED SCIENCES
OF
MIDDLE EAST TECHNICAL UNIVERSITY

BY

İSMAİL ELMA

IN PARTIAL FULFILLMENT OF THE REQUIREMENTS
FOR
THE DEGREE OF DOCTOR OF PHILOSOPHY
IN
ELECTRICAL AND ELECTRONICS ENGINEERING

FEBRUARY 2025

Approval of the thesis:

DAY-AHEAD MULTI-OBJECTIVE REACTIVE POWER OPTIMIZATION

submitted by **İSMAİL ELMA** in partial fulfillment of the requirements for the degree of **Doctor of Philosophy in Electrical and Electronics Engineering Department, Middle East Technical University** by,

Prof. Dr. Naci Emre Altun
Dean, Graduate School of **Natural and Applied Sciences** _____

Prof. Dr. İlkey Ulusoy
Head of Department, **Electrical and Electronics Engineering** _____

Prof. Dr. Ali Nezhil Güven
Supervisor, **Electrical and Electronics Engineering, METU** _____

Examining Committee Members:

Prof. Dr. Murat Göl
Electrical and Electronics Engineering, METU _____

Prof. Dr. Ali Nezhil Güven
Electrical and Electronics Engineering, METU _____

Prof. Dr. M. Cengiz Taplamacıođlu
Electrical and Electronics Engineering, Gazi University _____

Prof. Dr. Saffet Ayasun
Electrical and Electronics Engineering, Gazi University _____

Assist. Prof. Dr. Keyvan Firuzi
Electrical and Electronics Engineering, METU _____

Date: 11.02.2025

I hereby declare that all information in this document has been obtained and presented in accordance with academic rules and ethical conduct. I also declare that, as required by these rules and conduct, I have fully cited and referenced all material and results that are not original to this work.

Name, Surname: İSMAİL ELMA

Signature :

ABSTRACT

DAY-AHEAD MULTI-OBJECTIVE REACTIVE POWER OPTIMIZATION

ELMA, İSMAİL

Ph.D., Department of Electrical and Electronics Engineering

Supervisor: Prof. Dr. Ali Nezir Güven

February 2025, 116 pages

Transmission system operators (TSOs) need to control voltages along the grid to have an economic and reliable system operation. The coordination between the voltage set-points of power plants, transformer tap positions and switching of shunt elements may be defined as an optimum reactive dispatch problem. This thesis aims to develop an efficient algorithm for the optimum reactive power dispatch problem. The main objective of this problem is the minimization of transmission losses. Due to operational costs of switching equipment of shunt elements and transformer tap changers, TSOs also expect the number of switching of these devices to be minimized. In this study, the minimization of switching of shunt elements and transformer tap changes are included in the objective function. Hence, the problem is formulated as a multi-period and multi-objective optimization problem.

The optimum reactive power dispatch problem is a nonlinear and non-convex optimization problem due to the nonlinear power balance constraints. In addition, since the switch statuses of shunt elements and transformer tap positions are integer variables, the problem becomes a mixed integer nonlinear optimization problem (MINLP). Execution time for MINLP problems for large systems become imprac-

tical. Moreover, there is no guarantee for convergence. The main difficulty is the integer variables. Hence, in the first stage of the algorithm, the switch statuses of the shunt elements will be determined. Although the transformer tap variables are integer variables, these variables can be linearized without any practical loss of information. In the second stage of the algorithm the problem becomes a nonlinear optimization problem which can be solved using nonlinear interior point algorithm. the developed algorithm has been tested on IEEE 118 bus test network and convergence performance and execution time of the algorithm is considered as applicable for day ahead reactive power optimization.

Keywords: Day-Ahead Planning, Multi-Period Optimization, Multi-Objective Optimization, Optimal Power Flow, Reactive Power Control

ÖZ

GÜN ÖNCESİ ÇOK AMAÇLI REAKTİF GÜÇ OPTİMİZASYONU

ELMA, İSMAİL

Doktora, Elektrik ve Elektronik Mühendisliği Bölümü

Tez Yöneticisi: Prof. Dr. Ali Nezih Güven

Şubat 2025 , 116 sayfa

İletim sistem operatörleri ekonomik ve güvenli bir sistem işletmesi için şebekede gerilimleri kontrol etme ihtiyacı duymaktadır. Santral gerilim ayar değerleri, trafo kademe değerleri ve şönt ekipman anahtarlama koordinasyonu bir optimum reaktif güç tevzi problemi olarak tanımlanabilir. Bu tez, optimum reaktif güç tevzi problemi için bir etkin bir algoritma geliştirmeyi amaçlamaktadır. Bu problemin temel amacı iletim kayıplarının en aza indirilmesidir. Şönt elemanların anahtarlama ekipmanlarının ve trafo kademe değiştiricilerinin işletme maliyetleri nedeniyle, iletim sistemi operatörleri bu cihazların anahtarlama sayısının en aza indirilmesini beklemektedir. Bu çalışmada şönt elemanların anahtarlama sayıları ve trafo kademe değişimlerinin en aza indirilmesi amaç fonksiyonuna dahil edilmiştir. Bu nedenle, problem, çok dönemli ve çok amaçlı bir optimizasyon problemi olarak formüle edilmiştir.

Optimum reaktif güç tevzi problemi, doğrusal olmayan güç dengesi kısıtları nedeniyle doğrusal olmayan ve dışbükey olmayan bir optimizasyon problemidir. Ayrıca, şönt elemanlarının anahtarlama durumları ve trafo kademe konumlarının tamsayı değişkenler olması sebebiyle, problem karışık tam sayılı doğrusal olmayan bir optimi-

zasyon problem (MINLP) haline gelmektedir. Büyük sistemler için MINLP problemlerinin çözüm süresi uygulanamaz hale gelmektedir. Ayrıca, problemin yakınsama garantisi de olmamaktadır. Bu problemlerde başlıca zorluk tamsayı değişkenlerdir. Bu nedenle, ilk aşamada şönt elemanlarının anahtarlama durumları belirlenecektir. Trafo kademe değişkenleri tamsayı olmasına rağmen, bu değişkenler herhangi bir Pratik bilgi kaybı olmadan doğrusallaştırılabilir. İkinci aşamada, problem interior point algoritması ile çözülebilen bir optimizasyon problemi haline gelir. Geliştirilen algoritma IEEE 118 bara test şebekesinde test edilmiş ve algoritmanın yakınsama performansı ve yürütme süresi, gün öncesi reaktif güç optimizasyonu için uygulanabilir olarak kabul edilmiştir.

Anahtar Kelimeler: Gün Önesi Planlama, Çok Dönemli Optimizasyon, Çok Amaçlı Optimizasyon, Optimal Güç Akışı,Reaktif Güç Kontrolü.

To my beloved wife and precious daughters, with all my love,
you are my anchor and inspiration

ACKNOWLEDGMENTS

I would like to express my deepest gratitude to my supervisor Prof. Dr. Ali Nezhir Güven for his guidance, advice, encouragement and support throughout my Ph.D study. His teaching and guidance has profoundly shaped both my expertise and personal growth. I am also thankful to the members of the advisory committee for their insightful feedback and support.

I would also like to thank my colleagues at the TÜBİTAK MAM Power System Research Group. I am sincerely grateful for their contributions, support, both professionally and personally, and the inspiring discussions that have enriched my research journey.

Last but not least, I wish to express my heartfelt gratitude to my family, especially my daughters and my wife, along with my extended family, including our parents. Through all the challenges of my research, the unwavering encouragement, patience, and understanding of my wife have been truly invaluable. Likewise, the love and support of my entire family have been essential in making this journey possible.

TABLE OF CONTENTS

ABSTRACT	v
ÖZ	vii
ACKNOWLEDGMENTS	x
TABLE OF CONTENTS	xi
LIST OF TABLES	xiv
LIST OF FIGURES	xvii
LIST OF ABBREVIATIONS	xx
LIST OF SYMBOLS	xxi
CHAPTERS	
1 INTRODUCTION	1
1.1 Reactive Power Control	2
1.2 Voltage Control Tools	3
1.3 Motivation and Problem Definition	4
1.4 The Outline of the Thesis	5
2 GENERAL BACKGROUND	7
2.1 Optimal Power Flow	7
2.1.1 Objective Functions	8
2.1.2 Constraints	10

2.1.3	Reactive Power Optimization	13
2.1.4	Solution Methods	13
2.1.5	Approximations and Relaxations	15
3	LINEARIZED MULTI-PERIOD REACTIVE POWER OPTIMIZATION . .	17
3.1	Proposed Two-Stage Linearized Algorithm	18
3.1.1	First Stage of the Algorithm	19
3.1.2	Second Stage of the Algorithm	23
3.2	Simulation and Results	25
3.3	Evaluation and Limitations of the Proposed Algorithm	30
4	DAY-AHEAD MULTI-PERIOD REACTIVE POWER OPTIMIZATION . .	35
4.1	Problem Formulation	37
4.1.1	Objective and Constraints	38
4.2	Conventional Single-Period Optimization Approach	39
4.3	Proposed Two-Stage Multi-Period Optimization Approach	41
4.3.1	First Stage Single-Period Optimization and Shunt Switch Op- timization	43
4.3.1.1	Identification of Optimal Reactive Power Requirements	44
4.3.1.2	Shunt Switch Optimization	47
4.3.2	Second Stage Multi-Period Optimization	48
5	SIMULATION AND RESULTS	55
5.1	IEEE 118 Bus Test System and Loading Scenarios	56
5.2	Energy, Operational and Risk Costs	59
5.3	Conventional Single-Period Optimization Approach Results	63

5.3.1	Scenario 1	64
5.3.2	Scenario 2	70
5.4	Proposed Two-Stage Multi-Period Optimization Approach Results . .	76
5.4.1	Scenario 1	77
5.4.2	Scenario 2	83
5.5	Evaluation of the Proposed Algorithm	90
6	CONCLUSIONS	97
	REFERENCES	103
	APPENDICES	109
A	Simulation Data	109
A.1	IEEE 30 Bus Test System	109
A.2	IEEE 118 Bus Test System	110
	CURRICULUM VITAE	115

LIST OF TABLES

TABLES

Table 3.1	Shunt equipment in the IEEE 30 Bus test system	26
Table 3.2	Loss coefficients for shunt equipments for each time period	27
Table 3.3	Shunt switch statuses for the case $w_{sw} < 0.4$	28
Table 3.4	Shunt switch statuses for the case $w_{sw} > 0.4$	28
Table 4.1	Variable categories in day-ahead reactive power optimization	37
Table 4.2	Variable categories in the 2^{nd} stage of the proposed two-stage multi-period optimization approach	48
Table 5.1	Key network components in the IEEE 118 Bus test system	56
Table 5.2	Rated reactive power of shunt equipment in the IEEE 118 Bus test system	57
Table 5.3	Simulation Scenarios	57
Table 5.4	Annual maintenance and material costs for OLTC transformers	61
Table 5.5	Energy costs per tap change	62
Table 5.6	Calculation of operational cost per tap change	62
Table 5.7	Calculation of risk cost per tap change	63
Table 5.8	Total cost per tap change	63

Table 5.9 Non-varying switch statuses of shunt equipment for 24 hours - Scenario 1	66
Table 5.10 Varying switch statuses of shunt equipment for 24 hours - Scenario 1	66
Table 5.11 Non-varying transformer tap ratios for 24 hours - Scenario 1	68
Table 5.12 Transformer tap ratios of the Transformer 64-61 - Scenario 1	68
Table 5.13 Non-varying switch statuses of shunt equipment for 24 hours - Scenario 2	71
Table 5.14 Varying switch statuses of shunt equipment for 24 hours - Scenario 2	72
Table 5.15 Varying transformer tap ratios for 24 hours - Scenario 2	74
Table 5.16 Results of Stage I: Switch statuses of non-varying shunt equipment for 24 hours - Scenario 1	78
Table 5.17 Results of Stage I: Varying switch statuses of shunt equipment - Scenario 1	79
Table 5.18 Non-varying transformer tap ratios for 24 hours - Scenario 1	81
Table 5.19 Varying transformer tap ratios for 24 hours - Scenario 1	81
Table 5.20 Non-varying transformer tap ratios for 24 hours - Scenario 1	82
Table 5.21 Results of Stage I: Non-varying switch statuses of shunt equipment for 24 hours - Scenario 2	84
Table 5.22 Results of Stage I: Varying switch statuses of shunt equipment – Scenario 2	85
Table 5.23 Non-varying transformer tap ratios for 24 hours - Scenario 2	87
Table 5.24 Varying transformer tap ratios for 24 hours - Scenario 2	88
Table 5.25 Non-varying transformer tap ratios for 24 hours - Scenario 2	89
Table 5.26 Total duration of shunt equipment in service - Scenario 1	91
Table 5.27 Total duration of shunt equipment in service - Scenario 2	91

Table 5.28 Number of tap changes	93
Table 5.29 Resulting costs for transmission losses and transformer tap changes .	95
Table A.1 IEEE 30 Bus Test System	109
Table A.2 IEEE 118 Bus Test System	110

LIST OF FIGURES

FIGURES

Figure 3.1	The flowchart of the proposed two-stage linearized algorithm . . .	20
Figure 3.2	Successive linear programming approach for the 2^{nd} stage of the proposed two-stage linearized algorithm	24
Figure 3.3	Resulting objective function values	29
Figure 3.4	Resulting bus voltage magnitudes	30
Figure 3.5	Voltage differences between the 2^{nd} stage algorithm and power flow results	32
Figure 3.6	Active power flow differences between the 2^{nd} stage algorithm and power flow results	33
Figure 3.7	Reactive power flow differences between the 2^{nd} stage algorithm and power flow results	33
Figure 4.1	The flowchart of the proposed two-stage multi-period optimization approach	42
Figure 4.2	The flowchart of the 1^{st} stage of the proposed two-stage multi-period approach	44
Figure 5.1	Load Profile of Scenario 1	58
Figure 5.2	Load Profile of Scenario 2	58
Figure 5.3	Day-ahead market energy prices - 2024	60

Figure 5.4	Voltage profile of busbars with shunt equipment obtained via power flow calculations - Scenario 1	65
Figure 5.5	Voltage profile of busbars connected with transformers obtained via power flow calculations - Scenario 1	67
Figure 5.6	Resulting hourly voltage profiles of conventional single-period optimization approach - Scenario 1	69
Figure 5.7	Hourly and cumulative losses for conventional single-period optimization approach - Scenario 1	70
Figure 5.8	Voltage profile of busbars with shunt equipment obtained via power flow calculations - Scenario 2	71
Figure 5.9	Voltage profile of busbars connected with transformers obtained via power flow calculations - Scenario 2	73
Figure 5.10	Resulting hourly voltage profiles of conventional single-period optimization approach - Scenario 2	75
Figure 5.11	Hourly and cumulative losses for conventional single-period optimization approach - Scenario 2	76
Figure 5.12	Reactive power requirement of shunt equipment connected busbars - Scenario 1	78
Figure 5.13	Resulting hourly voltage profile for the two-stage optimization approach - Scenario 1	80
Figure 5.14	Hourly and cumulative losses - Scenario 1	83
Figure 5.15	Reactive power requirement of shunt equipment connected busbars - Scenario 2	84
Figure 5.16	Resulting voltage profile - Scenario 2	87
Figure 5.17	Hourly and cumulative losses - Scenario 2	90
Figure 5.18	The hourly switch statuses for the capacitor at Bus 44 in Scenario 1	92

Figure 5.19	The hourly switch statuses for the capacitor at Bus 48 in Scenario 2	92
Figure 5.20	Distribution of voltage magnitudes - Scenario 1	94
Figure 5.21	Distribution of voltage magnitudes - Scenario 2	94

LIST OF ABBREVIATIONS

OPF	Optimal Power Flow
FACTS	Flexible Alternating Current Transmission System
FCR	Frequency Containment Reserve
FRR	Frequency Restoration Reserve
HV	High Voltage
IEEE	Institute of Electrical and Electronics Engineers
KKT	Karush-Kuhn-Tucker
MINLP	Mixed Integer Nonlinear Programming
MVA	Mega Volt-Ampere
MVA _r	Mega Volt-Ampere reactive
MW	Mega Watt
MWh	Mega Watt hour
OLTC	On-Load Tap Changer
SDP	Semi-Definite Programming
SOCP	Second-Order Cone Programming
STATCOM	Static Synchronous Compensator
SVC	Static Var Compensator
TSO	Transmission System Operator
H#	Hour #
IS	Switch Status
P	Active Power
Q	Reactive Power
TP	Tap Position
V _{nom}	Nominal Voltage

LIST OF SYMBOLS

Sets

- \mathcal{N} Set of buses
- \mathcal{L} Set of lines
- \mathcal{K} Set of shunt equipment
- \mathcal{G}_i Set of generators connected to the busbar i
- \mathcal{N}^Q Set of busbars connected with generators and shunt equipment

Indices

- i, j Busbar index
- g Generator index
- l Line index
- t Transformer index
- k Shunt equipment index
- h Hour index

Parameters

- g_k Series Conductance of branch k
- g_{ij}^{tr} Series Conductance of transformer between busbar i and busbar j
- g_{ik} Series Conductance of branch k connected to busbar i
- b_{ij}^{tr} Series Susceptance of transformer between busbar i and busbar j
- b_{ik} Series Susceptance of branch k connected to busbar i
- G_{ij} Real part of ij^{th} entry of bus impedance matrix

- B_{ij} Imaginary part of ij^{th} entry of bus impedance matrix
- N_{bus} Number of busbars
- N_{gen} Number of generators
- N_{line} Number of lines
- $N_{transformer}$ Number of transformers
- $G_{ij}(h)$ Real part of ij^{th} entry of bus impedance matrix for hour h
- N_{shunt} Number of shunt equipment
- $B_{ij}(h)$ Imaginary part of ij^{th} entry of bus impedance matrix for hour h
- N_{hour} Number of hours
- N_{switch}^{max} Maximum allowable switching operations
- T_{change} Minimum time periods between consecutive switching operations
- a_g^P 2nd order quadratic active power cost function coefficient for generator g
- b_g^P 1st order quadratic active power cost function coefficient for generator g
- c_g^P Constant for quadratic active power cost function for generator g
- a_g^Q Cost coefficient for reactive power cost injection function coefficient for busbar i
- P_g^{min} Minimum active power generation of generator g
- P_g^{max} Maximum active power generation of generator g
- Q_g^{min} Minimum reactive power generation of generator g
- Q_g^{max} Maximum reactive power generation of generator g
- Q_k^{nom} Nominal reactive power of shunt equipment k
- $|V_g^{ref}|$ Voltage setpoint for the busbar connected with generator g
- V_i^{min} Minimum voltage limit of busbar i
- V_i^{max} Maximum voltage limit of busbar i

S_l^{max}	Maximum MVA capacity of line l
ϵ^{tol}	Convergence tolerance for linearized multi-period optimization problem
ϵ	A small positive constant used in second stage of the two-stage multi-period optimization approach
M	A sufficiently large constant used in second stage of the two-stage multi-period optimization approach
π_{loss}	Unit cost of transmission loss
π_{sw}	Unit cost per switching operation of shunt equipment
π_{tc}	Unit cost per tap change
w_{loss}	Weight of transmission loss
w_{sw}	Weight of number of switching operations of shunt equipment

Variables

$ V_i $	Voltage magnitude of busbar i
$ V_i(h) $	Voltage magnitude of busbar i for hour h
$ V_g $	Voltage magnitude of busbar connected with generator g
$ V_k $	Voltage magnitude of busbar connected with shunt equipment k
$ V_{li} $	Voltage magnitude of busbar i connected with line l
$ V_{li}(h) $	Voltage magnitude of busbar i connected with line l for hour h
θ_i	Voltage angle of busbar i
$\theta_i(h)$	Voltage angle of busbar i for hour h
$\theta_{ij}(h)$	Voltage angle difference between busbar i and busbar j for hour h
θ_{li}	Voltage angle of busbar i connected with line k
$\theta_{li}(h)$	Voltage angle of busbar i connected with line k for hour h
C_{total}^P	Total active power generation cost

- C_{total}^Q Total reactive injection cost
- C^T Total cost
- C_2^T Total cost of the optimization problem at the second stage of the proposed two-stage multi-period optimization approach
- C_g^P Active power cost function of generator g
- C_i^Q Reactive power injection cost function of busbar i
- P_{loss} Total transmission loss
- ∇P_{loss} Gradient of total transmission loss
- P_{loss}^T Total transmission loss from hour 1 to N_{hour}
- ΔP_{loss}^T Change in total transmission loss from hour 1 to N_{hour}
- $f(\mathbf{x}, \mathbf{u})$ Objective function of OPF problem
- $g(\mathbf{x}, \mathbf{u})$ Equality constraints of OPF problem
- $h(\mathbf{x}, \mathbf{u})$ Inequality constraints of OPF problem
- \mathbf{x} State variables of OPF problem
- \mathbf{V} Voltage magnitude vector
- θ Voltage angle vector
- \mathbf{x}^k State variables of OPF problem at k^{th} iteration
- x^k A state variable at k^{th} iteration
- \mathbf{u} Control variables of OPF problem
- P_g Active power generation of generator g
- Q_g Reactive power generation of generator g
- $Pinj_i$ Active power injection of busbar i
- $\nabla Pinj_i$ Gradient of active power injection of busbar i
- $Pinj_i(h)$ Active power injection of busbar i for hour h

- $Qinj_i$ Reactive power injection of busbar i
- $\nabla Qinj_i$ Gradient of reactive power injection of busbar i
- $Qinj_i(h)$ Reactive power injection of busbar i for hour h
- P_l Active power flow of line l
- Q_l Reactive power flow of line l
- S_l Apparent power flow of line l
- P_i^G Total active power generation of the generators connected to the busbar i
- P_i^L Total active power demand of the loads connected to the busbar i
- Q_i Reactive power injection at the busbar i
- Q_i^R Required reactive power injection at the busbar i
- Q_k^R Required reactive power injection at the busbar connected with shunt equipment k
- Q_i^G Total reactive power generation of the generators connected to the busbar i
- $Q_i^G(h)$ Total reactive power generation of the generators connected to the busbar i for hour h
- Q_i^L Total reactive power demand of the loads connected to the busbar i
- Q_k Reactive power output of shunt equipment k
- $Q_k(h)$ Reactive power output of shunt equipment k for hour h
- IS_i Switch Position of Shunt Equipment connected to busbar i
- IS_i Switch Position of Shunt Equipment connected to busbar i for hour h
- IS_k Switch Position of Shunt Equipment k
- $IS_k(h)$ Switch Position of Shunt Equipment k for hour h
- $ST_k(h)$ Change in Switch Position of Shunt Equipment k between hours $h - 1$ and h
- $\left. \frac{\Delta P_{loss}}{\Delta IS_k} \right|_h$ Loss coefficient for shunt equipment k at hour h

- $\left. \frac{\Delta|V_i|}{\Delta IS_k} \right|_h$ Voltage coefficient for busbar i for shunt equipment k
- f^W Wiegthed objective function of linearized multi-period reactive power optimization problem
- $T_t(h)$ Tap position of transformer t for hour h
- $\Delta T_t^+(h)$ Binary variable for positive tap change of transformer t for hour h
- $\Delta T_t^-(h)$ Binary variable for negative tap change of transformer t for hour h
- $\tilde{T}_t^+(h)$ Auxiliary variable for positive tap change of transformer t for hour h
- $\tilde{T}_t^-(h)$ Auxiliary variable for negative tap change of transformer t for hour h
- $t_{ij}(h)$ Tap position of transformer between busbar i and busbar j for hour h
- $TC_t(h)$ Tap change of transformer t for hour h
- n_{sw} The number of switching operations of shunt equipment
- n_{tc} The number of transformer tap changes
- n_{calc}^{PF} The number of Power Flow calculations

CHAPTER 1

INTRODUCTION

The fundamental objective of modern power systems is to ensure the continuity of supply. Although energy storage technologies and installations have significantly improved in recent decades, electrical energy cannot be stored and used when required for large power systems. As a result, electrical energy must be instantaneously consumed when it is generated to maintain a balance between supply and demand. In addition, power systems must be able to supply the required amount of electrical energy to supply all the load variations. To meet this requirement, adequate active power reserves must always be available to maintain the supply-demand balance.

Frequency control is essential for power system operation to ensure real-time balance between supply and demand. Electrical frequency is a key parameter for power balance. In the event of an imbalance between the supply and demand, the difference is temporarily absorbed or supplied by the kinetic energy of the rotating synchronous machines in the system. Consequently, any power imbalance leads to a change in the rotational speed of these machines, resulting in a corresponding deviation in electrical frequency [1].

Power balance is maintained through frequency control reserves, which are classified into two categories: frequency containment reserves (FCR) and frequency restoration reserves (FRR). Frequency containment reserves provide the initial response to frequency deviations, aiming to limit fluctuations in the event of power imbalance. Following this initial response, frequency restoration reserves act as a secondary mechanism to restore the frequency to its nominal value [2].

While ensuring the continuity of supply is a fundamental objective in power system operation, it is equally important to maintain supply quality. The quality of supply includes various aspects such as frequency control, voltage stability, and reliability of the power system. Frequency quality, which is closely related to the continuity of supply, refers to maintaining the frequency deviations within acceptable limits to maintain stability. In addition to frequency, voltage quality plays a crucial role in power system performance, as voltage deviations and fluctuations can negatively affect system stability. The voltage quality is directly controlled by reactive power management. Furthermore, reliability, defined as the ability of the power system to consistently supply electricity under normal and contingency conditions, is a key aspect of supply quality.

1.1 Reactive Power Control

Reactive power control is a fundamental aspect of power system operation that ensures that voltage levels remain within acceptable limits while minimizing transmission losses. The key elements of transmission systems, such as transmission lines and transformers, have inherent capacitive and inductive characteristics. This yields a reactive power requirement for maintaining the operation of these elements. To provide the necessary reactive power, power system operators utilize various reactive power resources, including synchronous generators, shunt capacitors, and shunt reactors. Transformer tap changers are used in reactive power control by regulating the voltage profiles across the grid.

Reactive power control can be categorized as a three-level hierarchical structure consisting of primary, secondary, and tertiary voltage controls [3], [4] and [5]. The primary voltage control is the control action of a local controller in generating units or FACTS devices with a voltage control capability. Local controllers of the reactive power resources generally control the terminal voltage at a given reference value. In the case of voltage deviation in the power system, these controllers provide or absorb reactive power to regulate the voltage at the desired value.

Secondary voltage control refers to the regional voltage regulation using regional voltage controllers. These controllers adjust the voltage of a designated pilot node within each voltage control region. The primary objective of secondary voltage control, also referred to as coordinated voltage control in some systems [6], is to regulate the voltage within an area where the voltage levels influence one another using a regional controller. Regional voltage controllers utilize the reactive power capabilities of generators within the voltage control region. They regulate the voltage setpoints of automatic voltage regulators, which are responsible for the primary voltage control.

Tertiary voltage control, on the other hand, ensures the coordination of these regional voltage controllers at the system level. A central voltage controller or system operator manages the voltage setpoints of the pilot nodes within each voltage control region.

Secondary and tertiary voltage controls were defined, with some differences in the Turkish power system. Instead of dividing the system into voltage control regions for secondary voltage control, each generator and high-voltage (HV) busbar, which serves as the connection point between the power plant and the power grid, are considered individual voltage control regions. In this approach, the HV busbar is assumed as the pilot node for its respective voltage control region [7].

All power plants directly connected to the transmission system must be equipped with a secondary voltage controller that regulates the HV busbar of the power plant and controls the voltage setpoints of the automatic voltage regulators of the generators. In this context, tertiary voltage control is defined as the determination of the voltage setpoints for power plants. These voltage setpoints are determined on an hourly basis as part of day-ahead reactive power planning.

1.2 Voltage Control Tools

Various network elements can influence the voltage magnitudes through their reactive power capabilities, or by altering the impedance characteristics of the network. Synchronous generators, shunt capacitors, shunt reactors, and FACTS devices, such as static VAR compensators (SVCs) and static synchronous compensators (STATCOMs), regulate voltage magnitudes by utilizing their reactive power capabilities.

Transformer tap changers and series capacitors, which indirectly affect the voltage levels, modify the voltage magnitudes by altering the impedance of the network elements.

These elements can be controlled either through discrete or continuous control depending on their characteristics. Synchronous generators regulate the voltage through automatic voltage regulators, which enable the continuous control of the generator terminal voltage. More recently, static synchronous compensators have been used to provide continuously adjustable reactive power to the grid.

However, shunt capacitors, shunt reactors, and static VAR compensators operate under discrete-control conditions. In most cases, they are switched on when needed, meaning that they are either in service or out of service. In addition, they can be designed in multiple steps, allowing the number of activated steps to be adjusted in a discrete manner.

Similarly, transformer tap changers are controlled discretely by adjusting the voltage levels by changing the transformer tap ratio in predefined steps. They can be classified into on-load tap changers (OLTCs), which allow tap changes while the transformer is in service, and off-load tap changers, which require de-energization for tap changes. In large transmission systems, voltage regulation primarily relies on the reactive power capabilities of power plants along with shunt capacitors, shunt reactors, and OLTC transformers. By contrast, STATCOMs are typically installed and utilized at the distribution level. Therefore, day-ahead reactive power planning for transmission systems involves the determination of voltage setpoints for power plants, switch statuses of shunt capacitors and reactors, and transformer tap positions.

1.3 Motivation and Problem Definition

Voltage control and reactive power management play critical roles in secure and efficient operation of modern power systems. With the expansion of transmission systems, the active power demand has increased, leading to higher transmission losses. Additionally, the share of renewable energy in the total electricity generation is growing. This results in a decrease in electricity generation from controllable power plants.

Therefore, loss minimization has become an important objective in power-system operations. Reactive power management is crucial in achieving this objective.

Conventional reactive power planning and voltage control methods rely on operator experience, often leading to voltage magnitudes outside the desired region and inefficient reactive power dispatches. Furthermore, day-ahead reactive power planning involves discrete control decisions, such as shunt equipment switching and transformer tap changes, which introduce intertemporal dependencies that cannot be effectively handled by conventional single-period optimization methods. This limitation necessitates the development of an advanced optimization framework capable of systematically determining the optimal reactive power dispatch while explicitly considering the temporal aspects of discrete control actions.

This thesis addresses the day-ahead reactive power planning problem by proposing a two-stage multi-period optimization approach that determines the voltage setpoints for generators, switch statuses of shunt equipment, and transformer tap positions. The formulated problem is nonlinear and non-convex, requiring an efficient solution methodology to obtain near-optimal solutions within a practical computation time. Unlike conventional single-period OPF approaches, the proposed methodology explicitly models temporal dependencies, allowing for more coordinated and cost-effective reactive power dispatch. The objective was to develop an optimization-based framework to enhance voltage stability, reduce transmission losses, and improve the overall efficiency of day-ahead reactive power scheduling.

1.4 The Outline of the Thesis

In this thesis, a general background and a review of the literature are provided in Chapter 2. This chapter presents the formulation of the optimal power flow (OPF) problem, including various objective functions and constraint sets for different approaches. Reactive power optimization, which is a specific formulation of the OPF, was also introduced. In addition, solution methods, as well as approximations and relaxations, are discussed.

Chapter 3 introduces the linearized multi-period reactive power optimization approach for the day-ahead reactive power planning problem, providing an outline of the proposed two-stage linearized algorithm. The details of the algorithm are explained, followed by a discussion of the simulation results, and an evaluation of the limitations of the proposed linearized algorithm.

Chapter 4 extends this discussion to the nonlinear day-ahead multi-period reactive power optimization problem and presents its mathematical formulation, including objective functions and constraints. This chapter also discusses the conventional single-period optimization approach before introducing the proposed two-stage multi-period optimization approach.

Chapter 5 presents simulation studies and results, focusing on the IEEE 118-bus test system. It also provides details on the cost calculations related to transmission losses, operational costs, and risk costs associated with tap changes, including the total cost per tap change. The performance of the conventional single-period approach was compared with that of the proposed multi-period approach, followed by an overall evaluation of the algorithm's performance.

Finally, Chapter 6 concludes the thesis with a summary of the important aspects and results of the proposed algorithm, and potential research problems for future work.

CHAPTER 2

GENERAL BACKGROUND

Active power dispatch is one of the fundamental challenges in the operation of modern power systems. The economic dispatch problem is employed as a key approach to obtain the optimum active power dispatch for the generating units. The goal of the economic dispatch problem is to minimize the generation costs without considering the power flows along the grid. With rapidly growing power systems, transmission system operators have started to develop strategies for operating the power system such that the transmission network elements are utilized with maximum capacities. In this environment, the optimum power flow problem has emerged as an extension of the economic dispatch problem. The necessity of operating the transmission system near its maximum capacity mandates the inclusion of network constraints in the active power dispatch problem. Since its introduction in 1962 by Carpentier [8], numerous studies have been conducted to address various objectives and constraints of the OPF problem by proposing diverse solution methodologies. Among these, reactive power optimization has emerged as one of the most common applications for the OPF problem.

2.1 Optimal Power Flow

Optimal power flow is an essential tool in power system operation and planning. The objectives and constraints have diversified significantly so far. The objective of the optimal power flow problem is to determine the optimal control conditions for the grid that optimizes the value for the specified objective function while satisfying the physical and operational constraints of power systems. The optimal power flow

problem can be formulated as a nonlinear optimization problem with equality and inequality constraints, and the general expression for the optimal power flow is given in (2.1)

$$\begin{aligned} \min f(\mathbf{x}, \mathbf{u}) \\ g(\mathbf{x}, \mathbf{u}) &= 0 \\ h(\mathbf{x}, \mathbf{u}) &\geq 0 \end{aligned} \tag{2.1}$$

The state variables, \mathbf{x} , are the uncontrollable variables such as voltage magnitudes of busbars without generators and voltage angles. The control variables, \mathbf{u} , are the controllable variables that are used to optimize the value of the objective function, such as voltage magnitudes of the busbars with generators, active power generation of the generators, transformer tap positions and switch statuses of the shunt equipment.

2.1.1 Objective Functions

The initial and most common objective function of the OPF problem is the minimization of generation costs [8],[9],[10],[11]. In addition to minimizing the generation costs, the minimization of system losses started to be considered in the OPF problem in the early periods [9],[11]. With these objectives, various objectives are utilized in OPF problems.

- Minimization of total generation cost
- Minimization of transmission losses
- Minimization of reactive injection costs [12]
- Maximization of reactive power reserves [13]
- Minimization of bus voltage deviation [14]
- Minimization of the switching numbers of discrete controllers [15],[16]

The minimization of generation costs is usually used to achieve the most economically active power dispatch for generators. The objective function is given in (2.2).

In OPF problems, the typical generation cost function is defined as in (2.3). The cost function may differ for different type of units, but the cost functions are generally approximated as convex quadratic functions.

$$\min C_{total}^P = \sum_{g=1}^{N_{gen}} C_g^P(P_g) \quad (2.2)$$

$$C_g^P(P_g) = a_g^P \cdot P_g^2 + b_g^P \cdot P_g + c_g^P \quad (2.3)$$

The minimization of transmission losses is usually utilized to obtain the optimum reactive power dispatch along the grid. The transmission losses can be obtained using the bus admittance matrix or line parameters directly as in (2.4) and (2.5) respectively. In fact, transmission loss calculations depend on both line and transformer parameters; however, transformer conductance can be neglected in most cases. This allows transmission loss calculations to be performed using only line parameters.

$$P_{loss} = \sum_{i=1}^{N_{bus}} \sum_{j=1}^{N_{bus}} G_{ij} |V_i| |V_j| \cos(\theta_i - \theta_j) \quad (2.4)$$

$$P_{loss} = \sum_{l=1}^{N_{line}} g_k (|V_{li}|^2 + |V_{lj}|^2 - 2 \cdot |V_{li}| \cdot |V_{lj}| \cdot \cos(\theta_{li} - \theta_{lj})) \quad (2.5)$$

The minimization of the reactive power injection costs is also used for reactive power planning [12]. The objective function will be given in (2.6). A linear cost function can be defined for reactive power injection cost for each busbar as in (2.7)

$$\min C_{total}^Q = \sum_{i \in \mathcal{N}^Q} C_i^Q(Q_i) \quad (2.6)$$

$$C_i^Q(Q_i) = a_i^Q \cdot Q_i \quad (2.7)$$

In recent studies, the OPF problem has been extended to address multi-objective optimization. Maximization of reactive reserves [13] and minimization of voltage deviations [14] are included with the minimization of transmission losses. Maximization

of reserves can be defined as in (2.8). In [13], Q_g^{max} is defined as a function of generator parameters. Although the maximum reactive power generation can vary with active power generation level, it can be approximated as the maximum reactive power generation at nominal active power level.

$$\max \sum_{g=1}^{N_{gen}} |Q_g^{max} - Q_g| \quad (2.8)$$

The minimization of voltage deviations is defined as in (2.9). V_g^{ref} is usually defined as 1.0 pu. In addition to the generator terminal voltages, voltages of the important busbars can be included in the objective function.

$$\min \sum_{g=1}^{N_{gen}} (|V_g| - |V_g^{ref}|)^2 \quad (2.9)$$

Due to maintenance problems of switching of shunt reactive power resources which can be used to control the voltage profile along the grid, minimization of the switching numbers of the discrete controller is utilized in the objective function of the optimal power flow problem [15],[16]. The minimization of the switching numbers of the shunt equipment is defined as:

$$\min n_{sw} = \sum_{h=0}^{N_{hour}} \sum_{k=0}^{N_{shunt}} ST_k(h) \quad (2.10)$$

where

$$ST_k(h) = |IS_k(h) - IS_k(h-1)| \quad (2.11)$$

2.1.2 Constraints

OPF mainly aims to determine the optimum settings for network elements to achieve the most economical and reliable system operation. A reliable system operation is ensured by the inclusion of network constraints, such as power balance equations, voltage limits of busbars, and flow limits for branch elements. The network constraints

included in the OPF problem to obtain physically realizable power flows along the grid are as follows:

- For each busbar, the sum of the power currents flowing into the busbar is equal to the sum of the currents flowing out of it.
- For each branch element, the current flowing through it should not exceed the maximum current capacity of the element.
- For each element, the voltage magnitude should not exceed the minimum or maximum voltage limits.

The first constraint is modeled as the sum of power balance equations given in (2.12) and (2.13). These two constraints are included in the OPF problem as equality constraints depending on the objective function of the OPF problem.

$$Pinj_i = |V_i| \sum_{j=1}^{N_{busbar}} |V_j| \cdot (G_{ij} \cos(\theta_i - \theta_j) + B_{ij} \sin(\theta_i - \theta_j)) \quad (2.12)$$

$$Qinj_i = |V_i| \sum_{j=1}^{N_{busbar}} |V_j| \cdot (G_{ij} \sin(\theta_i - \theta_j) - B_{ij} \cos(\theta_i - \theta_j)) \quad (2.13)$$

where

$$Pinj_i = P_i^G - P_i^L$$

$$Qinj_i = Q_i^G - Q_i^L$$

For OPF problems with minimization of generation costs as the objective, both active and reactive power generation of generators are variables. Hence, the minimum and maximum limits for both variables and should be included as inequality constraints. On the other hand, for OPF problems with minimization of transmission losses as the objective, the active power generation of generators is usually constant, whereas the reactive power generation of generators is variable. Therefore, the minimum and maximum limits for the reactive power generation variable should be included as the inequality constraints. The constraints for the minimum and maximum limits of these variables are given in (2.14). and (2.15).

$$\begin{aligned}
P_i^G &\geq \sum_{g \in \mathcal{G}_i} P_g^{min} \\
P_i^G &\leq \sum_{g \in \mathcal{G}_i} P_g^{max}
\end{aligned} \tag{2.14}$$

$$\begin{aligned}
Q_i^G &\geq \sum_{g \in \mathcal{G}_i} Q_g^{min} \\
Q_i^G &\leq \sum_{g \in \mathcal{G}_i} Q_g^{max}
\end{aligned} \tag{2.15}$$

Voltage limits for busbars and the flow limits for branch elements such as transformers and transmission lines are formulated as inequality constraints defined in (2.16) and (2.17). For each busbar, there are two inequality constraints corresponding to the minimum and maximum voltage levels. For each branch element, there are two inequality constraints corresponding to the maximum flow limits.

$$\begin{aligned}
|V_i| &\geq V_i^{min} & \forall i \in \mathcal{N} \\
|V_i| &\leq V_i^{max} & \forall i \in \mathcal{N}
\end{aligned} \tag{2.16}$$

$$\begin{aligned}
\sqrt{P_l^2 + Q_l^2} &= S_l & \forall l \in \mathcal{L} \\
S_l &\leq S_l^{max} & \forall l \in \mathcal{L}
\end{aligned} \tag{2.17}$$

With the constraints introduced to this point, grid security under normal operating conditions is ensured. To further enhance the reliability of the system, additional N-1 security constraints have attracted the attention of researchers [17],[18],[19]. In these studies, N-1 secure active and reactive power dispatch has been established with additional constraints.

In subsequent studies, new constraints have been proposed to ensure voltage stability [13],[15]. Researchers have sought to obtain increased voltage stability with an optimal power flow solution.

2.1.3 Reactive Power Optimization

Reactive power optimization is a special case of the OPF problem [20]. The primary objective of this process is to determine the optimal reactive power dispatch along the grid [21]. Typically, reactive power dispatch is determined after the energy markets are cleared. As a result, the active power dispatch is fixed before reactive power optimization begins. This implies that the active power generation is no longer considered as a control variable. Instead, the voltage setpoints of the generators and switchable reactive power resources remain as control variables. Additionally, transformer tap positions may be included as control variables because they have a significant impact on the reactive power flows within the grid.

The most common objective of reactive power optimization problems is the minimization of transmission losses, because excessive reactive power flows yield an increase in transmission losses [22]. Although the most common objective function is the minimization of transmission losses, other objective functions, such as the maximization of reserves and minimization of bus voltage deviations are also employed in reactive power optimization problems.

2.1.4 Solution Methods

Optimal Power Flow and reactive power optimization are critical aspects of power system operation, with various methodologies developed to address the challenges inherent in these complex problems. Newton's method is among the most prominent methods [9],[11],[17]. This is a numerical technique that iteratively solves nonlinear equations, where in each iteration, the nonlinear equations are linearized using a second-order Taylor series expansion [23]. This method is particularly effective for OPF problems due to its quadratic convergence characteristics, which lead to rapid convergence near the solution. In addition to the computational burden of calculating Jacobian and Hessian matrices in each iteration, the convergence performance of Newton's method is highly dependent on the initial conditions of the problem.

In later studies, the interior point algorithm emerged from [24] and has become widely utilized for OPF problems [12],[13],[14],[19]. The interior point algorithm is a pow-

erful method for solving constrained optimization problems in power systems [25]. It transforms constrained optimization problems into a series of unconstrained problems by incorporating constraints into the objective function using barrier terms. The solution is updated iteratively within the feasible region. This method is well suited for large-scale OPF problems because it can handle inequality constraints effectively as well as equality constraints. Additionally, it exhibits robust convergence characteristics that can handle nonlinear constraints. Despite its high computational complexity, the interior point algorithm is still the most preferred algorithm for large-scale OPF problems.

More recently, meta-heuristic algorithms such as genetic algorithms and particle swarm optimization have been used to address nonconvex and large-scale problems [26]. Heuristic algorithms, such as Genetic Algorithms and Particle Swarm Optimization, have become more popular in OPF applications because of their ability to effectively handle complex nonlinear problems [27]. Genetic Algorithm simulates the mechanism of natural selection by employing techniques such as selection, crossover, and mutation to develop a population of candidate solutions across successive generations, gradually converging toward the optimal solution [28]. In contrast, Particle Swarm Optimization is inspired by the social behaviour of swarms, where each particle in the population adjusts its position in the search space based on its own experience and the collective experience of the swarm [29],[30]. Both methods can handle the nonlinear and nonconvex characteristics of OPF problems. The advantages of these techniques include flexibility, global search capabilities, and the ability to avoid becoming trapped in local optima. However, these methods have certain drawbacks. Genetic Algorithms can be computationally intensive because of their dependence on iterative evaluations of populations. At the same time, Particle Swarm Optimization may experience premature convergence or face challenges in high-dimensional search spaces. Furthermore, neither method guarantees convergence to the global optimum, and their efficiency largely depends on proper parameter tuning [31].

2.1.5 Approximations and Relaxations

To simplify the inherently nonconvex and nonlinear OPF problems, various relaxations and approximations have also been investigated. Convex relaxations [32] provide lower bounds for the objective function, but may produce infeasible solutions [33]. Linear approximation methods simplify power flow equations while maintaining sufficient accuracy for small-sized electrical networks [16],[34],[35]. However, linearized methods often fail to accurately represent the reactive power flows in large systems.

Linear Programming provides an efficient solution framework for problems that can be linearized, ensuring fast computations and guaranteeing the global optimality in convex configurations [36],[37]. However, its applicability is limited to scenarios in which linear relationships can be established, and its inflexibility in managing nonlinear constraints diminishes its utility. Quadratic Programming addresses more complex scenarios by allowing quadratic objective functions [38]. Quadratic programming based algorithms have been utilized for OPF problems in many studies [39],[40],[41].

Sequential Linear Programming [42],[43] and Sequential Quadratic Programming [44] are an iterative approach that builds on the principles of Linear and Quadratic Programming methods, effectively solving a series of linear or quadratic subproblems to tackle nonlinear issues. Sequential Quadratic Programming demonstrates effective constraint management; however, its sensitivity to initial conditions and complexity can pose implementation challenges.

Convex relaxations are a fundamental approach for addressing Optimal Power Flow problems, particularly because of their ability to transform inherently nonconvex problems into convex optimization problems, thereby enabling the attainment of globally optimal solutions [45],[46]. The classical OPF problem, characterized by its nonlinear and nonconvex nature, often presents significant computational challenges due to its multiple local minima. Convex relaxation techniques such as Semidefinite Programming and Second-Order Cone Programming have been extensively studied and applied to overcome these challenges [47].

SDP relaxations work by reformulating the OPF problem into a semidefinite program, where the power flow constraints are approximated by semidefinite constraints, ensuring convexity and allowing the use of efficient interior-point methods [48],[49]. This approach not only guarantees global optimality, but also demonstrates robustness in handling a wide range of objective functions and constraints. However, it is computationally intensive, particularly for large-scale power systems, and may introduce approximation errors.

Similarly, SOCP relaxations transform the OPF problem by approximating the non-convex constraints with second-order cone constraints, thereby preserving convexity and enabling efficient solution algorithms [50]. The SOCP is popular because of its computational efficiency and flexibility in accommodating various constraints and objective functions, although it faces challenges related to approximation accuracy and complexity in large-scale scenarios [51]. Both the SDP and SOCP offer powerful tools for reactive power optimization, enhancing voltage stability, and minimizing power losses; however, their practical application necessitates careful consideration of computational resources and approximation fidelity.

In summary, the diverse methodologies for OPF and reactive power optimization present unique advantages and limitations, underscoring the need for tailored approaches that align with specific power system characteristics and requirements. Each method contributes to a broader understanding of power system optimization, aiding in the pursuit of a more reliable and efficient energy distribution.

CHAPTER 3

LINEARIZED MULTI-PERIOD REACTIVE POWER OPTIMIZATION

Day-ahead reactive power optimization focuses on the optimal dispatch of reactive power resources. The purpose of the day-ahead reactive power optimization is to allocate reactive power resources within the day-ahead time frame using the forecasted load and generation profiles. Reactive power resources, such as generators and shunt equipment, play a critical role in minimizing transmission losses by regulating reactive power injections across the grid. Transformer tap positions further support this process by adjusting voltage levels to manage reactive power flows efficiently. However, switching operations for shunt equipment and transformer tap changes introduce operational costs and risks, which could also be minimized. Transmission system operators therefore aim to reduce both the number of daily shunt equipment switching operations and transformer tap changes.

In the initial stage of the algorithm development process, minimization of the number of switching operations of the shunt equipment was the main focus of the problem, while transformer tap changes were excluded. The objective of the day ahead reactive power planning problem is defined as the minimization of transmission losses and the minimization of the number of switching operations of shunt equipment. Linear programming approach is utilized as the basis of the proposed algorithm to the nonconvex and nonlinear reactive power optimization problem at this point. In this chapter, the linearized multi-period reactive power optimization approach based on linear programming approach will be presented.

A two-stage algorithm is developed for the reactive power planning problem on a day-ahead basis based on the successive linear programming approach. In the first stage, a linearized optimization problem is formulated to determine the integer variables.

Then, in the second stage, it is aimed to find the optimal solution for continuous variables by iteratively updating the solution. In each iteration, the search direction is determined using a linearized optimization problem.

The day ahead reactive power planning problem interested in this chapter is a multi-objective optimization problem. The objective function of the problem is defined as the weighted sum of two independent objectives as can be seen in (3.1).

$$\min f^W = w_{loss}P_{loss}^T + w_{sw}n_{sw} \quad (3.1)$$

The objective functions are the minimization of total transmission losses, P_{loss} , given in (2.5) and the minimization of the number of switching operations of shunt equipment, n_{sw} , given in (2.10). However, since the problem is a multi-period optimization problem, the transmission loss function is calculated as multi-period as given in (3.2).

$$P_{loss}^T = \sum_{h=1}^{N_{hour}} \left(\sum_{l=1}^{N_{line}} g_k \left(|V_{li}(h)|^2 + |V_{lj}(h)|^2 - 2 \cdot |V_{li}(h)| \cdot |V_{lj}(h)| \cdot \cos(\theta_{li}(h) - \theta_{lj}(h)) \right) \right) \quad (3.2)$$

3.1 Proposed Two-Stage Linearized Algorithm

The successive linear programming methods search for the optimal solution by iteratively solving linearized optimization problems. In each iteration, the power balance constraints and the total loss function are approximated as linear functions using a first-order Taylor series expansion. However, since the switch statuses of shunt equipment are binary variables, the linearized objective function and constraints are not valid for both possible values of the shunt switch status variables. This implies that the solution of the linearly approximated optimization problem is only valid for the specific values at which the constraints were linearized.

To overcome this issue, a two-stage algorithm has been developed. The integer variables related with the switch statuses of shunt equipment are determined in the first

stage. The shunt switch optimization problem is formed with loss and voltage sensitivity factors in this stage. The solution of the shunt switch optimization problem gives the switch statuses of the shunt equipment.

Then in the second stage, only the minimization of transmission losses is remains as the objective function of the problem. Since there is no time coupling with the remaining variables, the reactive optimization problems for each hour are solved independently. The reactive power optimization problems for each hour in the second stage of the problem is solved based on a successive linear programming approach.

The algorithm flowchart is given in Figure 3.1. The relevant network parameters are read from the system database, and the bus admittance model is formed during the data preparation phase. The active power generation dispatch is retrieved from the market results and the demand data is formed according to the load forecast data. With the data preparation phase, overall system data and hourly active power generation and demand data has been determined. Then the two-stage algorithm will be run to optimize the reactive power dispatch along the grid.

3.1.1 First Stage of the Algorithm

In this stage, the main purpose is to determine the switch statuses of shunt equipment within a given time period. In the meantime, the aim of the optimization problem is to minimize number of switching of these shunt equipment while minimizing the total system losses. The optimization problem for this stage is formulated as a linear optimization problem. The objective function of the optimization problem in this stage is defined as in (3.3). The control variables consist only the switch statuses of shunt equipment in this stage; hence, the change in transmission losses due to the reactive power injection of shunt equipment is included in the objective function.

$$\min f^W = w_{loss}\Delta P_{loss}^T + w_{sw}n_{sw} \quad (3.3)$$

In order to include the effect of shunt equipment on system losses in the optimization problem, loss coefficients are introduced. These coefficients represent the effect of

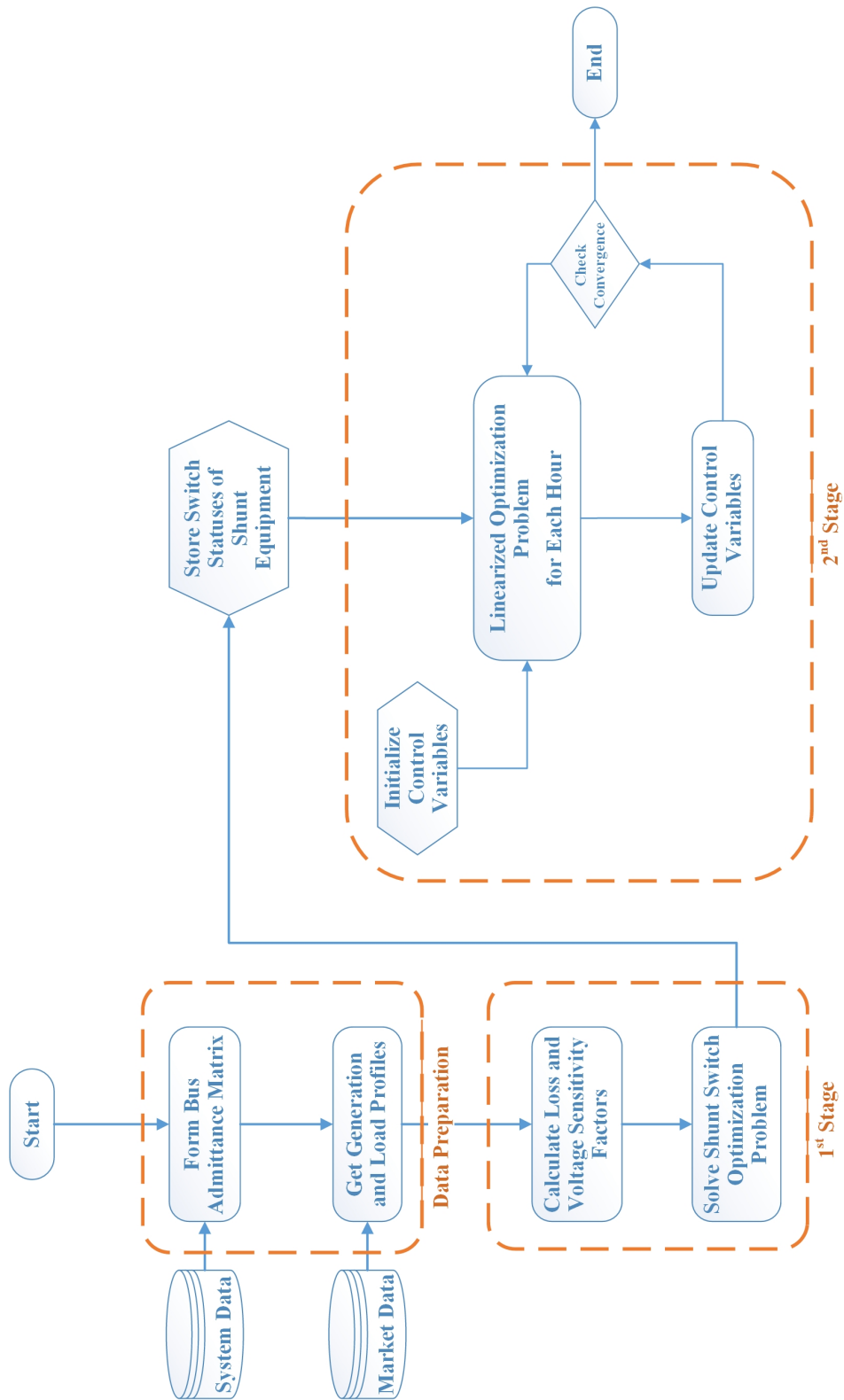


Figure 3.1: The flowchart of the proposed two-stage linearized algorithm

the change in switch statuses on system losses. The effect of switch statuses of shunt equipment to the transmission losses are included in the objective as in (3.4).

$$\Delta P_{loss}^T = \sum_{h=1}^{N_{hour}} \sum_{k \in \mathcal{K}} \left(IS_k(h) \cdot \frac{\Delta P_{loss}}{\Delta IS_k} \Big|_h \right) \quad (3.4)$$

The loss coefficients are defined for each shunt equipment and calculated as the difference between the system losses at hour h for the cases where the shunt equipment k is in service and out of service as in (3.5).

$$\frac{\Delta P_{loss}}{\Delta IS_k} \Big|_h = P_{loss}(h) \Big|_{IS_k(h)=1} - P_{loss}(h) \Big|_{IS_k(h)=0} \quad (3.5)$$

The number of switching operations, n_{sw} , is the sum of all the status change variables. The status change variable of shunt equipment k for hour h , $ST_k(h)$, is defined as the absolute value of the difference between switch status of shunt equipment k for consecutive hours. In order to eliminate the absolute value function and convert the expression into a linear function, the relation between the status change variables and switch status variables, three inequality constraints are introduced for each shunt equipment k and for each hour h . These constraints are defined as in (3.6), (3.7) and (3.8).

$$ST_k(h) \geq 0 \quad (3.6)$$

$$ST_k(h) \geq IS_k(h) - IS_k(h-1) \quad (3.7)$$

$$ST_k(h) \geq IS_k(h-1) - IS_k(h) \quad (3.8)$$

where

$$ST_k(h) \in [0, 1]$$

In addition, the voltage magnitudes of the busbars are influenced by the reactive power injections of shunt equipment, with a decrease in impact as the distance increases from the shunt equipment. Hence, the voltage limits are included in the shunt switch status optimization problem constraints as in (3.9) and (3.10) for all busbars.

$$|V_i(h)| + \sum_{k \in \mathcal{K}} \left(IS_k(h) \cdot \frac{\Delta |V_i|}{\Delta IS_k} \Big|_h \right) \leq V_i^{max} \quad (3.9)$$

$$|V_i(h)| + \sum_{k \in \mathcal{K}} \left(IS_k(h) \cdot \frac{\Delta |V_i|}{\Delta IS_k} \Big|_h \right) \geq V_i^{min} \quad (3.10)$$

In order to take the voltage limits into account, voltage coefficients are introduced similar to the loss coefficients. The voltage coefficients are defined as the difference of bus voltage magnitudes at hour k for the cases where the shunt equipment k is in service and out of service as given in (3.11). The voltage coefficients are calculated for each busbar. Voltage coefficients for the busbar i are calculated for each shunt equipment k .

$$\frac{\Delta |V_i|}{\Delta IS_k} \Big|_h = |V_i(h)|_{IS_k(h)=1} - |V_i(h)|_{IS_k(h)=0} \quad (3.11)$$

For each shunt equipment k , the values of $|V_i|(h)$ and $P_{loss}(h)$ for the cases where $IS_k(h) = 1$ and $IS_k(h) = 0$ are calculated using power flow solutions of the corresponding cases. Hence, there are $N_{shunt} + 1$ power flow calculations for each hour h required to obtain the loss and voltage coefficients .

Using these loss and voltage coefficients, a linear optimization problem is formulated to determine the switch statuses of shunt equipment. These coefficients is used to consider the effect of reactive power injection of shunt equipment to the voltage magnitudes of busbars and total transmission losses.

To summarize the shunt switch status optimization in the first stage, the objective of the optimization problem is defined as (3.3), where ΔP_{loss}^T is defined as (3.4). The constraints of the optimization problem are (3.6),(3.7),(3.8), (3.9) and (3.10).

The optimal solution for the shunt switch optimization problem is obtained using IBM CPLEX optimization solver. The optimal solution gives the switch statuses of each shunt equipment for each hour. At the end of the first stage of the algorithm, the bus admittance matrix is updated according to the results of the shunt switch optimization problem.

3.1.2 Second Stage of the Algorithm

The main purpose of the second stage of the algorithm is to determine the optimal voltage profile along the grid. Since the switch statuses of shunt equipment are determined in the first stage, there is no time coupling between the variables that remain unknown in the second stage. Consequently, the optimization problem in this stage is no longer a multi-period problem, allowing reactive power optimization to be executed independently for each hour. Furthermore, because the switch statuses are predetermined, the objective of minimizing the number of switching operations in the multi-objective optimization problem is eliminated. As a result, the objective function now solely focuses on minimizing transmission losses.

The objective function of the optimization problem for each hour h in the second stage is defined as in (2.5). The constraints are defined as (2.12), (2.13), (2.15) and (2.16). The active power generation of generators are assumed to be constant for this reactive power optimization since the active power generation of generators are determined in day-ahead market before the reactive power planning. Hence, the active power limits for generators and flow limits of the lines are not included in this optimization problem.

The second stage of the algorithm is based on the successive linear programming approach. The algorithm iteratively searches for the optimal solution independently for each time period. In every iteration, the objective function and constraints are linearized using a first-order Taylor series expansion at the current values of the state variables for that period. This linearized formulation results in a Linear Programming Problem, which is solved using the IBM CPLEX solver. The solution provides updated state variables for the given time step. At the end of each iteration, a convergence check is performed using the expression (3.12). This iterative process continues until the convergence criterion is met. The flowchart of the second stage of the algorithm is shown in Figure 3.2.

$$x^{k+1} - x^k < \epsilon^{tol} \quad (3.12)$$

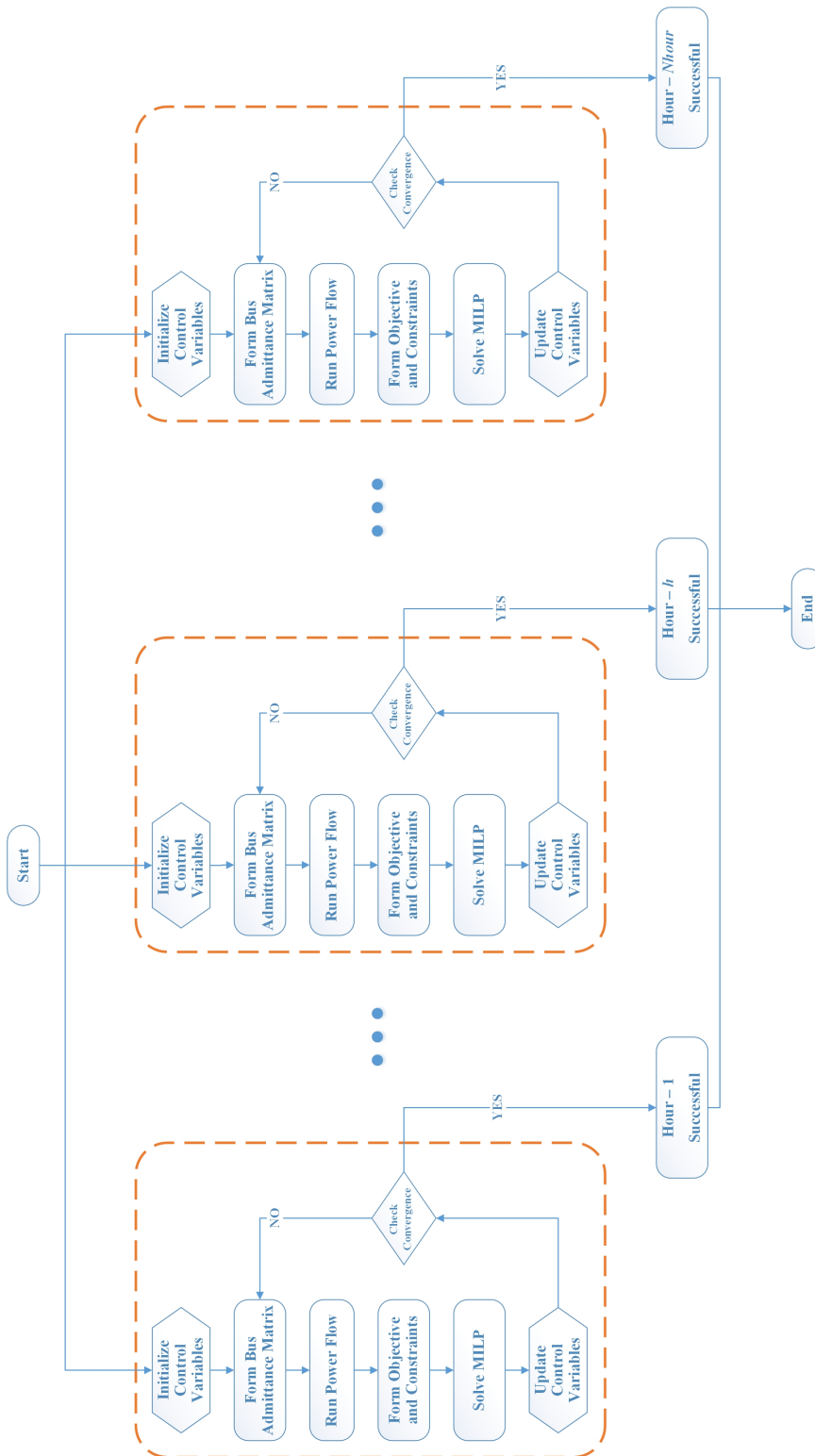


Figure 3.2: Successive linear programming approach for the 2nd stage of the proposed two-stage linearized algorithm

The linear optimization problem for each iteration for hour h , is formed using first order Taylor series expansion at the current values of the state vector. The objective function, which is only the minimization of transmission losses, is linearized as in (3.13). Similarly, the active and reactive power balance constraints are linearized as in (3.14) and (3.15).

$$P_{loss}(\mathbf{x}) = P_{loss}(\mathbf{x}^k) + \nabla P_{loss}(\mathbf{x}^k)^T \cdot (\mathbf{x} - \mathbf{x}^k) \quad (3.13)$$

$$Pinj_i(\mathbf{x}) = Pinj_i(\mathbf{x}^k) + \nabla Pinj_i(\mathbf{x}^k)^T \cdot (\mathbf{x} - \mathbf{x}^k) \quad (3.14)$$

$$Qinj_i(\mathbf{x}) = Qinj_i(\mathbf{x}^k) + \nabla Qinj_i(\mathbf{x}^k)^T \cdot (\mathbf{x} - \mathbf{x}^k) \quad (3.15)$$

where

$$\mathbf{x} = [\mathbf{V}, \boldsymbol{\theta}]$$

The active power dispatch is assumed to be determined before the reactive power optimization; therefore, any variations in reactive power flows will result in only minor changes in active power flows. Considering the strong coupling between active power and voltage angles in power systems, it is assumed that voltage angles remain unchanged throughout the optimization process. Hence the voltage angles, $\boldsymbol{\theta}$, is the only variable vector for the linear optimization problems for each time period.

3.2 Simulation and Results

The proposed algorithm has been tested on the IEEE 30-Bus Test System, which represents power networks at a fundamental level. This test system is widely used for power system optimization purposes because it includes the fundamental elements of a typical power network while maintaining minimal computational complexity compared to larger networks.

To evaluate the impact of shunt equipment on reactive power optimization, two shunt reactors have been added to the test system. The original model includes only two shunt capacitors at Bus 10 and Bus 24. Since the objective function focuses on minimizing the number of switching operations for the shunt equipment, two shunt reactors were added to ensure a sufficient number of shunt devices for evaluating the

minimization of switching operations. Shunt reactors are essential components for voltage regulation and reactive power management, especially in high-voltage transmission systems. Their inclusion in the test model helps demonstrate their effects on reactive power optimization.

Since standard test systems typically provide data for a single time period, an additional 8-hour dataset for generation and load values has been created to accommodate the algorithm’s requirements and enable its evaluation under time-varying conditions. The IEEE 30-Bus Test System is then used together with this dataset to test the proposed algorithm, which operates within a multi-period framework.

The details of the shunt equipment in the test system are given in Table 3.1.

Table 3.1: Shunt equipment in the IEEE 30 Bus test system

Bus ID	Vnom (kV)	Type	Q (MVar)
4	132	Reactor	-30
10	33	Capacitor	19
24	33	Capacitor	4,3
28	132	Reactor	-10

The first stage of the algorithm is basically a mixed integer linear programming problem. In order to form the MILP problem, loss coefficients, $\left. \frac{\Delta P_{loss}}{\Delta IS_k} \right|_h$, and voltage coefficients, $\left. \frac{\Delta |V_i|}{\Delta IS_k} \right|_h$, are required to be calculated. The coefficients are calculated using the equations (3.5) and (3.11).

For each time period h , and for each shunt equipment k , power flow calculation is performed to calculate the coefficients. The calculated loss coefficients are given in Table 3.2.

Table 3.2 shows the calculated loss coefficients for each shunt equipment and time period. Specifically, shunt reactors exhibit positive loss coefficients, indicating that their activation increases the overall system losses under specified network conditions. For example, the shunt equipment at Bus 4 causes relatively high loss coefficients, reaching 0.66 for certain time periods. Conversely, negative loss coefficients were observed

Table 3.2: Loss coefficients for shunt equipments for each time period

	H1	H2	H3	H4	H5	H6	H7	H8
Bus 4	0,66	0,24	0,66	0,36	0,23	0,66	0,24	0,36
Bus 10	-0,32	-0,09	-0,32	-0,13	-0,1	-0,32	-0,09	-0,13
Bus 24	-0,13	-0,06	-0,13	-0,09	-0,07	-0,13	-0,06	-0,09
Bus 28	0,17	0,07	0,17	0,08	0,06	0,17	0,07	0,08

for the shunt equipment at Bus 10 and Bus 24, suggesting that the activation of the shunt capacitors at these busbars reduces the system losses. In addition, the effect of shunt equipment on system losses varies with reactive power injection. The reactive power injection capacity of the shunt reactor at Bus 4 was higher than that of the shunt reactor at Bus 28. Similarly, the loss coefficient of the shunt reactor at Bus 4 was higher than that at Bus 28. These variations in the loss coefficients show the dependency of the shunt equipment's impact on the system losses for the amount and direction of reactive power injection. Without proper reactive power dispatch, the coordination of the shunt equipment may cause an undesired increase in system losses.

Due to the loss coefficients given in Table 3.2, the shunt switch optimization tends to switch on all the capacitors and switch off all the reactors. However, the reactive power injection from the shunt equipment alters the voltage magnitudes of the busbars electrically close to these devices. As a result, the switch statuses are determined as shown in Table 3.3 and Table 3.4 for different weighting factors of switching operations.

Specifically, for smaller values of the weighting factors of switching operations, shunt capacitor at Bus 10 remains switched on for most of the time periods, ensuring continuous reactive power support, while shunt capacitor at Bus 24 is switched on only at specific hours. This indicates that the shunt capacitor at Bus 10 plays a more active role in reactive power compensation, whereas the shunt capacitor at Bus 24 is utilized selectively in order to prevent over/under voltages along the grid. However, for larger values of the weighting factors of switching operations, shunt capacitor at Bus 10 is

Table 3.3: Shunt switch statuses for the case $w_{sw} < 0.4$

	Bus 10	Bus 24
H1	OFF	ON
H2	ON	ON
H3	ON	OFF
H4	ON	OFF
H5	ON	OFF
H6	ON	ON
H7	ON	OFF
H8	ON	OFF

Table 3.4: Shunt switch statuses for the case $w_{sw} > 0.4$

	Bus 10	Bus 24
H1	OFF	ON
H2	OFF	ON
H3	OFF	OFF
H4	OFF	OFF
H5	OFF	ON
H6	OFF	ON
H7	OFF	OFF
H8	OFF	OFF

switched off for all the time periods. This is because the algorithm tries to decrease the switching operations. The decrease in the system losses when the shunt capacitor at Bus 10, cannot compensate the number of switching operations of the shunt capacitor at Bus 10 with higher weighting factors.

The first stage of the algorithm has been simulated for different weighting factors, w_{loss} and w_{sw} , to analyze their impact on the optimization process. The results cor-

responding to different weighting factor values are illustrated in Figure 3.3. As observed in the figure, an increase in the weighting factor associated with switching operations w_{sw} leads to a reduction in the number of switching operations. This outcome aligns with expectations, as the optimization prioritizes minimizing switching when its associated weighting factor is increased. Conversely, as fewer switching operations are performed, the system experiences higher losses, reflected in an increase in the loss function ΔP_{loss} . Additionally, the total objective value demonstrates a trade-off between switching minimization and system losses, increasing progressively as w_{sw} increases. These results confirm that the weighting factors effectively regulate the balance between reducing switching operations and limiting system losses, enabling a more flexible optimization strategy depending on operational priorities.

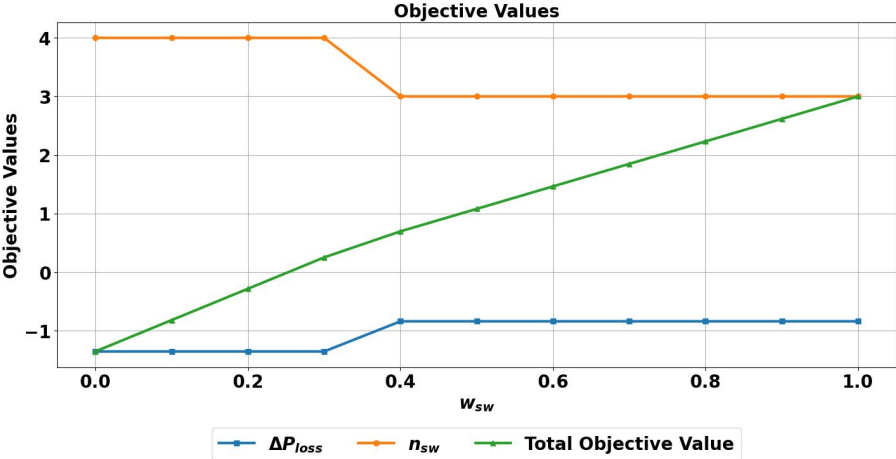


Figure 3.3: Resulting objective function values

In the second stage, with predetermined switch statuses for shunt equipment, the reactive power flows and inherently the voltage profile are optimized. The resulting voltages for busbars are shown in Figure 3.4. As can be seen in the figure, the voltages of the controllable busbars are maintained above 1 p.u., whereas the voltage magnitudes at electrically remote busbars tend to decline due to increased reactive power losses and reduced voltage support. Consequently, buses that are farther from the controllable nodes exhibit lower voltage levels, highlighting the impact of network topology and reactive power compensation on the overall voltage profile.

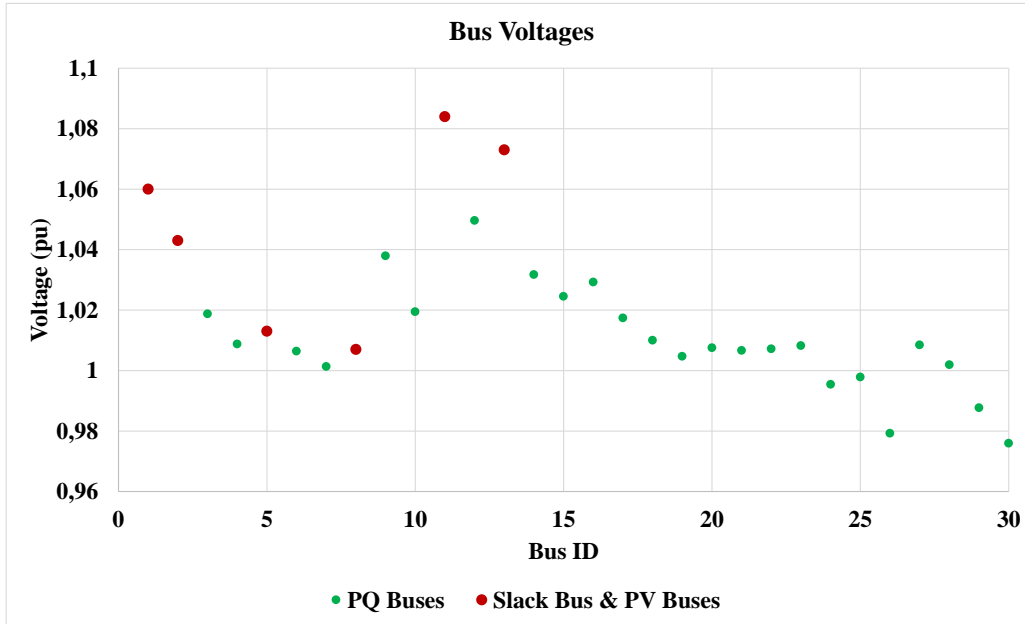


Figure 3.4: Resulting bus voltage magnitudes

3.3 Evaluation and Limitations of the Proposed Algorithm

A linearized reactive power optimization algorithm is introduced to address the challenges associated with multi-period and multi-objective reactive power optimization in this chapter. These problems are computationally intensive and may not always converge due to the inherent nonlinearity of power balance equations. To mitigate this issue, the nonlinear constraints are linearized, simplifying the problem formulation. However, this linearization remains valid only within a limited range of state variables. Therefore, the proposed algorithm employs a successive linear approximation approach to achieve an optimal reactive power dispatch. In addition to reactive power support of generators, shunt equipment play a crucial role in the voltage profile across the grid. However, the linearized power balance equations may not accurately represent the effects of discrete changes in shunt equipment statuses. To overcome this issue, the algorithm is formed as a two-stage optimization. The first stage formu-

lates the problem as a mixed-integer linear programming problem by excluding non-linear power balance equations. In the second stage, only reactive power injections of generators are determined while transmission losses are optimized. Successive linear approximations are applied in this stage to determine the optimum reactive power dispatch.

The primary limitation of the algorithm lies in the computational burden associated with the first-stage shunt switch optimization. This stage requires independent power flow calculations for each shunt device and each time period, which significantly increases the computational effort. While the test case analyzed in this chapter involves a manageable number of shunt elements and time periods, larger systems would require an impractically high number of power flow calculations, as expressed in (3.16).

$$n_{calc}^{PF} = N_{hour} \cdot (N_{shunt} + 1) \quad (3.16)$$

Another important issue with the first-stage shunt status optimization is the assumption that the effects of multiple shunt switching actions can be linearly superimposed. While the algorithm estimates the resulting loss and voltage changes by summing the individual linearized impacts of each shunt switching event, in reality, the simultaneous operation of multiple shunt elements can produce nonlinear interactions that are not accurately captured. In particular, the mutual influence of loss and voltage coefficients is disregarded, potentially leading to deviations from the actual system behavior.

Since the second stage relies on linearized power balance equations, it is essential to validate the resulting power flow solutions. To verify the accuracy of the second stage of the algorithm, a comparative analysis has been conducted between the power flows and bus voltages obtained from the algorithm results and via a Newton-Raphson Power Flow calculation, where the control variables from the second stage are used as inputs.

As shown in Figure 3.5, the voltage deviations at all buses remain below 0.01 p.u., demonstrating that the algorithm yields physically realizable voltage setpoints, an essential criterion in the reactive power optimization problem addressed in this study.

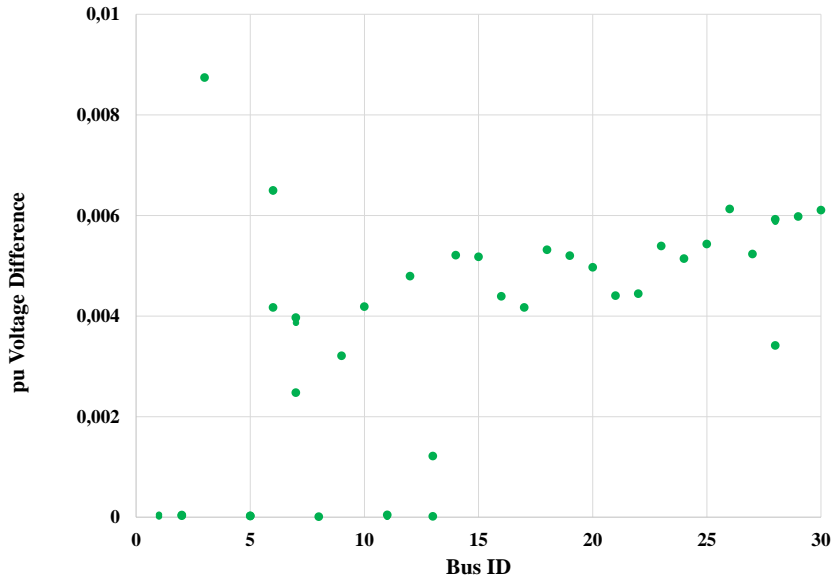


Figure 3.5: Voltage differences between the 2nd stage algorithm and power flow results

The differences in active and reactive power flows are shown in Figure 3.6 and Figure 3.7, respectively. The maximum absolute deviation in active power flows is found to be below 2 MW, while the absolute deviations in reactive power flows reach up to 16 MVar.

A further drawback of the algorithm is related to the second-stage successive linear optimization. While the discrepancy between the linearized and actual power balance equations remains within acceptable limits for active power flows, the deviation reaches significant levels for reactive power flows. Given that the primary objective of the algorithm is to determine the optimal reactive power dispatch, this issue represents a major limitation. The reliance on linearized constraints in the second stage may lead to suboptimal or inaccurate reactive power dispatch decisions, particularly in cases where the nonlinearity of reactive power flows is more pronounced.

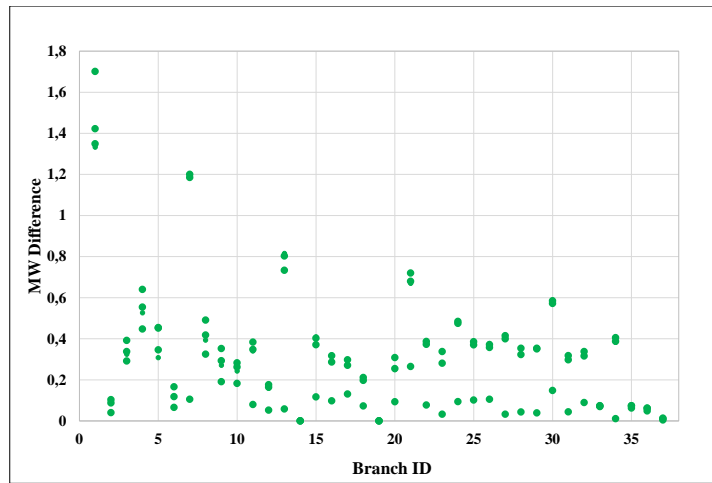


Figure 3.6: Active power flow differences between the 2nd stage algorithm and power flow results

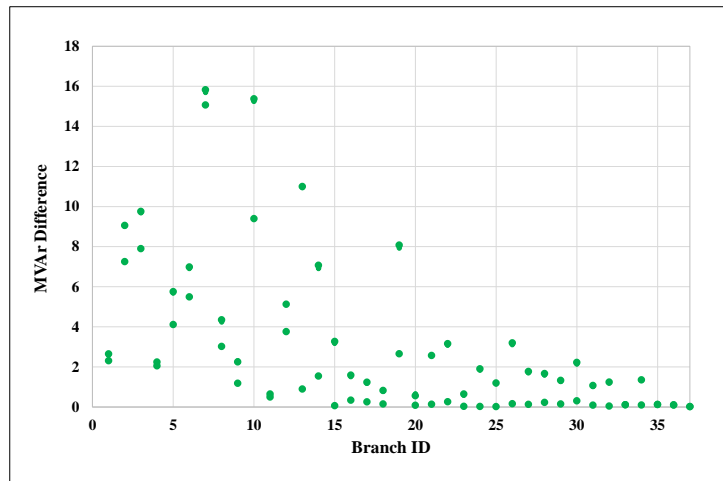


Figure 3.7: Reactive power flow differences between the 2nd stage algorithm and power flow results

Another limitation of the algorithm is that it does not incorporate transformer tap positions as decision variables. Inclusion of them in the first stage would drastically increase the computational burden, making the problem impractical for large networks. On the other hand, if tap positions were accounted for in the second stage, the discrepancies introduced by linearized equations, which are already problematic for reactive power flows, would become even more significant.

CHAPTER 4

DAY-AHEAD MULTI-PERIOD REACTIVE POWER OPTIMIZATION

Day-ahead reactive power optimization focuses on the optimal dispatch of reactive power resources. The main objectives are to ensure system reliability and security while minimizing transmission losses across the grid. Specifically, the purpose of the day-ahead reactive power optimization is to allocate reactive power resources within the day-ahead time frame using the forecasted load and generation profiles. Since the day-ahead energy market clears active power dispatch independent from reactive power, a coordinated plan for reactive power dispatch must be determined after the day-ahead market clearing.

Reactive power resources, such as generators and shunt equipment, play a critical role in minimizing transmission losses by regulating reactive power injections across the grid. Reactive power is required for the transmission of active power from generation to consumers. On the other hand, reactive power flows increase the magnitude of the current through the network elements, therefore the active power loss on these elements. In order to decrease the active power loss on network elements, the redundant reactive power flow must be removed from the grid. The principal method to eliminate the excessive reactive power flows along the grid is to support reactive power as close as possible to where it is required. In this context, the reactive power injections from generators and shunt equipment are the primary resources to minimize the total transmission losses.

Transformer tap positions further support this process by adjusting voltage levels to manage reactive power flows efficiently. Transformer tap positions are mainly used for regulating the voltage levels of both sides of the transformers. Generally, either the primary or secondary side of the transformer is stronger in terms of equivalent short

circuit MVA, hence the transformer tap positions can alter the voltage magnitudes of the weaker side of the transformer. The change in the voltages cause a change in reactive power requirement of the network elements. In such manner, the transformer tap positions may cause a change in transmission losses.

Therefore, the main resources that can be controlled to minimize the transmission losses and to obtain the optimum reactive power flows along the grid is the reactive power injection by the generators and shunt equipment and the transformer tap positions. However, switching operations for shunt equipment and transformer tap changes introduce operational costs and risks, which transmission system operators are trying to avoid from switching operations and tap changes.

In this context, the day-ahead hourly reactive power planning problem, which is a nonlinear and nonconvex optimization problem, is formulated to minimize the total cost. Although the problem inherently involves multiple objectives, these objectives are modeled within a single cost function, which consists of the energy cost of transmission losses and the operational and risk costs associated with transformer tap changes and switching operations of shunt equipment. To address this problem, a two-stage algorithm is proposed. In the first stage, the switching statuses of shunt equipment are determined. In the second stage, generator voltage setpoints and transformer tap positions are optimized to minimize transmission losses while ensuring system reliability and security.

In conventional power system operations, reactive power optimization is often performed on an hourly basis, where each hour is considered independently without accounting for inter-temporal dependencies. This widely used methodology, referred to as the Conventional Single-Period Approach, serves as a reference to evaluate the effectiveness of the proposed two-stage algorithm for the day-ahead hourly reactive power planning problem. The main objective of comparing the proposed two-stage algorithm with the Conventional Single-Period Optimization Approach is to evaluate improvements in efficiency, solution quality, and computational performance. Specifically, the limitations of the single-period optimization, such as the potential for suboptimal resource utilization and increased operational costs, can be analyzed in detail.

4.1 Problem Formulation

In reactive power optimization problems, variables can be divided into two categories: control variables and state variables. Control variables refer to the parameters that can be actively adjusted to regulate active and reactive power flows along the grid. In contrast, state variables cannot be directly modified; instead, their values are inherently determined based on the selected control variables. Variable categories in this study are given in Table 4.1.

Table 4.1: Variable categories in day-ahead reactive power optimization

	$ V $	θ	P	Q	IS	TP
Slack Busbar	Control	Control	State	State	-	-
Generator Busbar	Control	State	Constant	State	-	-
Non-Generator Busbar	State	State	Constant	Constant	-	-
Shunt Equipment	-	-	-	State	Control	-
Transformer	-	-	-	-	-	Control

As shown in Table 4.1, active power injection, voltage magnitude, and voltage angle for the slack busbar are classified as control variables. Although active power dispatch is determined prior to reactive power optimization, the active power injection at the slack busbar is retained as a variable to compensate for changes in active power equilibrium caused by variations in active power losses. Voltage magnitude is regulated by the slack generator, whereas voltage angle is designated as a control variable to fix the slack busbar's voltage angle at zero. This ensures that the slack busbar serves as the reference for the voltage angles of all other busbars. The reactive power injection at the slack busbar is classified as a state variable, primarily influenced by the voltage magnitude of the generator busbar.

For generator busbars, active power injections are assumed to be constant since active power dispatch is determined before the day-ahead reactive power planning process.

The only controllable variable for generator busbars is voltage magnitude. In contrast, voltage angle and reactive power injection are treated as state variables.

For non-generator busbars, active and reactive power injections are determined solely by the active and reactive power demands of loads, if present. Since the voltage magnitudes and angles of non-generator busbars cannot be directly controlled, they are classified as state variables.

For busbars with generators, slack busbar and generator busbars, either voltage magnitude or reactive power injection may be designated as a control variable, with the other classified as a state variable. The generator regulates its voltage magnitude by adjusting its reactive power injection, or alternatively, maintains a specified reactive power injection by modifying its excitation voltage. Consequently, both variables cannot simultaneously be classified as control or state variables; one must be a control variable while the other remains a state variable. In this study, since the objective is to determine the voltage set points of power plants, generator voltage magnitudes are designated as control variables, while reactive power generation is treated as a state variable.

Reactive power injections of the shunt equipment are determined by the switch statuses of the shunt equipment and the voltage magnitudes of the busbar that the shunt equipment is connected. Hence, the switch statuses of shunt equipment are classified as control variables whereas the reactive power injections of shunt equipment are categorized as state variables. Lastly, the transformer tap positions are the control variables that are defined relating with transformers.

4.1.1 Objective and Constraints

In this thesis, as the final solution for the day-ahead reactive power planning problem, the reactive power optimization is constituted by three objectives: minimization of transmission losses, minimization of shunt switching operations, and minimization of transformer tap changes. These objectives are combined under a cost minimization framework. The total cost includes energy costs for transmission losses and operational and risk costs for switching shunt equipment and transformer tap changes.

The objective function of the optimization problem is defined as (4.1). The transmission losses, P_{loss} , is defined using the line conductances as in (2.5). The number of switching operations of shunt equipment is defined as (2.10) and (2.11). Similar to the linearized multi-period reactive optimization presented in 3, the absolute function is represented as three linear inequality constraints, defined as (3.6), (3.7) and (3.8).

$$\min C^T = \pi_{loss}P_{loss} + \pi_{switch}n_{sw} + \pi_{tc}n_{tc} \quad (4.1)$$

The constraints of the reactive optimization problem are comprised by power balance equations which are indispensable for reactive power optimization problems. Each shunt switching operation and transformer tap change introduces a disturbance to the system. Especially, disturbances caused by shunt switching operations can be significant, making it essential to closely monitor and track them. Although the effect of transformer tap changes is not as large as that of shunt switching operations, transmission system operators pay close attention to tap change operations as well. Therefore, in addition to the power balance equations defined as (2.12) and (2.13), the maximum allowable number of switching operations and tap changes can be included in the optimization problem. These new operational constraints are defined as (4.2) and (4.3).

$$\sum_{h=2}^{N_{hour}} ST_k(h) \leq N_{switch}^{max} \quad (4.2)$$

$$\sum_{i=0}^{T_{change}} ST_k(h+i) \leq 1 \quad (4.3)$$

4.2 Conventional Single-Period Optimization Approach

This approach is developed based on personal experience with the Turkish transmission system operator and reflects conventional industry practices in reactive power dispatch. In this approach, reactive power optimization is carried out for each hour independently, without considering inter-temporal dependencies. The requirements related to the number of switching operations and transformer tap changes and reasons behind them are explained in the previous section. On the other hand, this ap-

proach does not consider the relation between time periods. To satisfy the need of the transmission system operators, the switching statuses and transformer tap positions are dealt with before conducting the single-period optimization problems.

Conventionally, shunt switch statuses and transformer tap positions are determined based on historical voltage profiles for the regions affected by each shunt device. It is assumed that shunt reactors are utilized when the voltage profile needs to be lowered, whereas shunt capacitors are used to increase voltages in the region. Based on historical voltage profile data, switch statuses are set accordingly. Additionally, the maximum allowable number of switching operations is considered in this process. Transmission system operators generally perform a maximum of two to four switching operations per day for each shunt device. The maximum allowable number of switching operations is determined based on the age and characteristics of the switching equipment associated with the shunt reactive resources.

Similarly, transformer tap positions are determined based on historical voltage profiles. Tap adjustments can modify the voltages of the busbars connected to the corresponding transformer. Transformer tap positions are adjusted to regulate the voltage of the weaker busbar, which has lower short-circuit power. As in the case of shunt equipment, transmission system operators aim to limit the number of tap changes to minimize mechanical stress and system disturbances. Therefore, in this approach, the maximum allowable number of transformer tap changes is also defined. However, this limit is typically set slightly higher than the maximum allowable number of switching operations for shunt equipment.

With predetermined shunt switch statuses and transformer tap positions, reactive power planning is carried out using single-period reactive power optimization models. For each time period, a nonlinear reactive power optimization problem is formulated and solved to determine the optimal reactive power dispatch.

The single-period reactive power optimization model for each time period is formulated with the objective of minimizing transmission losses, as shown in (4.4), and transmission losses are defined in (2.5).

$$\min P_{loss}(h) \quad \forall h \in \{1, 2, \dots, N_{hour}\} \quad (4.4)$$

The constraints of the single-period optimization models for each time period are defined using conventional OPF constraints, as in (2.12), (2.13), (2.15), and (2.16). The active power limits of the generators and branch flow limits are not considered in the optimization models, as the active power dispatch is assumed to be determined in the day-ahead energy market prior to the day-ahead reactive power planning process.

4.3 Proposed Two-Stage Multi-Period Optimization Approach

The day-ahead hourly reactive power planning problem is inherently nonlinear and nonconvex, posing significant challenges for optimization. To address these challenges, a novel two-stage multi-period optimization approach is proposed. This approach aims to provide an effective solution by considering the time coupling due to operational constraints related to shunt equipment and transformer tap positions, thus improving the overall efficiency of the reactive power planning process. The proposed algorithm introduces a structured methodology for optimizing reactive power dispatch, ensuring better performance and reduced operational costs. In this section, the details of the two-stage algorithm are provided, including its objectives, constraints, and the underlying approach.

The flowchart of the algorithm is given in Figure 4.1. During the data preparation phase, the relevant network parameters are extracted from the system database to represent the network topology for the following day, as the algorithm is executed in a day-ahead framework. The bus admittance model is then constructed to accurately reflect the system's electrical characteristics. The active power generation dispatch is obtained from market-clearing results, while the demand profile is formulated based on the latest load forecast data. This phase establishes a comprehensive dataset that includes the overall system parameters, as well as the hourly active power generation and demand values, providing the necessary input for the optimization stages.

In this study, a two-stage multi-period optimization approach is employed to optimize the reactive power dispatch. In the first stage, the switch statuses of the shunt equipment are determined. Here, the switch statuses of shunt equipment and transformer tap settings are treated as continuous variables, allowing the problem to be

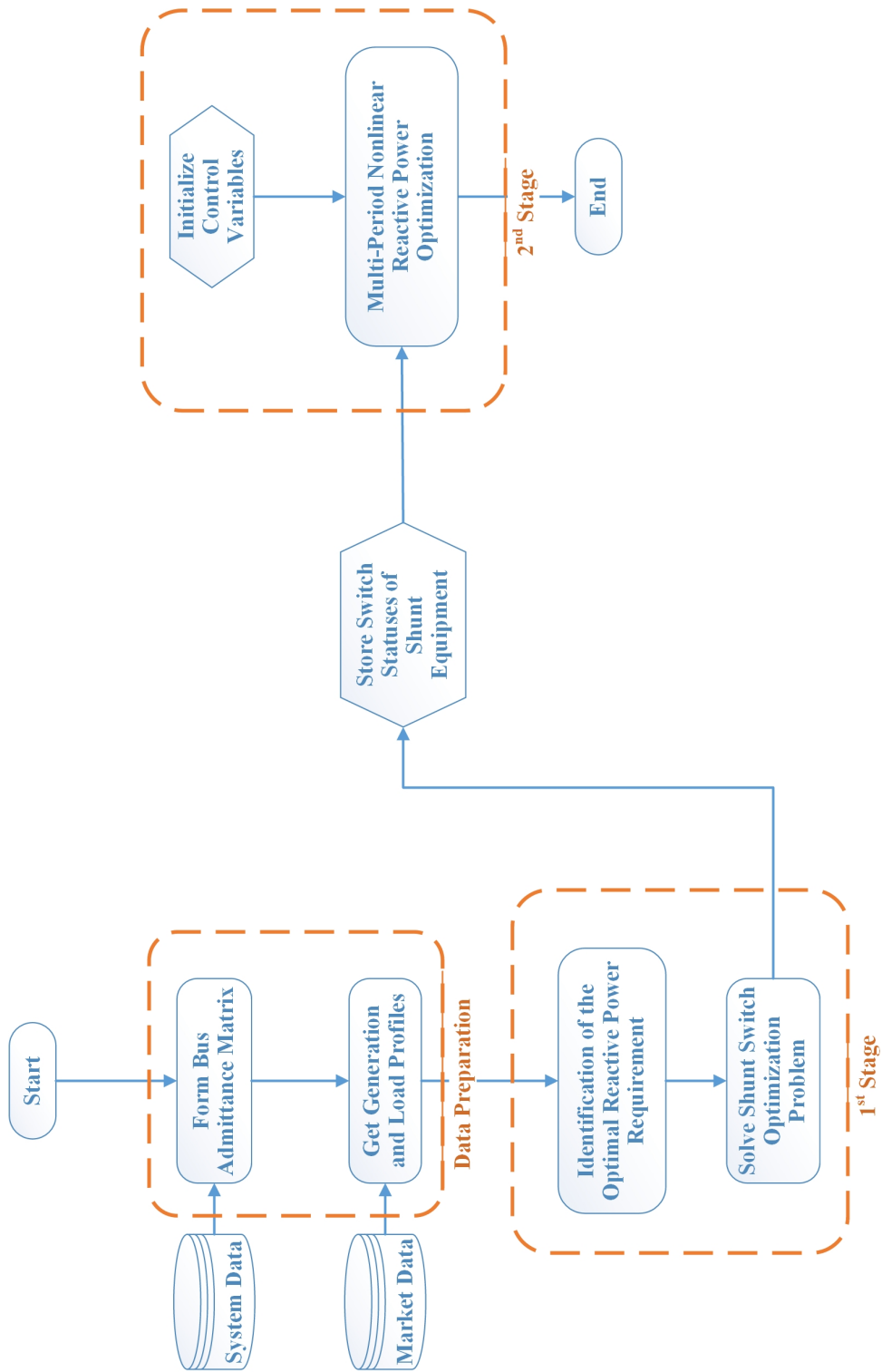


Figure 4.1: The flowchart of the proposed two-stage multi-period optimization approach

decomposed into single-period reactive optimization problems. For single-period optimization models, the transformer tap change and number of switching operations of the shunt equipment cannot be considered because they combine different time periods. The switch statuses of the shunt equipment were established based on the results of these single-period optimizations. In the second stage, a multi-period reactive power optimization problem is formed, where the switch statuses of the shunt equipment are fixed. In this stage, integer tap change variables are represented as continuous variables; however, additional quadratic constraints are implemented to ensure that these variables ultimately assume binary values.

4.3.1 First Stage Single-Period Optimization and Shunt Switch Optimization

The objective of the first stage of the algorithm is to decouple the integer decision variables associated with the switch statuses of shunt equipment from the main problem, allowing for a more straightforward and computationally efficient identification of these variables. To achieve this, the identification of the switch statuses of shunt equipment is carried out in two sequential steps as in Figure 4.2. In the first step, the problem is decomposed into separate subproblems for each time period. Operational constraints relating the inter-temporal dependencies are not considered in this step, since the only target is to determine the reactive power requirements for busbars with shunt equipment. The switch statuses will be determined according to these requirements with considering the operational constraints in the second step. Since the operational constraints relating the time coupling characteristics are not considered, it can be possible to decompose the multi-period optimization problem into subproblem for each time period.

The integer variables are relaxed to continuous variables within each single-period optimization problem. Following the solution of these subproblems, the optimal reactive power requirement for each time period and each busbar equipped with shunt devices is determined. These requirements represent the optimal reactive power injection at the corresponding busbar necessary to minimize transmission losses for that time period. In the second step, the shunt switch status optimization problem is formulated based on the identified reactive power requirements.

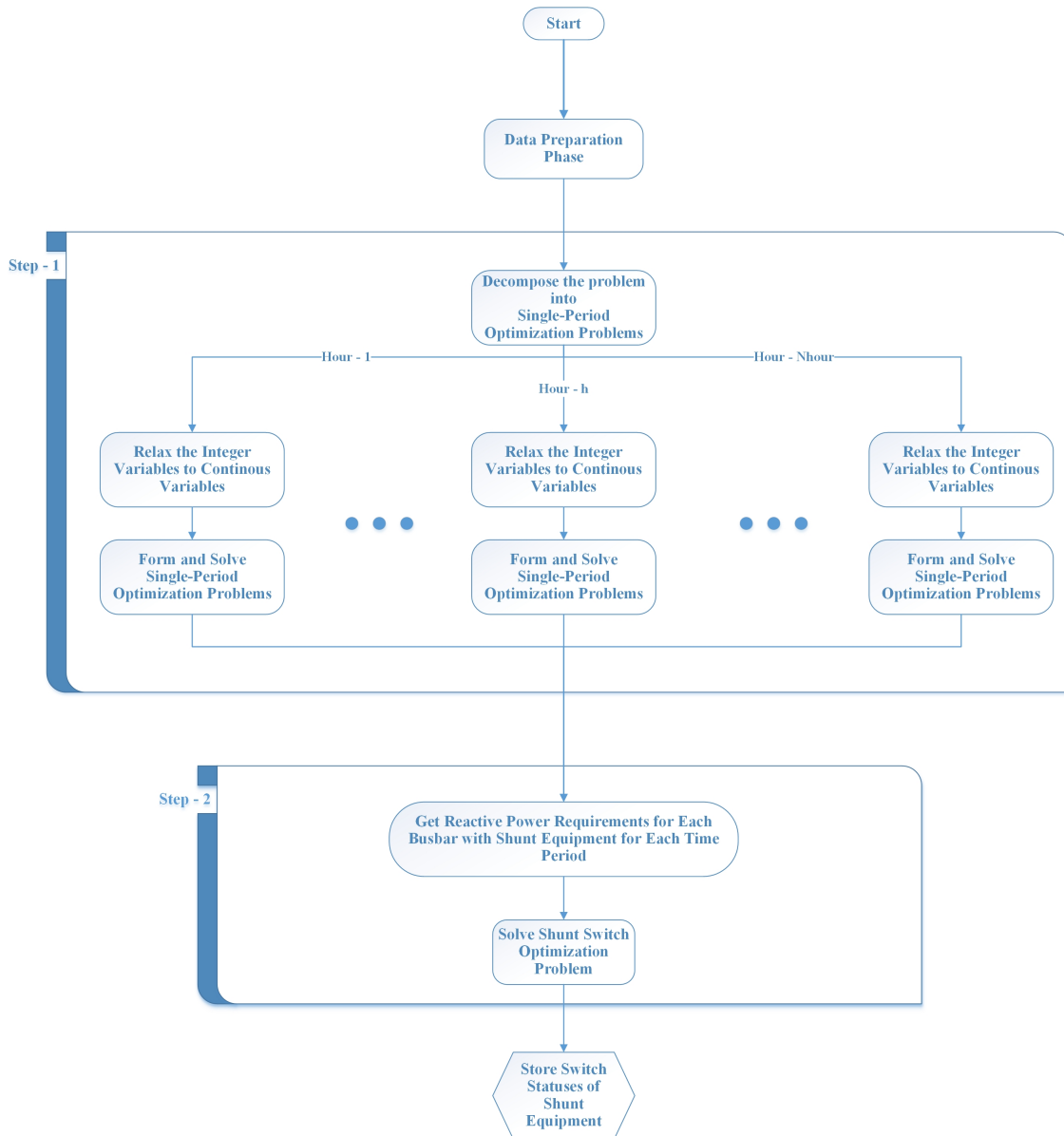


Figure 4.2: The flowchart of the 1st stage of the proposed two-stage multi-period approach

4.3.1.1 Identification of Optimal Reactive Power Requirements

Reactive power requirements serve as the basis for determining the switch statuses of shunt equipment. For busbars that have more than one controllable reactive power resource, including shunt equipment, the shunt equipment is switched on if the required reactive power cannot be supplied by the other reactive power resources. For busbars where shunt equipment is the only controllable reactive power resource, the shunt

equipment is switched on whenever there is a reactive power requirement. Therefore, before performing the shunt switch status optimization, the optimal reactive power requirements must first be determined.

Reactive power requirements are calculated based on the assumption that they are optimal when transmission losses are minimized. Accordingly, the optimal reactive power requirements are determined using a reactive power optimization formulation for each time period, where the objective function is the minimization of transmission losses. The objective function is defined as (4.4). The constraints are defined as active and reactive power balance constraints, reactive power generation limits for the generators and the voltage limits for the busbars which are defined as (2.12), (2.13), (2.15) and (2.16) respectively.

Active and reactive power injections calculated as (4.5), and (4.6) respectively.

$$P_{inj_i} = P_i^G - P_i^L \quad (4.5)$$

$$Q_{inj_i} = Q_i^G - Q_i^L + IS_i \cdot Q_i^R \quad (4.6)$$

For busbars with no generation, P_i^G and Q_i^G , are omitted from the equations (4.5) and (4.6).

For busbars with no shunt equipment, Q_i^R and IS_i are omitted from the equations (4.5) and (4.6).

For busbars with no loads, P_i^L and Q_i^L , are omitted from the equations (4.5) and (4.6).

Active power injections are all constants except the active power injection of slack busbar. Active power injection for the slack busbar is defined as variable to compensate the changes in transmission losses. Reactive power injections for only load connected busbars are constant. Reactive power injections for other busbars are variable.

The total reactive power injection of a shunt equipment is defined as (4.7). The reactive power injection is either zero or a non-zero value, $|V_k|^2 \cdot Q_k^R$. The switch statuses of shunt equipment are relaxed as continuous variables for the optimal re-

active power requirement process. Hence, the reactive power injection of a shunt equipment will take any value within the region $[0, |V_k|^2 \cdot Q_k^R]$. For this reason, the switch status of the shunt equipment are not included in the problem formulation of the single-period optimization problems in the first stage. A continuous variable, Q_k , with limits $[0, (|V_k|^{max})^2 \cdot Q_k^R]$ are defined for the reactive power injection of the shunt equipment.

$$Q_k = IS_k \cdot |V_k|^2 \cdot Q_k^R \quad (4.7)$$

The single period reactive optimization problems in the first stage of the algorithm are defined for all time periods, $\forall h \in \{1, 2, \dots, N_{hour}\}$, and can be summarized as in from (4.8) to (4.14).

$$\min P_{loss}(h) \quad (4.8)$$

such that

$$Pin_{j_i}(h) = |V_i(h)| \sum_{j=1}^{N_{busbar}} |V_j(h)| \cdot (G_{ij}(h) \cos(\theta_i(h) - \theta_j(h)) + B_{ij}(h) \sin(\theta_i(h) - \theta_j(h))) \quad (4.9)$$

$$Qin_{j_i}(h) = |V_i(h)| \sum_{j=1}^{N_{busbar}} |V_j(h)| \cdot (G_{ij}(h) \sin(\theta_i(h) - \theta_j(h)) - B_{ij}(h) \cos(\theta_i(h) - \theta_j(h))) \quad (4.10)$$

$$Q_i(h)^G \geq \sum_{g \in \mathcal{G}_i} Q_g^{min} \quad (4.11)$$

$$Q_i(h)^G \leq \sum_{g \in \mathcal{G}_i} Q_g^{max}$$

$$|V_i(h)| \geq V_i^{min} \quad (4.12)$$

$$|V_i(h)| \leq V_i^{max}$$

where equations (4.9), (4.10), (4.11) and (4.12) are formed for all busbars, $\forall i \in \mathcal{N}$ and

$$Pin_{j_i} = P_i^G - P_i^L \quad (4.13)$$

$$Qin_{j_i}(h) = Q_i^G(h) - Q_i^L + IS_i(h) \cdot Q_i^R \quad (4.14)$$

4.3.1.2 Shunt Switch Optimization

The key contribution of the two-stage algorithm is the decomposition of the switch statuses of shunt equipment from the original problem, as these integer variables introduce significant complexity. The presence of these discrete decision variables increases the computational burden and decreases the convergence probability of the original nonlinear and nonconvex optimization problem. To address this, the proposed approach decouples the determination of switch statuses from the main problem, allowing the integer complexity to be handled independently.

The determination of the switch statuses of shunt equipment is formulated as an integer programming problem. The shunt switch optimization problem is defined as (4.15), (4.16) and (4.17).

$$\min \sum_{h=1}^{N_{hour}} |IS_k(h) \cdot Q_k^{nom} - Q_k(h)| \quad (4.15)$$

such that

$$\sum_{h=2}^{N_{hour}} ST_k(h) \leq N_{switch}^{max} \quad (4.16)$$

$$\sum_{i=0}^{T_{change}} ST_k(h+i) \leq 1 \quad (4.17)$$

The objective of this process, given in (4.15), is to determine the switch statuses of the shunt equipment such that the difference between the resulting reactive power injections and the assigned optimal reactive power requirements is minimized. Since shunt equipment provides discrete levels of reactive power support, the optimal configuration should ensure that the deviation between the actual and required reactive power injections remains as small as possible across all time periods.

The constraints of the optimization problem, presented in (4.16) and (4.17), ensure that the switching operations of shunt equipment remain within predefined operational limits. Equation (4.16) imposes a maximum allowable limit on the total number of shunt switching operations across the planning horizon, preventing excessive switching actions that could increase operational costs and introduce reliability con-

cerns. Equation (4.17) enforces a minimum time interval between consecutive switching operations for each shunt device, ensuring that frequent switching is avoided. This constraint is crucial for maintaining the stability and longevity of shunt equipment, as frequent transitions between operational states may lead to higher maintenance requirements and potential operational issues. By incorporating these constraints, the optimization framework balances the need for precise reactive power support while adhering to practical operational restrictions.

4.3.2 Second Stage Multi-Period Optimization

The control variables defined for the day-ahead reactive power planning problem consist of generator voltage setpoints, transformer tap positions, and the switch statuses of shunt equipment, as presented in Table 4.1. The switch statuses of shunt equipment are determined in the first stage of the algorithm and remain fixed in the second stage. The categories of variables in the second stage are given in Table 4.2. The active power injection at the slack busbar is defined as a state variable to account for variations in transmission losses, while the voltage angle of the slack busbar is treated as a control variable, serving as the reference angle for all busbars. The primary control variables in the second stage are the generator voltage setpoints and transformer tap positions.

Table 4.2: Variable categories in the 2nd stage of the proposed two-stage multi-period optimization approach

	$ V $	θ	P	Q	IS	TP
Slack Busbar	Control	Control	State	State	-	-
Generator	Control	State	Constant	State	-	-
Busbar						
Non-Generator Busbar	State	State	Constant	Constant	-	-
Shunt Equipment						
Shunt	-	-	-	State	Fixed	-
Transformer	-	-	-	-	-	Control

The optimization problem remains a multiperiod optimization problem with inherent nonlinear and nonconvex characteristics. The number of switching operations is handled in the first-stage shunt switch optimization; therefore, the objective function in the second stage consists of two independent objectives, integrated within a cost-based framework. The objective function is formulated as given in (4.18), total transmission losses for all time periods are calculated as in (4.19). The number of tap changes and tap change variable are defined as (4.20) and (4.21) respectively.

$$\min C_2^T = \pi_{loss} \cdot P_{loss}^T + \pi_{tc} \cdot n_{tc} \quad (4.18)$$

where

$$P_{loss}^T = \sum_{h=1}^{N_{hour}} \sum_{l=1}^{N_{line}} g_k (|V_{li}(h)|^2 + |V_{lj}(h)|^2 - 2 \cdot |V_{li}(h)| \cdot |V_{lj}(h)| \cdot \cos(\theta_{li}(h) - \theta_{lj}(h))) \quad (4.19)$$

$$n_{tc} = \sum_{h=2}^{N_{hour}} \sum_{t=1}^{N_{transformer}} TC_t(h) \quad (4.20)$$

$$TC_t(h) = \begin{cases} 1, & \text{if } T_t(h) \neq T_t(h-1) \\ 0, & \text{if } T_t(h) = T_t(h-1) \end{cases} \quad (4.21)$$

The active and reactive power balance equations (4.22) and (4.23) are defined for all time periods, $h \in \{1, 2, \dots, N_{hour}\}$, and for all busbars, $i \in \mathcal{N}$. The

$$P_{inj_i}(h) = |V_i(h)| \sum_{j=1}^{N_{busbar}} |V_j(h)| \cdot (G_{ij}(h) \cos(\theta_{ij}(h)) + B_{ij}(h) \sin(\theta_{ij}(h))) \quad (4.22)$$

$$Q_{inj_i}(h) = |V_i(h)| \sum_{j=1}^{N_{busbar}} |V_j(h)| \cdot (G_{ij}(h) \sin(\theta_{ij}(h)) - B_{ij}(h) \cos(\theta_{ij}(h))) \quad (4.23)$$

where

$$\theta_{ij}(h) = \theta_i(h) - \theta_j(h)$$

The real and imaginary parts of the diagonal entries corresponding to busbars connected to a tap-changing transformer are computed using equations (4.24), (4.25), (4.26), and (4.27). Similarly, the real and imaginary parts of the off-diagonal entries associated with these busbars are determined by equations (4.28) and (4.29). As can be seen from the equations (4.24) to (4.29), the diagonal entries corresponding to a busbar on the secondary side of a tap-changing transformer, as well as the off-diagonal entries associated with busbars connected to tap-changing transformers, vary with transformer tap positions. These entries are, therefore, considered variable. In contrast, all remaining entries of the bus admittance matrix remain constant.

$$G_{ii}(h) = g_{ij}^{tr} + \sum_k g_{ik} \quad (4.24)$$

$$B_{ii}(h) = b_{ij}^{tr} + \sum_k b_{ik} \quad (4.25)$$

$$G_{jj}(h) = t_{ij}(h)^2 \cdot g_{ij}^{tr} + \sum_k g_{jk} \quad (4.26)$$

$$B_{jj}(h) = t_{ij}(h)^2 \cdot b_{ij}^{tr} + \sum_k b_{jk} \quad (4.27)$$

$$G_{ij}(h) = -t_{ij}(h) \cdot g_{ij}^{tr} \quad (4.28)$$

$$B_{ij}(h) = -t_{ij}(h) \cdot b_{ij}^{tr} \quad (4.29)$$

The bus admittance matrix entries, G_{ij} and B_{ij} , in equations (4.22) and (4.23), are not entirely constant due to the influence of transformer tap positions. While most elements remain unchanged, specific entries are directly affected by tap position adjustments. Changes in tap positions modify the effective impedance and admittance values, leading to variations in certain entries of the bus admittance matrix.

The day-ahead reactive power optimization problem is a nonconvex and nonlinear optimization problem. In addition to these characteristics, its size is 24 times larger than that of an hourly reactive optimization problem, leading to an exponential increase in problem complexity.

The integer complexity due to the shunt switch statuses is handled in the first stage of the algorithm; however, integer variables still remain in the optimization problem, specifically transformer tap positions and tap change variables. Transformers

with on-load tap changers generally have a 1% to 1.25% change in the tap ratio per step. Therefore, transformer tap positions can be defined as continuous variables with very small practical loss of information. However, this approach cannot be applied to transformer tap change variables. Although the minimization of shunt equipment switching is not included in the objective function and transformer tap positions can be treated as continuous variables with negligible practical loss, transformer tap change variables, $TC_t(h)$, remain as integer variables.

In addition to the integer complexity due to the tap change variable, equation (4.21) is a nonlinear equation. An initial reformulation is applied to handle this nonlinearity. To represent the nonlinear tap change equation, five linear inequality constraints, defined as (4.30), (4.31), (4.32), (4.33), and (4.34), are introduced. In addition to the binary variable, $TC_t(h)$, the newly introduced variables, $\Delta T_t^+(h)$ and $\Delta T_t^-(h)$, are binary variables as well.

$$TC_t(h) = \Delta T_t^+(h) + \Delta T_t^-(h) \quad (4.30)$$

$$T_t(h) - T_t(h-1) \leq \epsilon + M \cdot \Delta T_t^+(h) \quad (4.31)$$

$$T_t(h) - T_t(h-1) \geq \epsilon - M \cdot (1 - \Delta T_t^+(h)) \quad (4.32)$$

$$T_t(h) - T_t(h-1) \leq M \cdot (1 - \Delta T_t^-(h)) - \epsilon \quad (4.33)$$

$$T_t(h) - T_t(h-1) \geq -M \cdot \Delta T_t^-(h) - \epsilon \quad (4.34)$$

In these constraints, ϵ is introduced as a small positive constant to ensure numerical stability and enforce the condition that $\Delta T_t^+(h)$ and $\Delta T_t^-(h)$ is equal to zero when there is no change in the transformer tap position. This prevents unintended small deviations due to numerical errors and ensures that the model accurately represents the tap-changing action. Additionally, the parameter M is defined as a sufficiently large positive constant to guarantee that the constraints hold for all feasible values of $T_t(h)$. The selection of M is crucial, as choosing an excessively large value may lead to numerical instability, while a value that is too small may restrict feasible solutions. Hence, M is determined based on the known bounds of $T_t(h)$, ensuring that it is both sufficiently large and computationally efficient.

With the introduction of these constraints, new integer variables emerge in the formulation. The presence of these integer variables transforms the problem into a Mixed-

Integer Nonlinear Programming problem with nonconvex constraints. As a result, conventional continuous optimization techniques, such as the interior point method which is one of the most commonly used algorithms for solving large-scale nonlinear and nonconvex optimization problems, cannot be directly applied to solve this problem efficiently.

To address this challenge, the problem is reformulated in a way that eliminates the integer variables while preserving the essential characteristics of the transformer tap-changing actions. Specifically, in the second stage of the problem, transformer tap positions are treated as continuous variables with very small practical loss of information. Although $\Delta T_t^+(h)$ and $\Delta T_t^-(h)$ are originally binary variables, they are defined as continuous variables in the reformulation. To ensure that these variables represent the binary nature, auxiliary variables $\tilde{T}_t^+(h)$ and $\tilde{T}_t^-(h)$ are introduced, along with additional quadratic constraints. These constraints enforce that $\Delta T_t^+(h)$ and $\Delta T_t^-(h)$ can only take values of 0 or 1, thereby preserving the logical integrity of the tap-changing mechanism while maintaining a continuous optimization framework.

The equation (4.36) forces the variable $\tilde{T}_t^+(h)$ to be equal to -1 or 1. Similarly, the equation (4.38) forces the variable $\tilde{T}_t^-(h)$ to take the values -1 or 1. Then, the equations (4.35) and (4.37) transform -1 into 0 and 1 into 1. Hence, these newly introduced auxiliary variables and quadratic constraints guarantee that the variables $\Delta T_t^+(h)$ and $\Delta T_t^-(h)$ take only binary values.

$$\Delta T_t^+(h) = \frac{\tilde{T}_t^+(h) + 1}{2} \quad (4.35)$$

$$\tilde{T}_t^+(h)^2 = 1 \quad (4.36)$$

$$\Delta T_t^-(h) = \frac{\tilde{T}_t^-(h) + 1}{2} \quad (4.37)$$

$$\tilde{T}_t^-(h)^2 = 1 \quad (4.38)$$

The solution of the formulated nonlinear optimization problem is obtained using Artelys Knitro, which employs the interior point algorithm. The interior point method is one of the most widely used approaches for solving large-scale nonlinear and nonconvex optimization problems. Interior point algorithms traverse the interior of the

feasible region by iteratively improving a path that leads to the optimal solution. This method is particularly effective for handling inequality constraints, making it well-suited for nonlinear programming problems where the feasible set is defined by complex nonlinear constraints.

The interior point method introduces barrier functions to incorporate inequality constraints into the objective function. These barrier functions penalize solutions that approach the boundary of the feasible region, thereby ensuring that the state variables remain in feasible region throughout the iterations. The barrier parameter is progressively reduced, allowing the solution to converge toward the optimal point while maintaining numerical stability. The method relies on solving a series of Karush-Kuhn-Tucker (KKT) conditions, which are reformulated as a system of nonlinear equations. These equations are efficiently solved using Newton's method, ensuring rapid convergence, particularly for problems with a large number of variables and constraints.

To apply the interior point method using Artelys Knitro, in addition to the problem formulation, the gradient of the objective function and the Jacobian matrices of the constraints must be explicitly modeled. Given a general nonlinear optimization problem of the form (2.1), the gradient of the objective function is given by the equations (4.39), (4.40) and (4.41).

$$\nabla f(\mathbf{x}, \mathbf{u}) = \left[\nabla_x f(\mathbf{x}, \mathbf{u}) \quad \nabla_u f(\mathbf{x}, \mathbf{u}) \right]^T. \quad (4.39)$$

where

$$\nabla_x f(\mathbf{x}, \mathbf{u}) = \left[\frac{\partial f}{\partial x_1} \quad \frac{\partial f}{\partial x_2} \quad \dots \quad \frac{\partial f}{\partial x_n} \right]^T. \quad (4.40)$$

$$\nabla_u f(\mathbf{x}, \mathbf{u}) = \left[\frac{\partial f}{\partial u_1} \quad \frac{\partial f}{\partial u_2} \quad \dots \quad \frac{\partial f}{\partial u_n} \right]^T. \quad (4.41)$$

Similarly, the Jacobian matrix of the constraint functions is defined as

$$J_g(\mathbf{x}, \mathbf{u}) = \begin{bmatrix} \frac{\partial g_1}{\partial x_1} & \frac{\partial g_1}{\partial u_1} & \dots & \frac{\partial g_1}{\partial x_n} & \frac{\partial g_1}{\partial u_m} \\ \frac{\partial g_2}{\partial x_1} & \frac{\partial g_2}{\partial u_1} & \dots & \frac{\partial g_2}{\partial x_n} & \frac{\partial g_2}{\partial u_m} \\ \vdots & \vdots & \ddots & \vdots & \vdots \\ \frac{\partial g_m}{\partial x_1} & \frac{\partial g_m}{\partial u_1} & \dots & \frac{\partial g_m}{\partial x_n} & \frac{\partial g_m}{\partial u_m} \end{bmatrix}, \quad (4.42)$$

where $g_i(\mathbf{x}, \mathbf{u})$ are the equality constraint functions. Similarly, for the inequality constraints $h_j(\mathbf{x}, \mathbf{u})$, the Jacobian matrix is defined as:

$$J_h(\mathbf{x}, \mathbf{u}) = \begin{bmatrix} \frac{\partial h_1}{\partial x_1} & \frac{\partial h_1}{\partial u_1} & \cdots & \frac{\partial h_1}{\partial x_n} & \frac{\partial h_1}{\partial u_m} \\ \frac{\partial h_2}{\partial x_1} & \frac{\partial h_2}{\partial u_1} & \cdots & \frac{\partial h_2}{\partial x_n} & \frac{\partial h_2}{\partial u_m} \\ \vdots & \vdots & \ddots & \vdots & \vdots \\ \frac{\partial h_p}{\partial x_1} & \frac{\partial h_p}{\partial u_1} & \cdots & \frac{\partial h_p}{\partial x_n} & \frac{\partial h_p}{\partial u_m} \end{bmatrix}. \quad (4.43)$$

The Jacobian matrices $J_g(\mathbf{x}, \mathbf{u})$ and $J_h(\mathbf{x}, \mathbf{u})$ contain the first-order partial derivatives of the inequality and equality constraint functions with respect to the decision variables \mathbf{x} and \mathbf{u} . These matrices are essential for efficiently solving the optimization problem using the interior point algorithm, as they provide the necessary information to update the search direction at each iteration.

The Artelys Knitro solver automatically calculates the Hessian matrix based on the given problem formulation for the objective function, constraints, and the corresponding gradient and Jacobian functions. Therefore, there is no need to explicitly formulate the Hessian matrix, as Knitro internally handles its computation, ensuring a more efficient solution process.

CHAPTER 5

SIMULATION AND RESULTS

The main objective of day-ahead reactive power planning is to determine the optimal hourly reactive dispatch of various reactive power resources. The proposed algorithm aims to determine the voltage setpoints for generators, the switch statuses of shunt equipment, and transformer tap positions within the day-ahead reactive power planning process. To demonstrate the contributions of the proposed algorithm, a test system is required. This test system must include the fundamental network elements of large-scale electrical grids while also being minimal in size for implementation purposes. The IEEE 118-bus test system meets both requirements effectively, allowing for fast implementation while representing the key characteristics of a large-scale network.

To simulate inter-temporal dependencies, a 24-hour generation and load dataset is constructed based on typical load and generation profiles of the Turkish power system. This dataset reflects the hourly variations in demand and generation over a daily cycle. By incorporating actual fluctuations in power consumption and generation availability, the constructed dataset ensures that the simulation framework accurately represents practical operating conditions.

Simulation studies are conducted based on two distinct scenarios, each representing different loading and dispatch conditions. These scenarios are designed to analyze the impact of variable system states on reactive power optimization and to assess the robustness of the proposed approach under different operating conditions.

5.1 IEEE 118 Bus Test System and Loading Scenarios

For power system optimization problems, IEEE test systems are commonly used. The IEEE 118-bus test system is selected for its fast implementation and adequate representation of large-scale networks [52]. This model includes 118 busbars, 54 generators, and 170 transmission lines, providing a detailed framework for evaluating the proposed algorithm for day-ahead reactive power optimization. The system operates at two voltage levels, 138 kV and 345 kV, which represent the high-voltage grids of most large-scale networks. These voltage levels are interconnected by 9 transformers. To provide additional reactive power support, 12 shunt capacitors and 2 shunt reactors are connected at the 138 kV voltage level. The number of key network components for reactive power optimization are given in Table 5.1 and the rated reactive powers of shunt equipment in the model are given in Table 5.2.

Table 5.1: Key network components in the IEEE 118 Bus test system

Component	Quantity
Tap-Changing Transformers	9
Shunt Capacitors	12
Shunt Reactors	2

As can be seen in the Table 5.2, majority of the shunt equipment are the shunt capacitors. There are only two shunt reactors in the test system. Generally, shunt capacitors are utilized when low voltage levels occurred in the system to increase the voltage magnitudes locally. Shunt reactors, on the other hand, used to decrease the voltage magnitudes in case of overvoltages.

To demonstrate the effect of time dependencies, a 24-hour load and generation profile is required. Simulations are conducted for two different load scenarios, each representing typical operating conditions of the Turkish power system in winter and summer seasons. Each scenario is constructed based on a typical day from the respective season. The hourly load variations are derived from the selected days' actual demand patterns. To ensure consistency, the daily load profiles are normalized with

Table 5.2: Rated reactive power of shunt equipment in the IEEE 118 Bus test system

Bus ID	Type	Qrated (MVAR)	Bus ID	Type	Qrated (MVAR)
5	Reactor	40	74	Capacitor	12
34	Capacitor	14	79	Capacitor	20
37	Reactor	25	82	Capacitor	20
44	Capacitor	10	83	Capacitor	10
45	Capacitor	10	105	Capacitor	20
46	Capacitor	10	107	Capacitor	6
48	Capacitor	15	110	Capacitor	6

respect to their peak values and then scaled to match the IEEE 118-bus test system’s peak demand. For the summer scenario, the peak demand of the IEEE 118-bus test system is set to 4609 MW, whereas for the winter scenario, it is set to 4242 MW. The peak demand values for both scenarios are provided in Table 5.3.

Table 5.3: Simulation Scenarios

Scenario	Season	Renewable Generation	Total Daily Maximum Load (MW)
Scenario 1	Winter	Low	4242
Scenario 2	Summer	High	4609

In Scenario 1, which represents a typical winter day, renewable generation, especially solar generation, is significantly lower. As a result, the load profile exhibits a steady increase in the morning hours, reaching its peak demand of 4,242 MW at 14:00, as shown in Figure 5.1. Following the peak, the demand gradually declines in the late afternoon and evening hours. Unlike in summer, there is no substantial mid-day reduction in demand, as solar generation is minimal. This trend highlights the higher dependency on conventional generation sources during winter season.

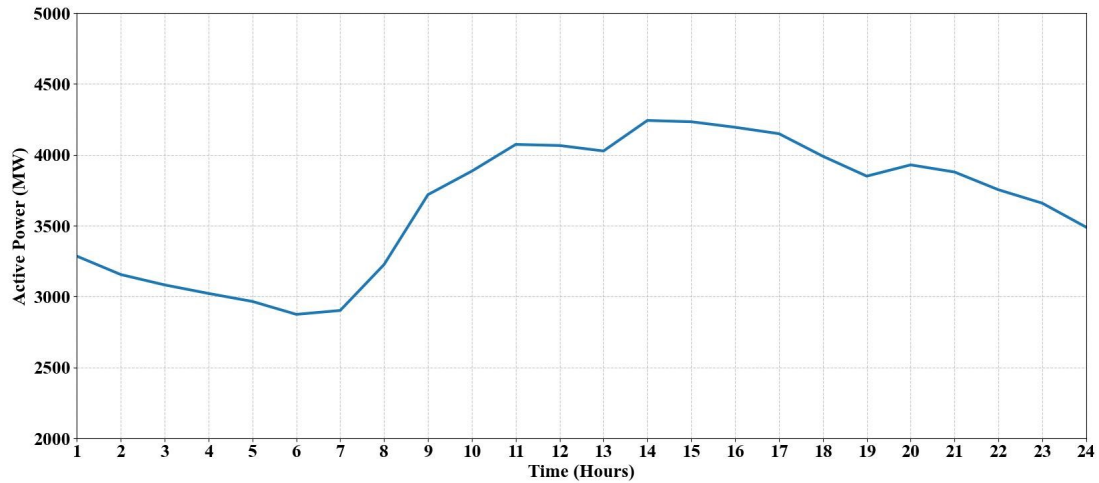


Figure 5.1: Load Profile of Scenario 1

In Scenario 2, a typical summer day is considered as a reference day. Due to higher solar generation, the load profile exhibits a distinct mid-day reduction, as shown in Figure 5.2. In the morning hours, the demand gradually increases until noon, after which it starts to decline due to the contribution of distributed solar generation. This mid-day dip is a key characteristic of summer load profiles, where solar power offsets a portion of the demand. However, as solar generation decreases in the late afternoon, the demand rises again, reaching its peak at 21:00 with a value of 4,609 MW.

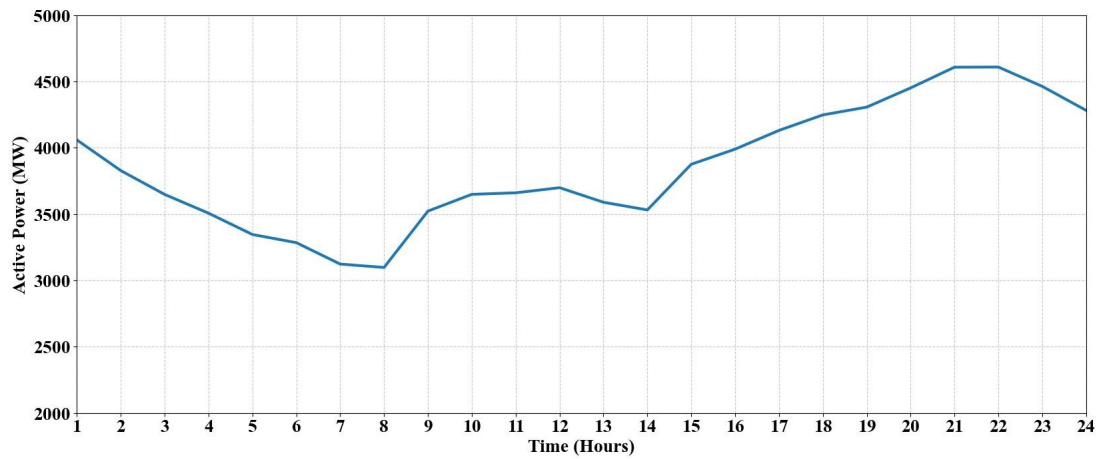


Figure 5.2: Load Profile of Scenario 2

The defined load and generation scenarios establish a comprehensive framework for evaluating the effect of different optimization approaches in day-ahead reactive power planning. By considering seasonal variations and their impact on system demand, the simulations enable a detailed assessment of reactive power dispatch under diverse operating conditions. The following sections present a comparative analysis of the Conventional Single-Period Optimization Approach and the Proposed Two-Stage Multi-Period Optimization Approach, focusing on their effectiveness in optimizing reactive power resources while ensuring system stability and operational efficiency.

5.2 Energy, Operational and Risk Costs

In energy markets, the market is cleared by matching bid prices and quantities between sellers, including generation companies, and buyers, such as individual consumers and electricity retail companies. In addition to the electricity purchased by consumers and retail companies, additional generation is required to compensate for transmission system losses, leading to a total generation amount exceeding the market volume. The treatment and pricing of these transmission losses vary across different countries and are incorporated into electricity markets through various mechanisms. In the Turkish electricity market, transmission system losses are procured by the transmission system operator (TSO) through electricity markets [53]. Accordingly, the day-ahead market prices have been used for the valuation of transmission system losses. Figure 5.3 shows the day-ahead market prices throughout 2024 in \$/MWh. The volume-weighted average electricity price in the day-ahead market for 2024 is approximately \$69/MWh [54].

Transformer tap changers are essential for regulating voltage by modifying the transformation ratio to maintain system voltages within acceptable limits. However, transmission system operators are generally conservative regarding tap-changing operations, as frequent adjustments increase operational costs due to mechanical degradation and power losses. Each tap change introduces an energy cost associated with the losses, as well as a maintenance cost due to component degradation over time. In the Conventional Single-Period Optimization Approach, tap changes are typically minimized to avoid excessive operational expenses. However, when operational and risk

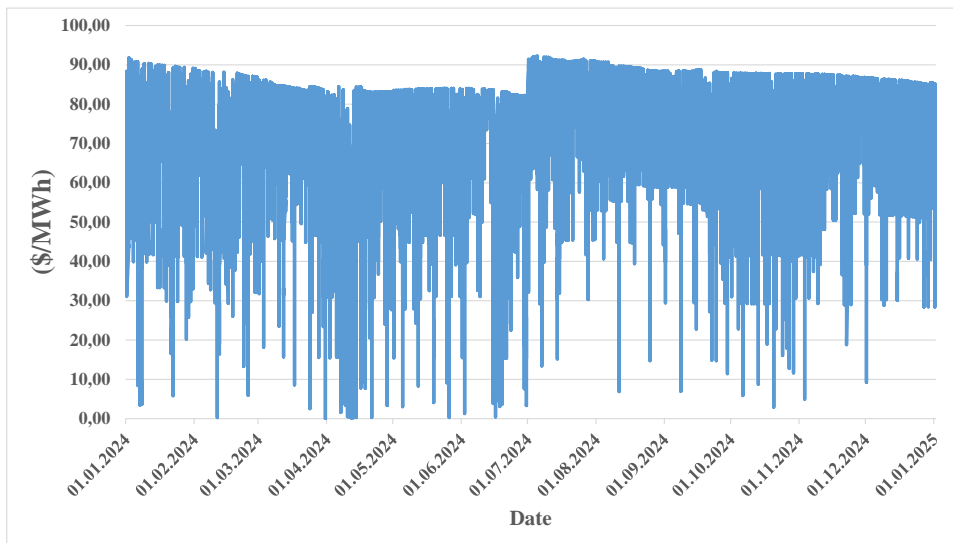


Figure 5.3: Day-ahead market energy prices - 2024[54]

costs are explicitly considered in the optimization framework, the optimal dispatch strategy may indicate a higher number of tap-changing operations, suggesting a potential trade-off between minimizing tap movements and achieving improved voltage control.

In addition to direct operational costs, excessive tap-changing operations introduce reliability concerns, contributing to risk costs. Frequent mechanical movements accelerate the aging of tap changers, increasing the likelihood of failures and necessitating unplanned maintenance. Transmission system operators often prefer to limit tap changes to reduce these risks and maintain long-term asset reliability. However, when an optimization approach explicitly accounts for operational and risk costs, it may suggest a different strategy, where a more proactive use of tap changers could enhance overall system performance. This indicates that a careful balance must be established between the long-term reliability of transformer assets and the potential benefits of a more flexible tap-changing strategy in voltage control.

Transformer tap changers are essential for regulating voltage by modifying the transformation ratio to maintain system voltages within acceptable limits. However, the operational costs associated with tap-changing operations must be carefully evaluated. These costs include maintenance and material expenses, energy costs due to transition losses, and risk costs related to mechanical wear and failure probabilities.

The operational costs of on-load tap-changing (OLTC) transformers primarily consist of maintenance and material expenses, which are necessary to ensure the long-term reliability of these critical components in power systems. The mechanical nature of tap changers leads to wear and tear over time, requiring periodic maintenance and part replacements to sustain proper functionality. For OLTC autotransformers used in large-scale power networks, the combined maintenance and material costs are assumed to be \$5,500 per year. This value reflects industry estimates for scheduled servicing, component replacements, and general maintenance, ensuring that tap changers operate efficiently while minimizing unexpected failures due to mechanical degradation. A breakdown of these costs is presented in Table 5.4.

Table 5.4: Annual maintenance and material costs for OLTC transformers

Cost Component	Annual Cost (\$)
Scheduled Maintenance	3,000
Component Replacement	2,000
General Upkeep	500
Total Annual Cost	5,500

In addition to maintenance and material costs, tap-changing operations introduce additional energy losses, contributing to overall operational expenses. When a tap change occurs, transient losses arise due to variations in impedance and circulating currents, leading to minor but cumulative energy dissipation. The energy cost associated with these losses is assumed to be \$0.069 per tap change, as shown in Table 5.5. While this cost per individual operation is relatively small, frequent tap-changing events across multiple transformers in a large-scale system can result in a significant cumulative expense. Therefore, accurately accounting for these energy losses is essential for comprehensive operational cost assessments.

Table 5.5: Energy costs per tap change

Parameter	Value
Energy Loss per Tap Change (MWh)	0.001
Energy Price (\$/MWh)	69
Energy Cost per Tap Change (\$)	0.069

To determine the operational cost per tap change, the expected number of yearly tap-changing operations must be considered. In practical power system operations, each transformer typically undergoes a maximum of three or four tap changes per day. This results in approximately 1,000 tap-changing operations in average annually. By distributing the yearly maintenance, material, and energy costs across these operations, the operational cost per tap change is calculated as approximately \$5.569, as summarized in Table 5.6.

Table 5.6: Calculation of operational cost per tap change

Parameter	Value
Annual Maintenance and Material Cost (\$)	5,500
Annual Number of Tap Changes	1,000
Energy Cost per Tap Change (\$)	0.069
Operational Cost per Tap Change (\$)	5.569

Beyond direct operational expenses, the risk costs associated with transformer tap changers must also be considered. Frequent tap-changing operations accelerate the mechanical aging of components, increasing the probability of failure and the need for unplanned maintenance. The cost of a failure event for an OLTC transformer is assumed to be approximately \$500,000, reflecting expenses related to repairs, replacements, and potential system disruptions. Given an estimated failure probability of 1% per year, the expected annual risk cost is calculated as \$5,000. When distributed over an estimated 1,000 tap-changing operations per year, the risk cost per tap change amounts to approximately \$5. The breakdown of risk costs is presented in Table 5.7.

Table 5.7: Calculation of risk cost per tap change

Parameter	Value
Failure Cost (\$)	500,000
Failure Probability per Year (%)	1
Estimated Annual Tap Changes	1,000
Risk Cost per Year (\$)	5,000
Risk Cost per Tap Change (\$)	5.00

By combining both operational and risk costs, the total cost per tap change is determined to be \$10.569, as summarized in Table 5.8. This value highlights the economic impact of each tap adjustment and the importance of optimizing tap-changing operations in reactive power planning.

Table 5.8: Total cost per tap change

Cost Component	Cost per Tap Change (\$)
Operational Cost	5.58
Risk Cost	5.00
Total Cost per Tap Change	10.58

5.3 Conventional Single-Period Optimization Approach Results

The Conventional Single-Period Model is based on the conventional day-ahead hourly reactive power planning performed by transmission system operators (TSOs). With the clearing of day-ahead energy market, active power dispatch has been determined unless a congestion occurs in the transmission network. Transmission system operators are required to determine reactive power dispatch after the energy market clearing on a day-ahead basis.

The fundamental tool for solving the day-ahead reactive power planning problem available to transmission system operators is the optimal power flow formulation. Transmission system operators obtain OPF solutions using industrial OPF solvers.

These solvers efficiently compute optimal power flow solutions; however, they are limited to single-period optimization. As previously mentioned, the day-ahead reactive power planning problem involves inter-temporal dependencies due to the switch statuses of shunt equipment and transformer tap changes. Since industrial OPF solvers are not designed for multi-period optimization problems, they cannot be directly utilized for this purpose.

For this reason, transmission system operators determine the switch statuses of shunt equipment and transformer tap positions during a pre-optimization process. In this stage, they rely on historical data and operator experience to set these variables before the optimization process. The maximum allowable switching operations and tap changes are also taken into account in this pre-optimization step. Once these variables are determined, single-period optimization problems are solved with the predefined switch statuses and tap positions. The solutions of these single-period optimization problems yield the final reactive power dispatch across the grid.

In this study, conventional single-period optimization approach is utilized to compare the results of the proposed two-stage multi-period optimization approach with the conventional approach.

The conventional single-period optimization approach exploits the historical data that a transmission system operator has. However, there are not any historical voltage profiles for IEEE 118 bus test system. In this study, historical voltage profile is constructed using power flow solutions for the test system and load and generation profiles. The switch statuses of the shunt equipment and transformer tap positions are determined according to the power flow results.

5.3.1 Scenario 1

Power flow calculations were performed to determine the shunt switch statuses of the shunt equipment and transformer tap positions. The fast decoupled Newton-Raphson algorithm was implemented in Java to perform these power-flow calculations. The voltage profiles for each busbar are calculated using power flow calculations. The voltages of the busbars with the shunt equipment are shown in Figure 5.4.

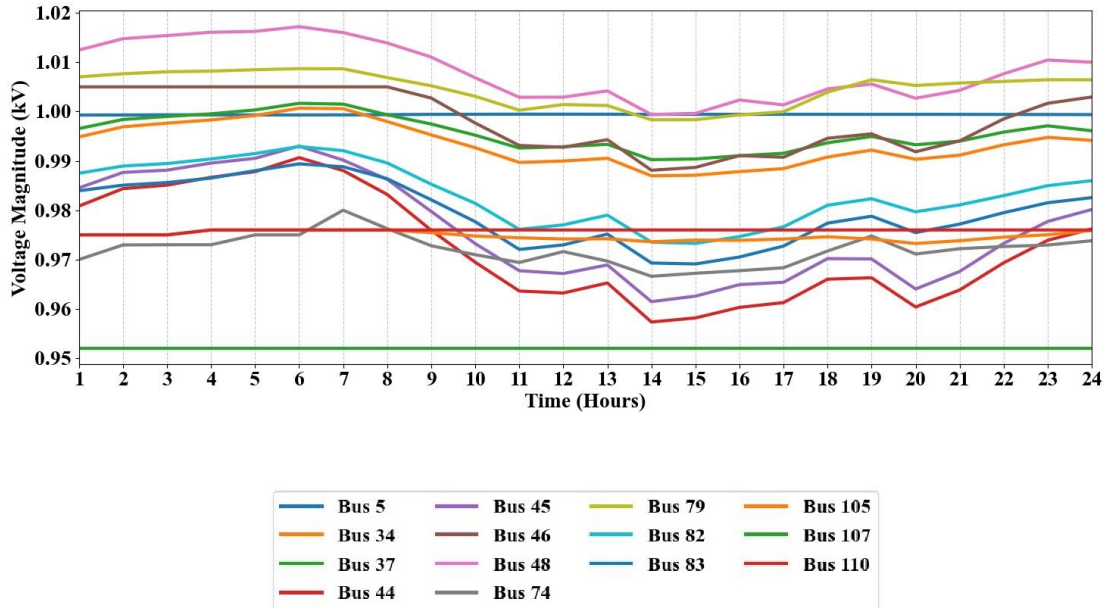


Figure 5.4: Voltage profile of busbars with shunt equipment obtained via power flow calculations - Scenario 1

As can be seen in Figure 5.4, the voltage magnitudes of the busbars are lower during peak hours. With the increased load demand, the voltage drop in the transmission lines increases owing to increased loading. Shunt capacitors are used for hours with lower voltage magnitudes to improve the voltage profiles for these hours. There are four shunt capacitors, and the voltage magnitudes of the busbars connected to these shunt capacitors do not fall below 0.99 p.u.; hence, these shunt capacitors are not taken into service during the day. On the other hand, there are four shunt capacitors and one shunt reactor in which the voltage magnitudes of the busbars connected to these shunt equipment are always close to 0.95 p.u.; hence, the shunt reactor is not in service, whereas the shunt capacitors are in service throughout the day. The switch statuses of these nonvarying shunt equipment are listed in Table 5.9. The hourly switch status of the remaining shunt equipment is listed in Table 5.10.

Table 5.9: Non-varying switch statuses of shunt equipment for 24 hours - Scenario 1

Switch Status		Switch Status	
Reactor 5	0	Capacitor 79	0
Capacitor 34	0	Capacitor 105	1
Capacitor 46	0	Capacitor 107	1
Capacitor 48	0	Capacitor 110	1
Capacitor 74	1		

Table 5.10: Varying switch statuses of shunt equipment for 24 hours - Scenario 1

	Reactor 37	Capacitor 44	Capacitor 45	Capacitor 82	Capacitor 83
H1	0	0	0	0	0
H2	0	0	0	0	0
H3	1	0	0	0	0
H4	1	0	0	0	0
H5	1	0	0	0	0
H6	1	0	0	0	0
H7	1	0	0	0	0
H8	0	0	0	0	0
H9	0	0	0	0	0
H10	0	1	1	0	1
H11	0	1	1	1	1
H12	0	1	1	1	1
H13	0	1	1	1	1
H14	0	1	1	1	1
H15	0	1	1	1	1
H16	0	1	1	1	1
H17	0	1	1	1	1
H18	0	1	1	1	1
H19	0	1	1	1	1

Table 5.10 – continued from previous page

	Reactor	Capacitor	Capacitor	Capacitor	Capacitor
	37	44	45	82	83
H20	0	1	1	1	1
H21	0	1	1	0	1
H22	0	1	1	0	1
H23	0	1	1	0	0
H24	0	0	0	0	0

The shunt reactor at Bus 37 is in service only for 5 hours during the morning hours when the voltage profiles are higher, whereas the other shunt capacitors are in service after the morning hours when the voltage magnitudes are lower. The voltage profiles corresponding to the shunt equipment with varying switch statuses are strongly correlated with the loading profile, as shown in Figure 5.1 and Figure 5.4. In conclusion, nine shunt equipment do not experience any switch operation during the day, whereas there are a total of ten switch operations for five shunt equipment.

Similarly, the transformer tap positions were determined according to the voltages of the busbars connected to the transformers. The voltages of the busbars connected to the transformers are presented in Figure 5.5.

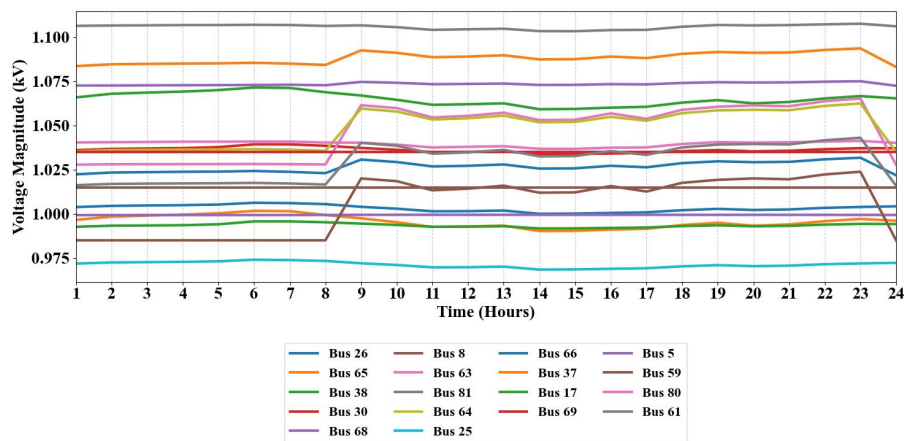


Figure 5.5: Voltage profile of busbars connected with transformers obtained via power flow calculations - Scenario 1

The transformer tap positions of the eight transformers are changed from their initial values used in power flow calculations, but they remain unchanged throughout the day. The nonvarying transformer tap positions are listed in Table 5.11.

Table 5.11: Non-varying transformer tap ratios for 24 hours - Scenario 1

Tap Ratio		Tap Ratio	
Tr. 8-5	1.0	Tr. 64-61	0.985
Tr. 26-25	0.97	Tr. 65-66	0.935
Tr. 30-17	1.0	Tr. 68-69	0.935
Tr. 38-37	1.0	Tr. 81-80	0.935

On the other hand, due to the high variations in the hourly voltage magnitudes of Bus 64 and Bus 61, the tap position of the transformer between Bus 64 and Bus 61 varies, as shown in Table 5.12.

Table 5.12: Transformer tap ratios of the Transformer 64-61 - Scenario 1

Tap Ratio		Tap Ratio		Tap Ratio	
H1	0.98	H9	1.04	H17	1.04
H2	0.98	H10	1.04	H18	1.04
H3	0.98	H11	1.04	H19	1.04
H4	0.98	H12	1.04	H20	1.04
H5	0.98	H13	1.04	H21	1.04
H6	0.98	H14	1.04	H22	1.04
H7	0.98	H15	1.04	H23	0.98
H8	0.98	H16	1.04	H24	0.98

With these fixed shunt switch statuses of the shunt equipment and transformer tap positions, single-period reactive power optimization problems are formulated. The Artelys Knitro nonlinear solver was used to solve single-period reactive power optimization problems. The resulting voltage profile for Scenario 1 is shown in Figure 5.6.

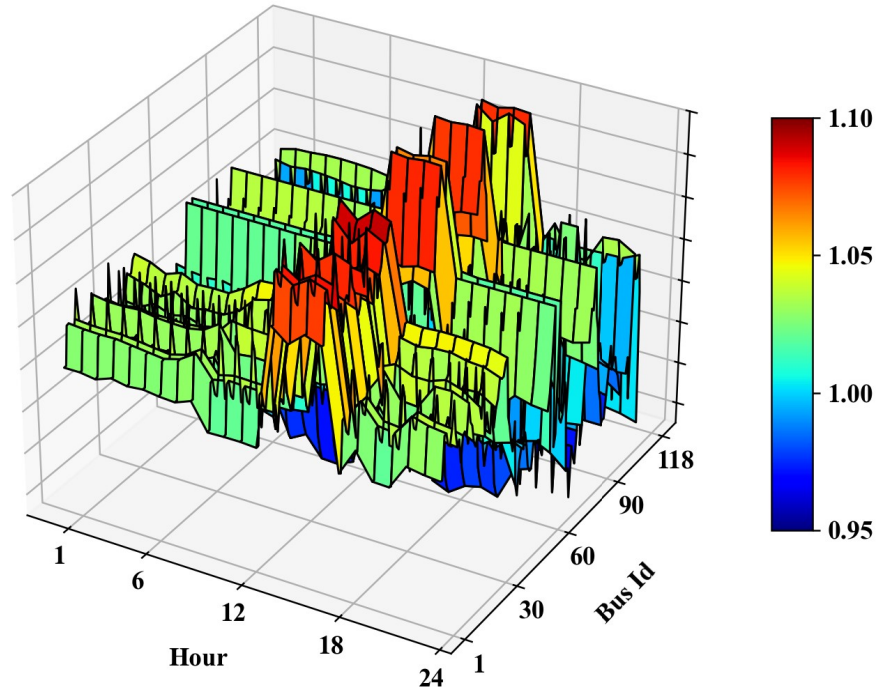


Figure 5.6: Resulting hourly voltage profiles of conventional single-period optimization approach - Scenario 1

Single-period optimization problems with predetermined switch statuses of shunt equipment and transformer tap positions do not converge with voltage limits, [0.95 - 1.05] p.u. for all time periods; hence, the voltage limits are relaxed to [0.9–1.1] p.u. for time periods from 14:00 to 17:00. The voltage magnitudes in these time periods were higher than those in other time periods.

The hourly and cumulative losses for the conventional single-period optimization approach for Scenario 1 are shown in Figure 5.7. The minimum loss occurs at 06:00, reaching 62 MW when the load is at its lowest level. On the other hand, the maximum loss occurs at 11:00, reaching 134 MW, even though the load peaks at 14:00. In general, higher demand results in higher hourly losses, as increased demand leads to greater transmission losses. However, the transmission losses from 14:00 to 17:00 do not increase despite the rising demand, as the voltage limits are relaxed during these periods.

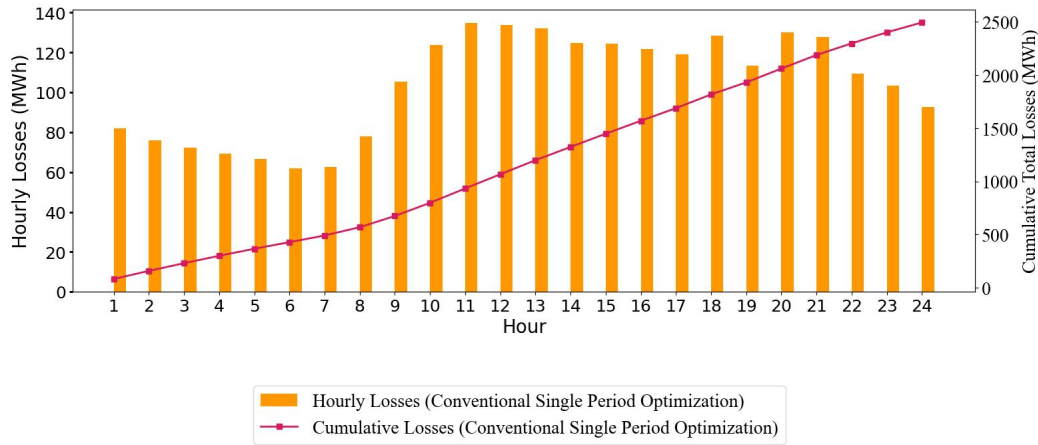


Figure 5.7: Hourly and cumulative losses for conventional single-period optimization approach - Scenario 1

As seen in Figure 5.7 and Figure 5.1, the hourly losses and load demand directly correlated, the average hourly loss is 104 MW and total daily loss is 2494 MWh. Given the energy price as 69\$/MWh, total daily energy cost for transmission losses is \$172,086. As shown in Table 5.12, total number of tap changes is two for all of the transformers, and with the assumed total cost per tap changes is \$10.58, the total operational and risk cost related with transformer tap changes is \$21.16 in scenario 1 for conventional single-period optimization approach.

5.3.2 Scenario 2

As a result of power flow calculations which performed to determine the shunt switch statuses of the shunt equipment and transformer tap positions in Scenario 2, the voltages of the busbars with the shunt equipment are shown in Figure 5.8.

As can be seen in Figure 5.8, the voltage magnitudes of the busbars are lower during peak hours which occurred from 20:00 to 23:00. With the shift in peak hours, the low voltage hours are shifted as well. Shunt capacitors are switched on to increase the voltages at these hours. One of the shunt capacitors is switched off during the day because the voltage magnitude of the busbar that this capacitor is connected do

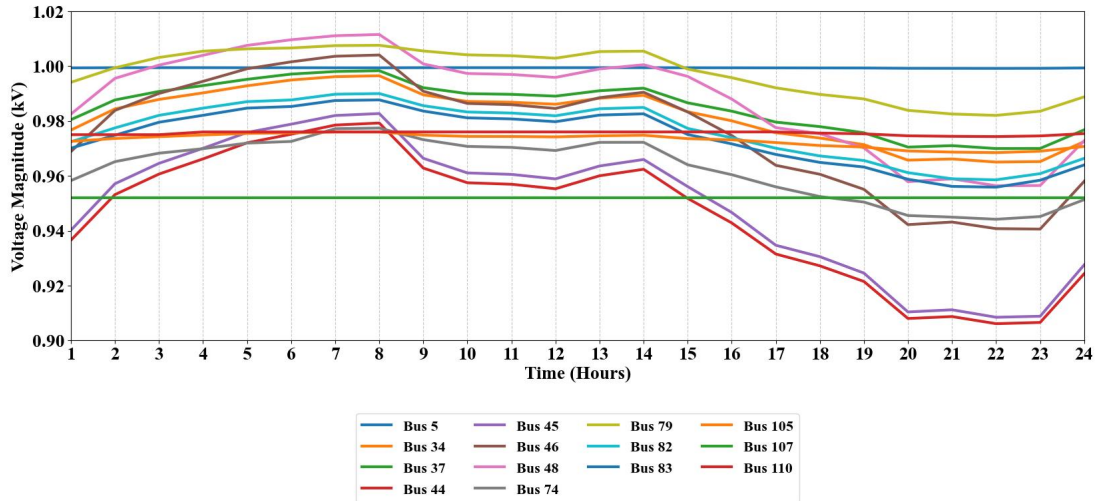


Figure 5.8: Voltage profile of busbars with shunt equipment obtained via power flow calculations - Scenario 2

not fall below 0.975 p.u. limit. Similarly, the two shunt reactors are not required to switch on since the voltages do not exceed the 1.0 p.u limit. The shunt capacitors at Bus 79, Bus 105, Bus 107 and Bus 110 are switched on during the day since the voltage magnitudes are equal to or below 0.975 p.u voltage limit all the day. Since the voltages of these busbars do not exceed the voltage limit, the shunt capacitors are in service for all time periods. The switch statuses of the non-varying shunt equipment are listed in Table 5.13.

Table 5.13: Non-varying switch statuses of shunt equipment for 24 hours - Scenario 2

Switch Status		Switch Status	
Reactor 5	0	Capacitor 105	1
Reactor 37	0	Capacitor 107	1
Capacitor 74	1	Capacitor 110	1
Capacitor 79	0		

The remaining shunt capacitors are switched on where the voltage magnitudes are lower; hence in the first few hours and the last hours of the day, the shunt capacitors are switched on. The voltage levels increase within the first hours of the day; how-

ever, the voltage magnitudes exceed the 0.975 p.u. voltage limit at 2:00 to 4:00 for different busbars. The voltage levels are over the voltage limit until the load demand is increased. The shunt capacitors are switched on at 15:00 to 19:00 and stay in service until the end of the day where the peak hours occurred. The hourly switch status of the remaining shunt equipment is listed in Table 5.14.

Table 5.14: Varying switch statuses of shunt equipment for 24 hours - Scenario 2

	Cap. 34	Cap. 44	Cap. 45	Cap. 46	Cap. 48	Cap. 82	Cap. 83
H1	0	1	1	1	0	1	1
H2	0	1	1	0	0	1	1
H3	0	1	1	0	0	0	0
H4	0	1	0	0	0	0	0
H5	0	0	0	0	0	0	0
H6	0	0	0	0	0	0	0
H7	0	0	0	0	0	0	0
H8	0	0	0	0	0	0	0
H9	0	1	1	0	0	0	0
H10	0	1	1	0	0	0	0
H11	0	1	1	0	0	0	0
H12	0	1	1	0	0	0	0
H13	0	1	1	0	0	0	0
H14	0	1	1	0	0	0	0
H15	0	1	1	0	0	1	1
H16	0	1	1	0	0	1	1
H17	0	1	1	1	0	1	1
H18	1	1	1	1	0	1	1
H19	1	1	1	1	1	1	1
H20	1	1	1	1	1	1	1
H21	1	1	1	1	1	1	1
H22	1	1	1	1	1	1	1
H23	1	1	1	1	1	1	1
H24	1	1	1	1	1	1	1

Similarly, the transformer tap positions were determined according to the voltages of the busbars connected to the transformers. The voltages of the busbars connected to the transformers are presented in Figure 5.9.

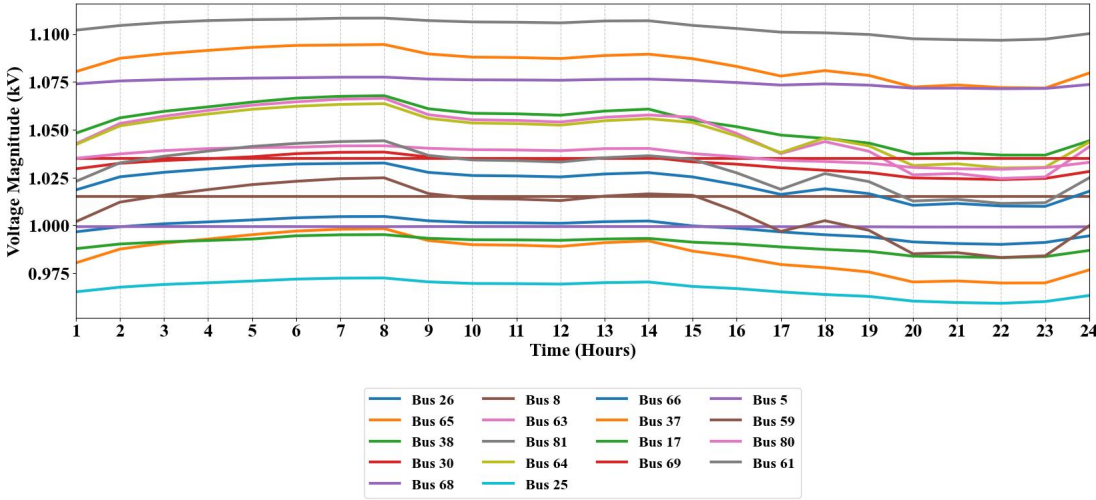


Figure 5.9: Voltage profile of busbars connected with transformers obtained via power flow calculations - Scenario 2

The transformer tap positions of the five transformers are kept as their initial values used in power flow calculations, and they remain unchanged throughout the day. Transformer tap positions of the remaining transformers varies according to the voltage profiles. The varying transformer tap positions are given in Table 5.15. The voltage magnitudes fall to their lowest values at the peak hours from 20:00 to 23:00. In order to increase the voltage magnitudes at these hours, the transformer tap positions are adjusted so as to decrease the tap ratio of the transformers. Tap changes for the first three transformers in Table 5.15 are minor changes 2%-3%. However, tap change in the last transformer, Transformer 63-59, is 6%.

There are two tap changes per transformer during the day. Transformer tap positions are constant until 16:00. Tap changes are occurred at 17:00 to 19:00 for different transformers. Transformer tap positions are altered to their morning positions at 23:00 to 24:00. As can be seen in Table 5.15, the total number of transformer tap changes is eight tap changes for the day.

Table 5.15: Varying transformer tap ratios for 24 hours - Scenario 2

	Tr.	Tr.	Tr.	Tr.		Tr.	Tr.	Tr.	Tr.
	26-25	38-37	30-17	63-59		26-25	38-37	30-17	63-59
H1	0.97	1	1	1.04	H13	0.97	1	1	1.04
H2	0.97	1	1	1.04	H14	0.97	1	1	1.04
H3	0.97	1	1	1.04	H15	0.97	1	1	1.04
H4	0.97	1	1	1.04	H16	0.97	1	1	1.04
H5	0.97	1	1	1.04	H17	0.97	0.97	1	0.98
H6	0.97	1	1	1.04	H18	0.95	0.97	1	0.98
H7	0.97	1	1	1.04	H19	0.95	0.97	1	0.98
H8	0.97	1	1	1.04	H20	0.95	0.97	0.98	0.98
H9	0.97	1	1	1.04	H21	0.95	0.97	0.98	0.98
H10	0.97	1	1	1.04	H22	0.95	0.97	0.98	0.98
H11	0.97	1	1	1.04	H23	0.95	0.97	0.98	0.98
H12	0.97	1	1	1.04	H24	0.95	0.97	1	0.98

With these fixed shunt switch statuses of shunt equipment and transformer tap positions, single-period reactive power optimization problems are formulated. For the solution of the single-period reactive power optimization problems, the Artelys Knitro nonlinear solver is utilized. The resulting voltage profile is given in Figure 5.10.

As can be seen in Figure 5.10, voltage magnitudes are the highest at the morning hours and evening hours where the load is higher at these hours. With the increased distributed solar power in Scenario 2, the net load at the midday hours are decreased. The single-period optimization problems cannot be solved with [0.95 - 1.05] p.u. voltage limits for the hours with high demand. The voltage limits are relaxed for these hours. Hence, higher voltage magnitudes are obtained from the single-period optimization problems in Scenario 2.

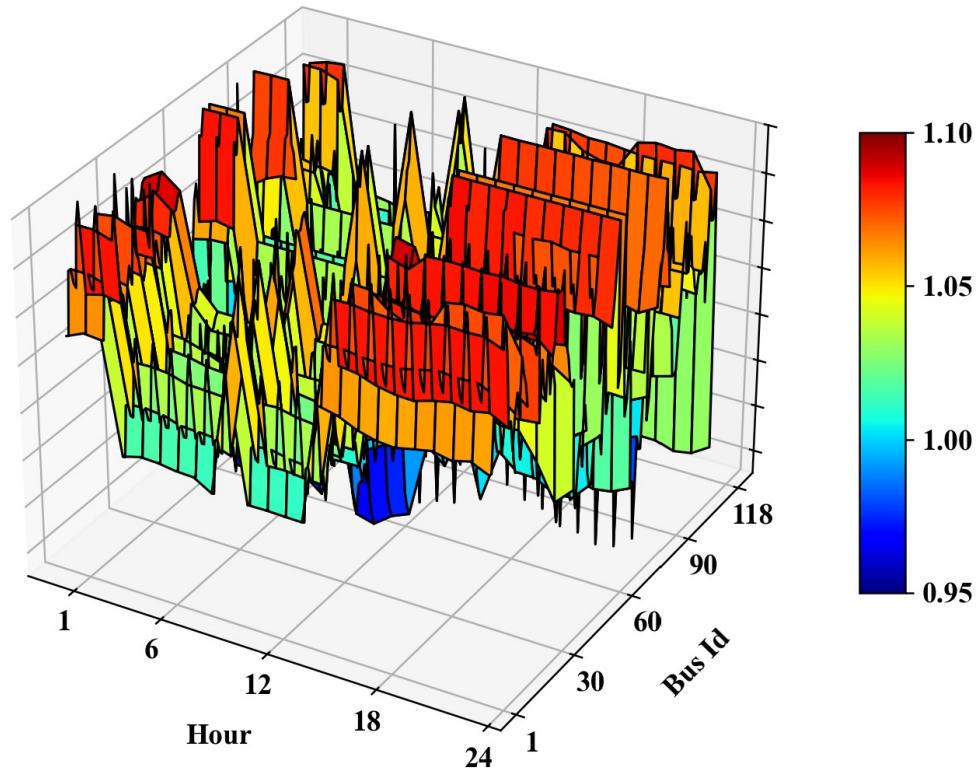


Figure 5.10: Resulting hourly voltage profiles of conventional single-period optimization approach - Scenario 2

As can be seen in Figure 5.10, there are fourteen time periods that the voltage limits are relaxed in single-period optimization problems. Hence, the conventional single-period optimization approach cannot guarantee the desired voltage limits.

Lastly, the hourly and cumulative transmission losses which the objective of the problem is to minimize it, is given in Figure 5.11. The minimum loss occurs at 08:00, reaching 82.5 MW when the load is at its lowest level and the maximum loss occurs at 22:00, reaching 167 MW, when the load is at its maximum level. The loss profile is correlated with the load profile; however, for some of the time periods, transmission losses are decreased when compared with the overall profile since the voltage limits are relaxed for these time periods.

The average hourly loss is 127 MW and total daily loss is 3040 MWh. Given the energy price as 69\$/MWh, total daily energy cost for transmission losses is \$209,760.

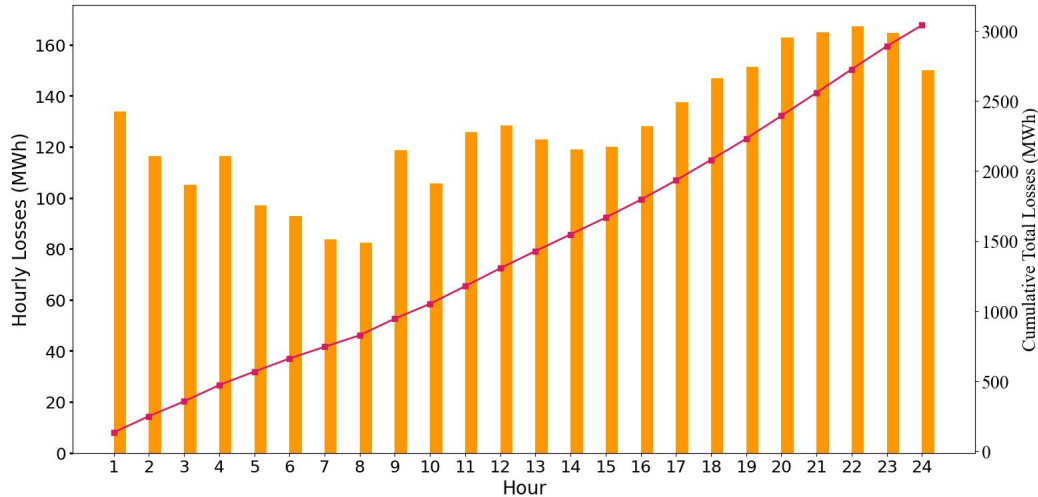


Figure 5.11: Hourly and cumulative losses for conventional single-period optimization approach - Scenario 2

As shown in Table 5.15, total number of tap changes is five for all of the transformers, and with the assumed total cost per tap changes is \$10.58, the total operational and risk cost related with transformer tap changes is \$52.9 in Scenario 2 for conventional single-period optimization approach.

The total daily load demand levels for Scenario 1 and Scenario 2 is similar with 4609 MW peak and 4242 MW peak respectively. Although the the peak load of Scenario 1 is higher than Scenario 2, the active power dispatch for the generators in Scenario 2 is increased the transmission losses. Since the scop of this study is to optimize the reactive power flows along the grid, the active power dispatch is not optimized.

5.4 Proposed Two-Stage Multi-Period Optimization Approach Results

Proposed two-stage multi-period optimization approach is a novel approach for the day-ahead reactive power planning problem. The switch statuses of shunt equipment are decomposed and determined in the first stage of the algorithm, then in the second stage the voltage setpoints and transformer tap positions are obtained using multi-period multi-objective reactive power optimization formulation.

The switch statuses of shunt equipment are determined in the shunt switch status optimization step of the first stage. The shunt switch optimization step needs reactive power requirements for the busbars with shunt equipment. These reactive power requirements are calculated using single-period reactive power optimization problems. The formulation of these single-period optimization problems are described in the previous chapter.

The reactive power requirements for busbars equipped with shunt devices represent the additional reactive power demand that can be supplied by these devices. In cases where a generator is connected to a busbar with a shunt equipment, the primary responsibility of the reactive power control is attributed to the generator. Consequently, if the calculated reactive power injections at such busbars exceeds the generator's maximum reactive power capacity or falls below its minimum reactive power capacity, the reactive power requirement is determined as the difference between the calculated reactive power injection and the generator's maximum or minimum reactive power limits.

In the second stage of the algorithm, switch statuses are fixed and the multi-period reactive optimization problem is formed to obtain the optimum voltage profile and the transformer tap positions. The single-period optimization problems in the first stage and the multi-period optimization problem in the second stage is solved using Artelys Knitro nonlinear optimization solver.

5.4.1 Scenario 1

The first loading scenario, Scenario 1, represents the loading variations of a typical day with low distributed solar generation. All of the single-period optimization problems are converged to an optimal solution and the calculated reactive power requirements are shown in Figure 5.12.

As can be seen in Figure 5.12, for eleven of the fourteen busbars with shunt elements, the reactive power requirement does not vary through the day. The reactive power requirement for the six busbars with shunt equipment is close to its maximum value, and the corresponding shunt equipment are switched on for the entire day. For

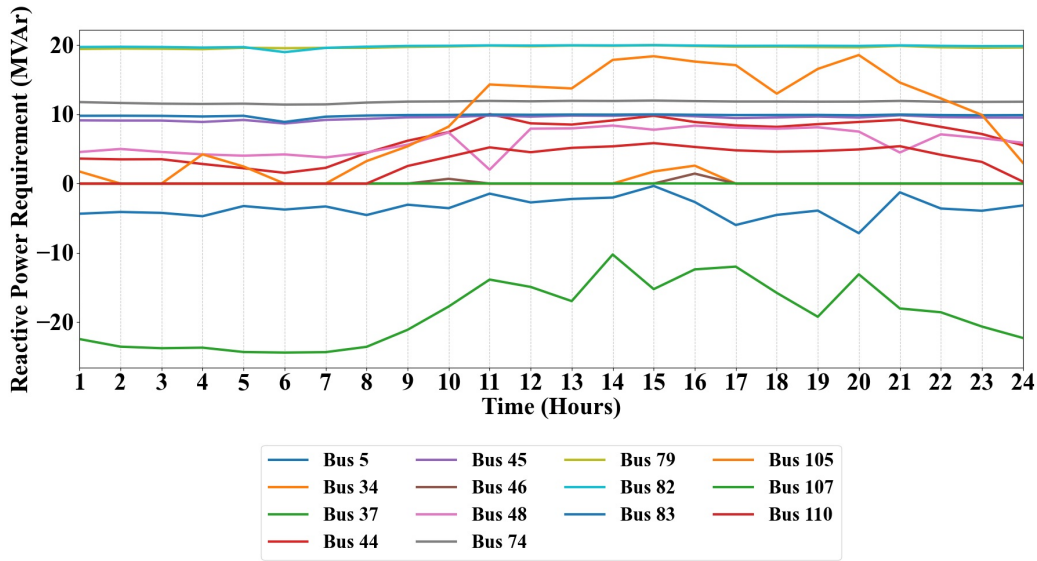


Figure 5.12: Reactive power requirement of shunt equipment connected busbars - Scenario 1

the five busbars, the reactive power requirements are close to zero; hence the shunt equipment are not required to be switched on. The switch statuses of these non-varying shunt equipment are given in Table 5.16.

Table 5.16: Results of Stage I: Switch statuses of non-varying shunt equipment for 24 hours - Scenario 1

Status		Status	
Reactor 5	0	Capacitor 79	1
Capacitor 34	0	Capacitor 82	1
Reactor 37	1	Capacitor 83	1
Capacitor 45	1	Capacitor 105	0
Capacitor 46	0	Capacitor 107	0
Capacitor 74	1		

The reactor at Bus 5 is switched on whereas the reactor at Bus 37 is not required to be switched on during the entire day. The shunt capacitors connected to the busbars Bus 74, Bus 79, Bus 82 and Bus 83 are electrically close to each other. Because of the reactive power requirement in this region, all four shunt capacitors connected to these

aforementioned busbars are switched on during the entire day. The shunt capacitors connected to Bus 105 and Bus 107 are not required to be switched on during the entire day. For the remaining busbars ,the shunt switch optimization gives the switch statuses shown in Table 5.17.

Table 5.17: Results of Stage I: Varying switch statuses of shunt equipment - Scenario 1

	Cap. 44	Cap. 48	Cap. 110		Cap. 44	Cap. 48	Cap. 110
H1	0	0	0	H13	1	1	0
H2	0	0	0	H14	1	1	1
H3	0	0	0	H15	1	1	1
H4	0	0	0	H16	1	0	1
H5	0	0	0	H17	1	0	1
H6	0	0	0	H18	1	0	1
H7	0	0	0	H19	1	0	1
H8	0	0	0	H20	1	0	1
H9	0	0	0	H21	1	0	1
H10	0	0	0	H22	1	0	0
H11	1	0	0	H23	0	0	0
H12	1	0	0	H24	0	0	0

The reactive power requirements emerge in the midday hours for the remaining busbars with shunt equipment. The shunt capacitor that remains in service for the longest time duration in the varying status capacitors is the shunt capacitor connected to Bus 44, and it is switched on at 11:00 and switched off at 23:00. The shunt capacitor that remains in service for the shortest time duration is the shunt capacitor at Bus 48, and it is switched on 13:00 and switched off at 16:00.

After the determination of switch statuses of shunt equipment, the second stage of the algorithm is performed to obtain the optimum voltage profiles along the grid and the transformer tap positions. The resulting voltages are shown in Figure 5.13. The voltages are kept within [0.95,1.05] p.u. voltage limits.

As can be seen in Figure 5.13, there is no big voltage differences between time periods; hence, the reactive power disturbances between time periods due to the voltage differences are small with the proposed algorithm. With the proposed two-stage multi-period optimization approach, voltage magnitudes can be guaranteed to be within the desired voltage limits.

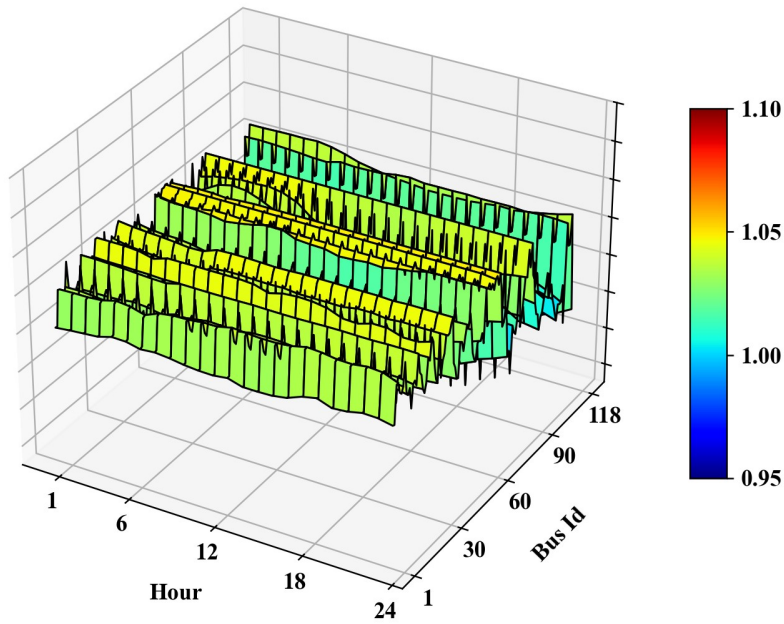


Figure 5.13: Resulting hourly voltage profile for the two-stage optimization approach - Scenario 1

Together with the voltage profiles, the transformer tap positions are determined in the second stage of the algorithm. The multi-period reactive optimization problem gives the optimum transformer tap positions to minimize the total losses and transformer tap changes together, where these two objectives are merged a cost-based framework. The results of the multi-period optimization problem shows that tap positions of the two transformers are constant during the day. The tap positions of these transformers are 1.0 through the entire day. The non-varying tap positions are given in Table 5.18. This results show that the voltage profile between the two sides of these transformers can be maintained at optimum levels without using the transformer tap positions.

Table 5.18: Non-varying transformer tap ratios for 24 hours - Scenario 1

Tap Ratio	
Tr. 30-17	1.0
Tr. 63-59	1.0

Tap positions of the remaining seven transformers varies during the day. The resulting tap ratios of these transformers are given in Table 5.19.

Table 5.19: Varying transformer tap ratios for 24 hours - Scenario 1

	Tr. 8-5	Tr. 26-25	Tr. 38-37	Tr. 64-61	Tr. 65-66	Tr. 68-69	Tr. 81-80
H1	0.99	0.99	1	0.98	1	1.01	1
H2	0.98	0.98	1	1.01	1	0.98	1
H3	1.02	1.02	1	1	1	1.02	1
H4	0.98	0.98	1	1	1	0.98	1
H5	0.98	0.98	1	1	1	0.98	1
H6	1.02	1.02	1	1.01	1	1.01	1
H7	0.97	0.97	1	0.97	1	1	1
H8	1.01	1.01	1	1.01	1	1	1
H9	1.01	1.01	1	1	1.01	1.01	1
H10	0.98	0.98	1	1.01	0.97	0.97	1
H11	0.99	0.99	1	0.98	1.01	1.01	1
H12	0.98	0.98	1	0.98	1	1	1
H13	1.02	1.02	1	1.01	1	1.03	1.01
H14	0.98	0.98	1	1	1	0.99	0.98
H15	0.98	0.98	1	1	1	0.99	0.98
H16	1.02	1.02	1	1	1	1.02	1.02
H17	0.98	0.98	1	1	1	0.98	0.98
H18	1.01	1.01	1.01	1	1	1.02	1.02
H19	0.98	0.98	0.97	1	1	0.98	0.98
H20	1.01	1.01	1.01	1	1	1.02	1.02
H21	0.97	0.97	1	1	1	0.97	0.98
H22	1.01	1.01	1	1	1	1.01	1.01
H23	1	1	1	1	1	1	1.01
H24	1	1	1	1	1	1	1.01

Since the transformer tap positions are determined using the multi-period and multi-objective reactive power optimization problem formed in the second stage of the algorithm, tap positions may be changed to minimize the losses by regulating the voltage profile or simply to keep the voltages within the desired voltage limits as long as the additional operational and risk costs for the tap change does not exceed the decrease in the energy cost of transmission losses.

The total daily number of tap changes for the transformers given in Table 5.20. The number of tap changes for transformers Tr. 8-5, Tr. 26-25 and Tr. 68-69 are very high. Although the tap positions of these transformers are changing almost for every hour, the changes are small with 0.97 tap ratio is the minimum and 1.03 tap ratio is the maximum.

Table 5.20: Non-varying transformer tap ratios for 24 hours - Scenario 1

Number of Tap Changes	
Tr. 8-5	19
Tr. 26-25	19
Tr. 38-37	4
Tr. 64-61	10
Tr. 65-66	4
Tr. 68-69	19
Tr. 81-80	9
Total	84

Hourly and cumulative losses are shown in Figure 5.14, where the bars represent the hourly losses and the lines represent the cumulative losses. The minimum loss occurs at 06:00, reaching 58 MW when the load is at its lowest level, while the maximum loss occurs at 14:00, reaching 130 MW when the load is at its peak. The loss profile is directly correlated with the load profile, as both share the same minimum and peak hours. Furthermore, the hourly variations in loss and load follow the same directional trend.

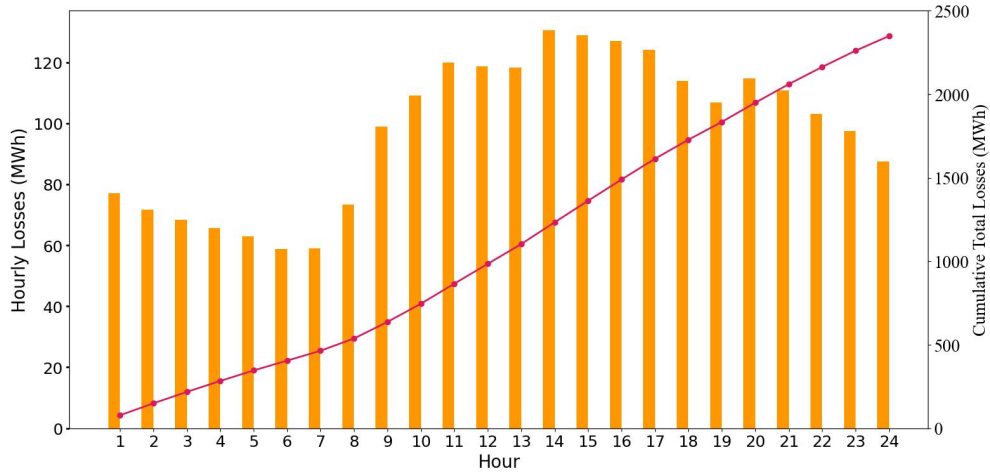


Figure 5.14: Hourly and cumulative losses - Scenario 1

The average hourly loss is 97.8 MW and total daily loss is 2347 MWh. Given the energy price as 69\$/MWh, total daily energy cost for transmission losses is \$161,943. As shown in Table 5.20, total number of tap changes is 84 for all of the transformers, and with the assumed total cost per tap changes is \$10.58, the total operational and risk cost related with transformer tap changes is \$888.72 in scenario 1 for two-stage multi-period optimization approach.

5.4.2 Scenario 2

The second loading scenario, Scenario 2, represents the loading variations of a typical day with high distributed solar generation. The results of the proposed algorithm for Scenario 2 is presented here. Single-period optimization problems, obtained by decomposing the original multi-period optimization problem, are solved using Artelys Knitro. Since each single-period optimization problem represents a specific time period, a total of 24 problems are formulated for the day-ahead hourly reactive power planning. Among these 24 single-period optimization problems, one problem fails to reach an optimal solution, while the remaining 23 problems successfully converge to an optimal solution. The calculated reactive power requirements are shown in Figure 5.15.

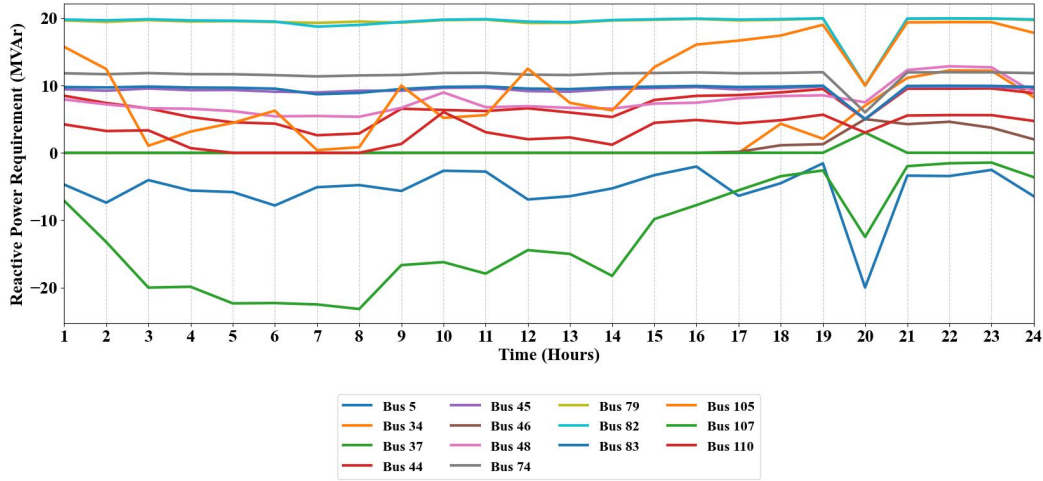


Figure 5.15: Reactive power requirement of shunt equipment connected busbars - Scenario 2

As can be seen in Figure 5.15, for eight of the fourteen busbars with shunt elements, the reactive power requirement does not vary through the day. The reactive power requirement for the five busbars with shunt equipment is close to its maximum value, and the corresponding shunt equipment are switched on for the entire day. For the three busbars, the reactive power requirements are close to zero; hence the shunt equipment are not required to be switched on. The switch statuses of these non-varying shunt equipment are given in Table 5.21.

Table 5.21: Results of Stage I: Non-varying switch statuses of shunt equipment for 24 hours - Scenario 2

Status		Status	
Reactor 5	0	Capacitor 79	1
Capacitor 45	1	Capacitor 82	1
Capacitor 46	0	Capacitor 83	1
Capacitor 74	1	Capacitor 107	0

The reactor at Bus 5 is not switched on whereas the reactor at Bus 37 is required to be switched on for 13 hours. The shunt capacitors connected to the busbars Bus 74, Bus 79, Bus 82 and Bus 83 are electrically close to each other. Because of the reactive power requirement in this region, all four shunt capacitors connected to these aforementioned busbars are switched on during the entire day. The shunt capacitor connected to Bus 107 is not required to be switched on during the entire day. For the remaining busbars, the shunt switch optimization gives the switch statuses shown in Table 5.22.

Table 5.22: Results of Stage I: Varying switch statuses of shunt equipment – Scenario 2

	Cap. 34	Reac. 37	Cap. 44	Cap. 48	Cap. 105	Cap. 110
H1	0	0	1	1	1	0
H2	0	1	1	0	1	0
H3	0	1	1	0	0	0
H4	0	1	1	0	0	0
H5	0	1	0	0	0	0
H6	0	1	0	0	0	0
H7	0	1	0	0	0	0
H8	0	1	0	0	0	0
H9	0	1	1	0	0	1
H10	0	1	1	0	0	1
H11	0	1	1	0	0	1
H12	0	1	1	0	0	0
H13	0	1	1	0	0	0
H14	0	1	1	0	0	0
H15	0	0	1	0	1	1
H16	0	0	1	0	1	1
H17	0	0	1	1	1	1
H18	0	0	1	1	1	1
H19	0	0	1	1	1	1
H20	1	0	1	1	1	1

Table 5.22 – continued from previous page

	Cap. 34	Reac. 37	Cap. 44	Cap. 48	Cap. 105	Cap. 110
H21	1	0	1	1	1	1
H22	1	0	1	1	1	1
H23	1	0	1	1	1	1
H24	1	0	1	1	1	1

The reactor at Bus 37 is switched on from the early hours of the day until midday. The capacitors at Bus 48 and Bus 105, on the other hand, need to be switched on from the evening until the end of the day. This demonstrates that the reactive power requirements at these busbars are parallel, considering that reactors and capacitors have opposing effects. The capacitor at Bus 34 is switched on only for five hours during peak hours. On the other hand, the capacitors at Bus 44, Bus 48, and Bus 110 are switched on for over twelve hours. In fact, the capacitor at Bus 44 remains switched on for as long as twenty hours.

After the determination of switch statuses of shunt equipment, the second stage of the algorithm is performed to obtain the optimum voltage profiles along the grid and the transformer tap positions. The resulting voltages are shown in Figure 5.16.

The voltages are kept within [0.95,1.05] p.u. voltage limits. The optimum voltage profile is obtained with the multi-period reactive power optimization problem since it can control both the voltage setpoints and transformer tap positions. As can be seen in Figure 5.16, there is no big voltage differences between time periods; hence, the reactive power disturbances between time periods due to the voltage differences are small with the proposed algorithm. With the proposed two-stage multi-period optimization approach, voltage magnitudes can be guaranteed to be within the desired voltage limits.

Together with the voltage profiles, the transformer tap positions are determined in the second stage of the algorithm. The multi-period reactive optimization problem gives the optimum transformer tap positions to minimize the total losses and transformer tap changes together, where these two objectives are merged a cost-based framework. The results of the multi-period optimization problem shows that tap positions of the

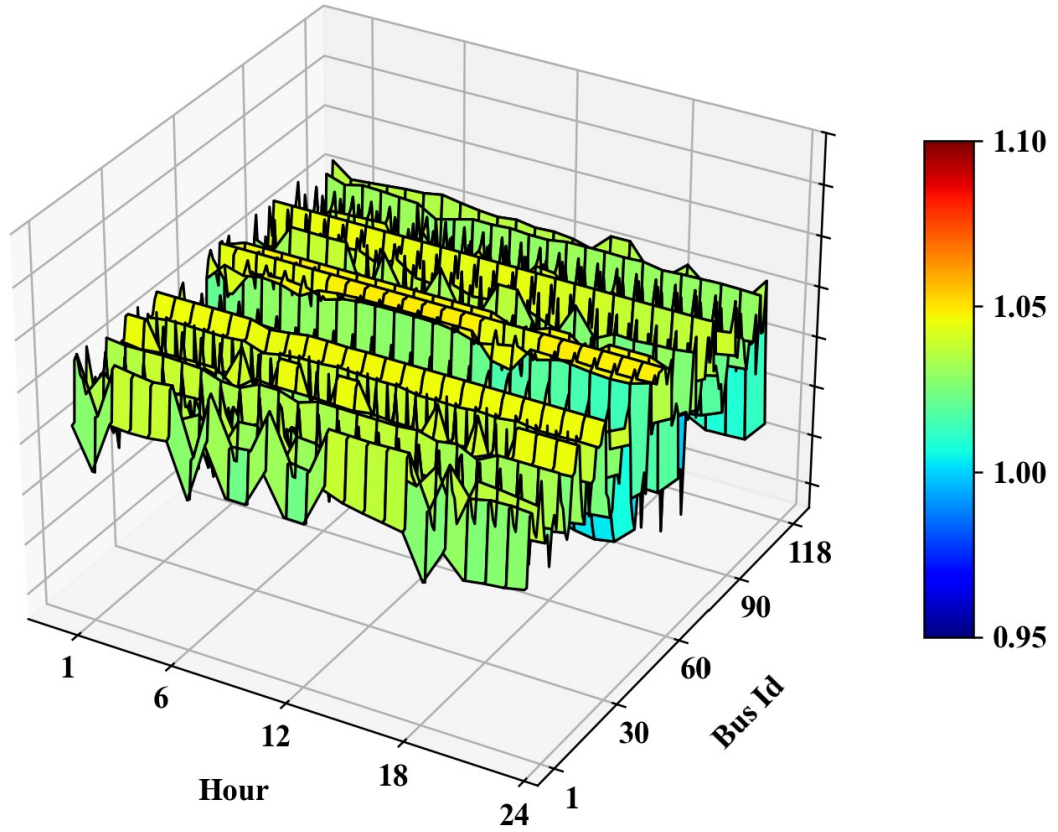


Figure 5.16: Resulting voltage profile - Scenario 2

four transformers are constant during the day. The tap positions of these transformers are 1.0 through the entire day. The non-varying tap positions are given in Table 5.23. This results show that the voltage profile between the two sides of these transformers can be maintained at optimum levels without using the transformer tap positions.

Table 5.23: Non-varying transformer tap ratios for 24 hours - Scenario 2

Tap Ratio	
Tr. 30-17	1.0
Tr. 38-37	1.0
Tr. 63-59	1.0
Tr. 65-66	1.0

Tap positions of the remaining five transformers varies during the day. The resulting tap ratios of these transformers are given in Table 5.24.

Table 5.24: Varying transformer tap ratios for 24 hours - Scenario 2

	Tr. 8-5	Tr. 26-25	Tr. 64-61	Tr. 68-69	Tr. 81-80
H1	0.98	1.00	0.98	0.99	1.01
H2	1.02	1.01	1.01	1.01	1.01
H3	0.99	0.98	0.98	1.01	0.99
H4	0.99	0.99	0.99	1.00	0.99
H5	0.99	0.99	0.99	1.00	0.99
H6	0.99	0.99	0.98	1.00	0.99
H7	1.01	1.01	1.00	1.00	1.02
H8	0.98	0.98	1.00	1.00	0.98
H9	1.01	1.01	1.00	1.00	1.01
H10	1.01	1.01	1.00	1.00	1.01
H11	0.98	0.98	1.00	1.00	0.98
H12	1.01	1.01	1.00	1.00	1.01
H13	1.01	1.01	1.00	1.00	1.01
H14	0.99	0.98	1.00	1.01	0.99
H15	0.99	0.99	1.00	1.01	0.99
H16	0.99	0.98	0.98	0.99	1.01
H17	0.99	1.01	0.98	0.99	1.01
H18	0.99	0.98	1.00	1.01	0.98
H19	1.01	1.01	1.00	1.01	1.01
H20	0.98	0.98	1.00	0.98	1.01
H21	1.00	1.00	1.00	1.01	1.00
H22	1.00	1.00	1.00	1.01	1.00
H23	1.00	1.00	1.00	1.01	1.00
H24	1.00	1.00	1.00	1.01	1.00

Since the transformer tap positions are determined using the multi-period and multi-objective reactive power optimization problem formed in the second stage of the algorithm, tap positions may be changed to minimize the losses by regulating the voltage profile or simply to keep the voltages within the desired voltage limits as long as the additional operational and risk costs for the tap change does not exceed the decrease in the energy cost of transmission losses.

The total daily number of tap changes for the transformers given in Table 5.25. The number of tap changes for transformers Tr. 8-5, Tr. 26-25 and Tr. 81-80 are high. Although the tap positions of these transformers are changing almost for every two hours, the changes are small with 0.98 tap ratio is the minimum and 1.02 tap ratio is the maximum.

Table 5.25: Non-varying transformer tap ratios for 24 hours - Scenario 2

Number of Tap Changes	
Tr. 8-5	11
Tr. 26-25	16
Tr. 64-61	7
Tr. 68-69	7
Tr. 81-80	11
Total	52

Hourly and cumulative losses are shown in Figure 5.17, where the bars represent the hourly losses and the lines represent the cumulative losses. The minimum loss occurs at 08:00, reaching 62 MW when the load is at its lowest level, while the maximum loss occurs at 22:00, reaching 140 MW when the load is at its peak. The loss profile is directly correlated with the load profile, as both share the same minimum and peak hours. Furthermore, the hourly variations in loss and load follow the same directional trend.

The average hourly loss is 101 MW and total daily loss is 2426 MWh. Given the energy price as 69\$/MWh, total daily energy cost for transmission losses is \$167,394. As shown in Table 5.25, total number of tap changes is 52 for all of the transformers,

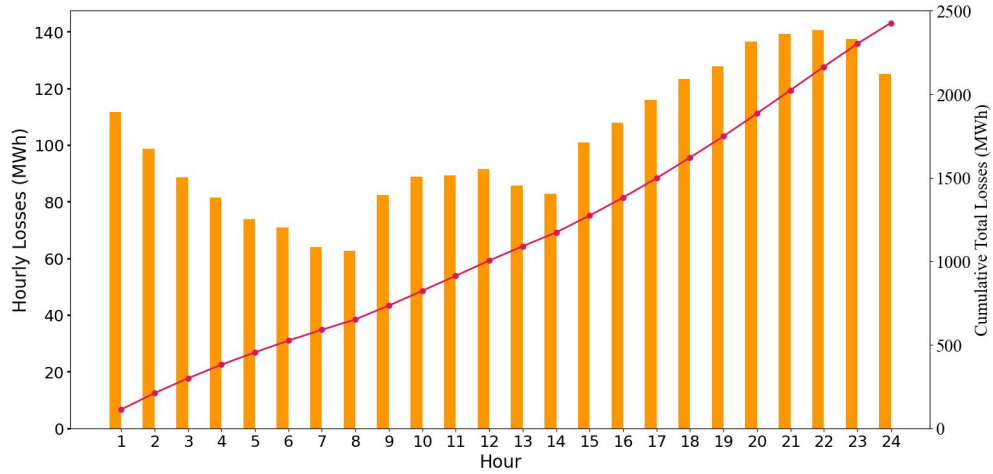


Figure 5.17: Hourly and cumulative losses - Scenario 2

and with the assumed total cost per tap changes is \$10.58, the total operational and risk cost related with transformer tap changes is \$550.16 in scenario 2 for two-stage multi-period optimization approach.

5.5 Evaluation of the Proposed Algorithm

The proposed two-stage optimization approach for the day-ahead reactive power planning problem is simulated under two different loading scenarios, and the results are presented in the previous sections. Previously, the results of the conventional single-period optimization approach, developed to represent common day-ahead reactive power planning applications, were presented.

The switch statuses of the shunt equipment are determined prior to the main optimization problems in both approaches, conventional approach and the proposed approach. Switch statuses are determined according to the voltage profiles calculated via power flow calculations in this study whereas they are obtained using the reactive power requirements calculated as a result of single-period optimization problems in the proposed approach. The proposed approach has the advantage that the switch statuses are determined according to the optimal reactive requirements. Table 5.26 and Table 5.27

show the number of hours that the shunt equipment are switched on for Scenario 1 and Scenario 2 respectively. This demonstrate that in the conventional approach, the shunt equipment are used less than required in a large part of the system; on the other hand, the capacitors at Bus 105, Bus 107 and Bus 110 are utilized more than required. The proposed approach is based on optimal reactive power requirements; hence, the shunt equipment is utilized at optimum level.

Table 5.26: Total duration of shunt equipment in service - Scenario 1

	Conventional Approach	Two-Stage Approach		Conventional Approach	Two-Stage Approach
Reac. 5	0	0	Cap. 74	24	24
Cap. 34	0	0	Cap. 79	0	24
Reac. 37	6	24	Cap. 82	12	24
Cap. 44	13	12	Cap. 83	13	24
Cap. 45	11	24	Cap. 105	24	0
Cap. 46	0	0	Cap. 107	24	0
Cap. 48	0	3	Cap. 110	24	8

Table 5.27: Total duration of shunt equipment in service - Scenario 2

	Conventional Approach	Two-Stage Approach		Conventional Approach	Two-Stage Approach
Reac. 5	0	0	Cap. 74	24	24
Cap. 34	7	5	Cap. 79	0	24
Reac. 37	0	13	Cap. 82	12	24
Cap. 44	20	20	Cap. 83	12	24
Cap. 45	19	24	Cap. 105	24	12
Cap. 46	9	0	Cap. 107	24	0
Cap. 48	6	9	Cap. 110	24	13

On the other hand, for some of the shunt equipment, the shunt equipment are switched on at similar time periods in both approaches. The hourly switch statuses for the capacitor at Bus 44 in Scenario 1 and for the capacitor at Bus 48 in Scenario 2 are given in Figure 5.18 and Figure 5.19 respectively. It can be seen that the switch statuses of the shunt equipment for both approaches largely coincide with each other.

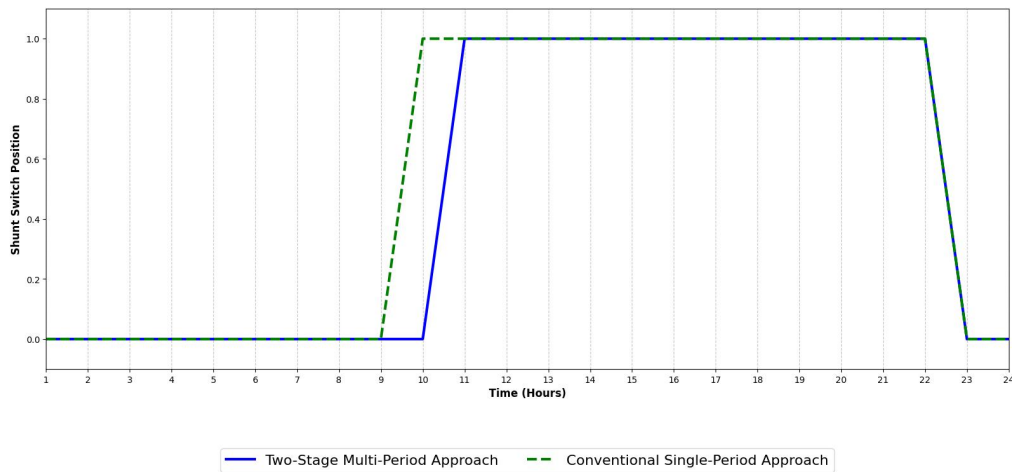


Figure 5.18: The hourly switch statuses for the capacitor at Bus 44 in Scenario 1

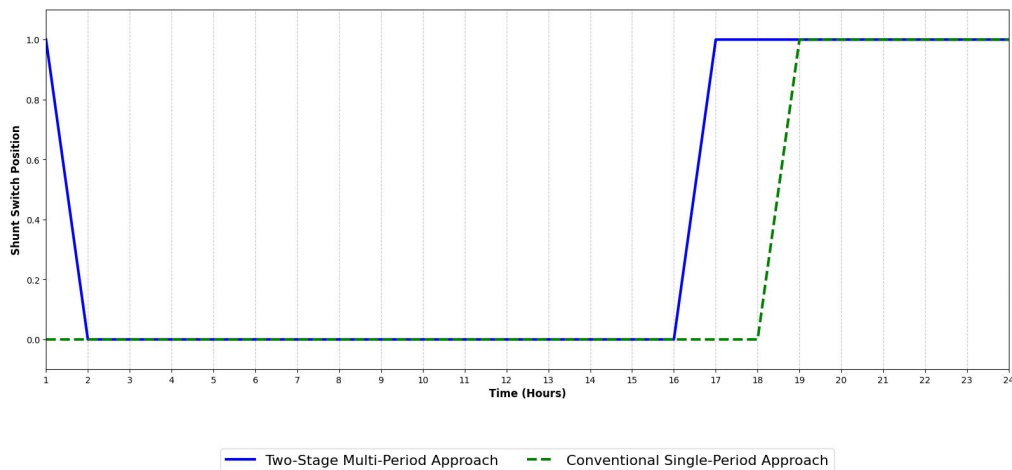


Figure 5.19: The hourly switch statuses for the capacitor at Bus 48 in Scenario 2

In the conventional single-period optimization approach, transformer tap positions are determined based on voltage profiles, similar to the switch statuses of shunt equipment. However, in the proposed two-stage multi-period optimization approach, transformer tap positions are obtained in the second stage of the algorithm as a result of the multi-period optimization problem. The total number of daily tap changes in both approaches for Scenario 1 and Scenario 2 is shown in Table 5.28. The number of tap changes in the conventional approach is significantly smaller compared to the proposed approach. This is because the conventional approach places excessive emphasis on minimizing tap changes. In the conventional approach, the minimization of tap changes and the minimization of losses cannot be optimized simultaneously, as loss minimization is handled through single-period optimization problems, whereas tap positions are determined based on voltage profiles and the practical experience of transmission system operators. In contrast, the proposed approach integrates loss minimization and tap change minimization within a cost-based framework. Thus, the proposed approach ensures a balanced trade-off between the minimization of losses and minimization of tap changes by formulating them within a unified multi-period optimization framework, leading to a more systematic and cost-effective determination of tap positions.

Table 5.28: Number of tap changes

	Conventional Approach		Two-Stage Approach	
	S1	S2	S1	S2
Tr. 8-5	0	0	19	11
Tr. 26-25	0	1	19	16
Tr. 30-17	0	2	0	0
Tr. 38-37	0	1	4	0
Tr. 63-59	0	1	0	0
Tr. 64-61	2	0	10	7
Tr. 65-66	0	0	4	0
Tr. 68-69	0	0	19	7
Tr. 81-80	0	0	9	11
Total	2	5	84	52

To evaluate the results of the proposed two-stage multi-period optimization approach, the voltage profiles are compared. The voltage distribution graphs for Scenario 1 and Scenario 2 are shown in Figure 5.20 and Figure 5.21, respectively. The y-axis represents the voltage magnitude, while the width of the distribution along the x-axis indicates the frequency of occurrence. The figures compare the results of the conventional single-period optimization approach and the proposed two-stage multi-period optimization approach. As shown in the figures, the proposed two-stage approach improves the voltage profile.

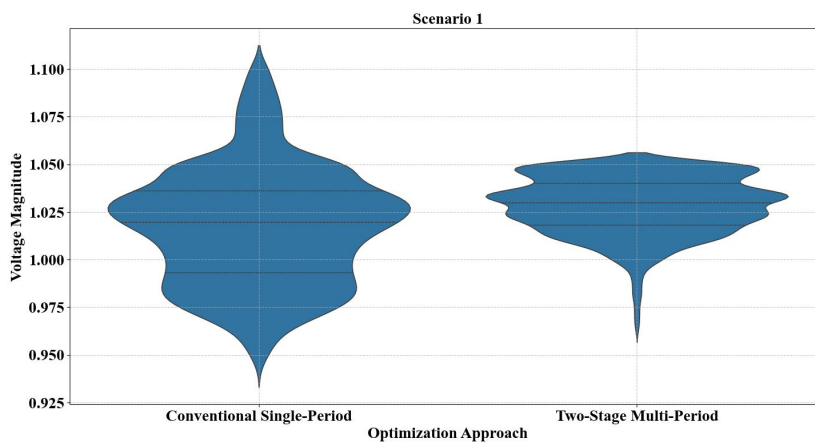


Figure 5.20: Distribution of voltage magnitudes - Scenario 1

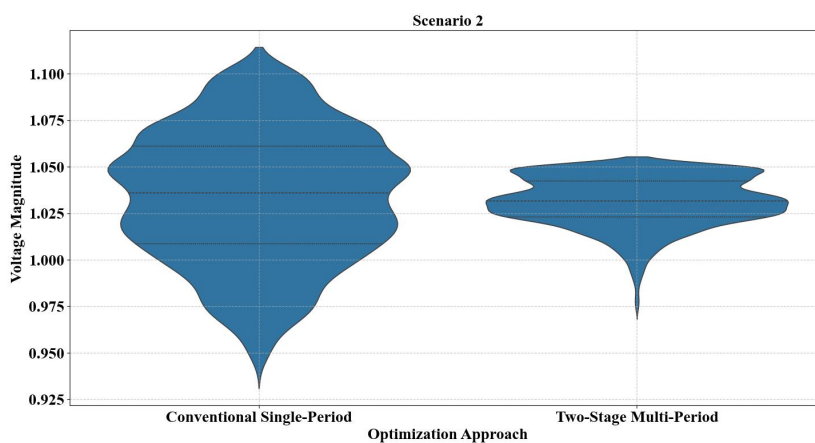


Figure 5.21: Distribution of voltage magnitudes - Scenario 2

In Scenario 1, the results of the conventional approach indicate that voltages are primarily distributed within the [0.95, 1.05] p.u. limits. However, for certain busbars and time periods, voltage deviations beyond these limits occur. In Scenario 2, the number of occurrences outside this range is even higher for the conventional single-period optimization approach. The proposed two-stage multi-period optimization approach enhances the voltage profile for both loading scenarios. As shown in both figures, the proposed approach exhibits a higher probability of maintaining voltages within the [0.95, 1.05] p.u. limits.

The number of tap changes, total losses and associated costs for both models are shown in Table 5.29. The proposed two-stage multi-period optimization approach resulted in a high number of transformer tap changes in both scenarios, as the operational and risk costs associated with transformer tap changes are significantly lower compared to the energy costs of transmission losses. Despite the increase in the cost due to transformer tap changer operations, the proposed algorithm achieves a 5.89% and 20.2% reduction in transmission losses for Scenario 1 and Scenario 2 respectively. The proposed algorithm provides 5.56% and 19.96% improvement in overall costs for Scenario 1 and Scenario 2 respectively.

Table 5.29: Resulting costs for transmission losses and transformer tap changes

	Conventional Approach		Two-Stage Approach	
	S1	S2	S1	S2
Total Daily Loss (MWh)	2494	3040	2347	2426
Cost of Transmission Losses (\$)	\$172,086	\$209,760	\$161,943	\$167,394
Number of Transformer Tap Changes	2	5	84	52
Cost of Transformer Tap Changes (\$)	\$21.16	\$52.9	\$888.72	\$550.16
Total Cost	\$172,107.16	\$209,812.9	\$162,831.72	\$167,944.16

CHAPTER 6

CONCLUSIONS

Modern power systems are designed to transport energy from generation facilities to consumers. Various network elements are utilized in these systems. Transmission lines and transformers, which are the fundamental components of transmission networks, exhibit capacitive and inductive effects, making reactive power indispensable for the operation of modern power systems. Although reactive power is essential, it must be supplied as close as possible to where it is needed, as excessive reactive power flows increase the transmission losses. To mitigate this issue, the reactive power flows must be optimized. In addition, the voltage magnitude is directly affected by the reactive power balance in the system. Insufficient reactive power leads to voltage drops, whereas excessive reactive power causes voltage rises. Effective reactive power management is required to maintain voltage levels within acceptable limits. Therefore, reactive power optimization is crucial for modern power systems with voltage/reactive power control.

The reactive power capabilities of power plants are the primary source of reactive power control, followed by shunt reactors and capacitors. In addition, transformers with tap changers participate in reactive power control because they can regulate voltages by altering their impedances. Consequently, reactive power optimization aims to optimize the utilization of these elements.

Day-ahead reactive power optimization mainly focuses on determining the hourly operation schedule of the elements participating in the reactive power control. This is achieved using nonlinear reactive power optimization. The main objective of this optimization is to minimize total transmission losses. In addition, the number of shunt equipment switching operations and transformer tap changes are a concern for

transmission system operators because of operational and risk costs. These objectives are combined using a cost-based optimization framework.

The control variables for the day-ahead reactive power optimization problem can be classified into discrete and continuous variables. Reactive power capabilities of power plants, which are defined as continuous variables, are the main source for the reactive power control. Power plants supply reactive power according to their local automatic voltage regulators; therefore, the voltage setpoints are considered as the control variables. The remaining control variables, switch statuses of shunt equipment and transformer tap positions are discretely controlled variables. The integer variables affect the convergence probability of the optimization problem. As the number of integer variables increases, the probability of convergence decreases, whereas the execution time grows significantly. In particular, the effect of the switch statuses of the shunt equipment is greater than that of the transformer tap changes. Transformer tap changes result in minor impedance changes; however, a switching operation causes a large disturbance to the system. Therefore, integer variables are treated with particular attention.

Furthermore, the operational constraints related to switching and tap-changing operations complicate the problem, making it a multi-period optimization problem. The number of variables and constraints is multiplied by the number of time periods. For the day-ahead hourly reactive power optimization problem, the problem size increased to more than 24 times that of a single-period optimization problem. Because the problem is nonconvex and nonlinear because of the power balance constraints, the complexity of the problem increases such that, in addition to the decrease in convergence probability, the execution time increases to a level that makes the problem computationally impractical.

The day-ahead reactive power optimization problem has been explored in this study. As a first step, possible solution methods are investigated for the challenges introduced by nonlinearity. For this purpose, a successive linear optimization method is proposed to overcome the nonlinearity of the original problem. To deal with the integer variables, a two-stage linearized optimization method is developed for the day-ahead reactive power optimization problem and tested on the IEEE 30 Bus test

system. One limitation of this method is the computational burden of the necessary calculations before the successive linear optimization method. The determination of integer variables depends on the power flow calculations in this method; hence, the number of required power flow calculations for the determination of integer variables in large systems will be impractically large. Moreover, the proposed approach for determining integer variables does not consider the mutual effects of integer control variables. In the proposed approach, the incremental loss and voltage deviations due to the change in integer control variables are summed to estimate the total loss and voltage deviations. In reality, the simultaneous operation of multiple integer control variables can lead to nonlinear interactions.

Another limitation of the two-stage linearized optimization method is related to the successive linear optimization approach. There is an inconsistency between the linearized and actual reactive power balance constraints, although the difference between the linearized and actual active power balance constraints is within acceptable limits. Because the main goal of the day-ahead reactive power optimization problem, obtaining the optimal reactive power flows, depends on the correct representation of reactive power flows, this approach may lead to suboptimal or inaccurate reactive power dispatches.

Since the proposed two-stage linearized optimization has the limitations discussed previously, the interior point algorithm is chosen for the solution of the day-ahead reactive power optimization problem, as it is widely used for solving nonlinear and nonconvex optimization problems. However, the interior point algorithm cannot provide a solution for the integer variables. The complexity arising from the integer variables, intensified by the increased problem size due to its multi-period nature, has been specifically addressed and mitigated in this study.

In this thesis, a two-stage multi-period optimization approach is developed for the day-ahead reactive power optimization problem. The proposed approach first decomposes the problem into single-period optimization problems to handle the switch statuses of shunt equipment. After determination of these switch statuses based on optimum reactive power requirements for each busbar with shunt equipment, reactive power dispatch is optimized so that the voltage setpoints for the power plants

and transformer tap positions are determined using the interior point algorithm on the proposed multi-period multi-objective reactive power optimization formulation.

The proposed two-stage multi-period optimization approach is tested on the IEEE 118 Bus test system. To evaluate the performance of the proposed approach, a conventional single-period optimization approach is introduced and tested on the IEEE 118 Bus test system.

Although the switch statuses of the shunt equipment are determined prior to the main optimization problem in the proposed approach, as in the conventional approach, the proposed approach has the advantage that the switch statuses are determined according to the optimal reactive requirements. This yields the optimum utilization of shunt equipment in the proposed two-stage multi-period optimization approach.

In the proposed two-stage multi-period optimization approach, transformer tap positions are defined as control variables of the reactive optimization problem, and the optimum transformer tap positions are obtained, whereas they are determined according to the voltage profiles in the conventional approach. The conventional approach may overstate the minimization of tap changes, where in the proposed approach, the optimum number of tap changes and losses are obtained since the objective of the optimization problem consists of two objectives merged in a cost based framework.

Simulation studies demonstrate that the proposed two-stage multi-period optimization approach achieves improvement in transmission losses along with the total cost, including the operational and risk costs of transformer tap changes. Unlike the conventional approach, the proposed approach provides a robust solution for hourly reactive power planning, balancing efficiency and reliability while dealing with the nonlinear and nonconvex nature of the problem. Moreover, simulation studies show that the proposed approach is particularly well suited to the day-ahead reactive power planning problem because of its acceptable execution times, making it practical for operational use while ensuring system reliability and efficiency.

In the simulation studies, the energy price for the losses is assumed to be constant for each time period. However, the energy prices vary throughout the day. Because the losses are purchased by transmission system operators based on day-ahead market

prices, simulation studies can also be performed with hourly energy prices. Thus, the effect of changing energy prices on the determination of optimum voltage profiles can be explored in future work.

Finally, simulation studies are performed on the IEEE 118 Bus test system. Although this test system can provide the fundamentals of a transmission network, simulation studies can be performed for large power systems using real load and generation data in the future.

REFERENCES

- [1] P. Kundur, *Power system stability and control*. EPRI power system engineering series, McGraw-Hill Inc., 1994.
- [2] E. Commission, “Commission regulation (EU) 2017/1485 of 2 August 2017 establishing a guideline on electricity transmission system operation.” Official Journal of the European Union, L220, pp. 1-120, August 2017.
- [3] J. P. Paul, J. Y. Leost, and J. M. Tesson, “Survey of the secondary voltage control in France : Present realization and investigations,” *IEEE Transactions on Power Systems*, vol. 2, no. 2, pp. 505–511, 1987.
- [4] J. Sancha, J. Fernandez, A. Cortes, and J. Abarca, “Secondary voltage control: analysis, solutions and simulation results for the Spanish transmission system,” in *Proceedings of Power Industry Computer Applications Conference*, pp. 27–32, 1995.
- [5] S. Corsi, M. Pozzi, C. Sabelli, and A. Serrani, “The coordinated automatic voltage control of the Italian transmission grid-part I: Reasons of the choice and overview of the consolidated hierarchical system,” *IEEE Transactions on Power Systems*, vol. 19, no. 4, pp. 1723–1732, 2004.
- [6] J. van Hecke, N. Janssens, J. Deuse, and F. Promel, “Coordinated voltage control experience in Belgium,” in *CIGRE Session 2000*, (Paris, France), pp. 38–111, 2000.
- [7] İsmail Elma, “Determination of optimum values for voltage setpoints of power stations in Turkey,” m.s. thesis, Middle East Technical University, Ankara, Türkiye, February 2014.
- [8] J. Carpentier, “Contribution to the economic dispatch problem (in french),” *Bulletin de la Societe Francaise des Electriciens*, vol. 3, no. 8, 1962.

- [9] H. W. Dommel and W. F. Tinney, "Optimal power flow solutions," *IEEE Transactions on Power Apparatus and Systems*, vol. PAS-87, no. 10, pp. 1866–1876, 1968.
- [10] H. Happ, "Optimal power dispatch - A comprehensive survey," *IEEE Transactions on Power Apparatus and Systems*, vol. 96, no. 3, pp. 841–854, 1977.
- [11] D. I. Sun, B. Ashley, B. Brewer, A. Hughes, and W. F. Tinney, "Optimal power flow by Newton approach," *IEEE Transactions on Power Apparatus and Systems*, vol. PAS-103, no. 10, pp. 2864–2880, 1984.
- [12] S. Granville, "Optimal reactive dispatch through interior point methods," *IEEE Transactions on Power Systems*, vol. 9, no. 1, pp. 136–146, 1994.
- [13] F. Dong, B. Chowdhury, M. Crow, and L. Acar, "Improving voltage stability by reactive power reserve management," *IEEE Transactions on Power Systems*, vol. 20, no. 1, pp. 338–345, 2005.
- [14] Q. Li, M. Liu, and H. Liu, "Piecewise normalized normal constraint method applied to minimization of voltage deviation and active power loss in an AC–DC hybrid power system," *IEEE Transactions on Power Systems*, vol. 30, no. 3, pp. 1243–1251, 2015.
- [15] A. Rabiee and M. Parniani, "Voltage security constrained multi-period optimal reactive power flow using Benders and optimality condition decompositions," *IEEE Transactions on Power Systems*, vol. 28, no. 2, pp. 696–708, 2013.
- [16] I. Elma and A. N. Guven, "Multi-period reactive power optimization for determination of switch statuses of shunt elements and voltage setpoints of power plants," in *2021 13th International Conference on Electrical and Electronics Engineering (ELECO)*, pp. 6–10, 2021.
- [17] O. Alsac and B. Stott, "Optimal load flow with steady-state security," *IEEE Transactions on Power Apparatus and Systems*, vol. PAS-93, no. 3, pp. 745–751, 1974.
- [18] A. Monticelli, M. V. F. Pereira, and S. Granville, "Security-constrained optimal power flow with post-contingency corrective rescheduling," *IEEE Transactions on Power Systems*, vol. 2, no. 1, pp. 175–180, 1987.

- [19] F. Capitanescu, M. Glavic, D. Ernst, and L. Wehenkel, "Contingency filtering techniques for preventive security-constrained optimal power flow," *IEEE Transactions on Power Systems*, vol. 22, no. 4, pp. 1690–1697, 2007.
- [20] N. Dandachi, M. Rawlins, O. Alsac, M. Prais, and B. Stott, "OPF for reactive pricing studies on the ngc system," *IEEE Transactions on Power Systems*, vol. 11, no. 1, pp. 226–232, 1996.
- [21] T. Wolgast, S. Ferez, and A. Nieße, "Reactive power markets: A review," *IEEE Access*, vol. 10, pp. 28397–28410, 2022.
- [22] J. Barquin Gil, T. San Roman, J. Alba Rios, and P. Sanchez Martin, "Reactive power pricing: A conceptual framework for remuneration and charging procedures," *IEEE Transactions on Power Systems*, vol. 15, no. 2, pp. 483–489, 2000.
- [23] C. W. Sanders and C. A. Monroe, "An algorithm for real-time security constrained economic dispatch," *IEEE Transactions on Power Systems*, vol. 2, no. 4, pp. 1068–1074, 1987.
- [24] N. Karmarkar, "A new polynomial-time algorithm for linear programming," *Combinatorica*, vol. 4, p. 373–395, Dec 1984.
- [25] L. Vargas, V. Quintana, and A. Vannelli, "A tutorial description of an interior point method and its applications to security-constrained economic dispatch," *IEEE Transactions on Power Systems*, vol. 8, no. 3, pp. 1315–1324, 1993.
- [26] J. Yuryevich and K. P. Wong, "Evolutionary programming based optimal power flow algorithm," *IEEE Transactions on Power Systems*, vol. 14, no. 4, pp. 1245–1250, 1999.
- [27] M. Niu, C. Wan, and Z. Xu, "A review on applications of heuristic optimization algorithms for optimal power flow in modern power systems," *Journal of Modern Power Systems and Clean Energy*, vol. 2, no. 4, pp. 289–297, 2014.
- [28] L. Lai, J. Ma, R. Yokoyama, and M. Zhao, "Improved genetic algorithms for optimal power flow under both normal and contingent operation states," *International Journal of Electrical Power & Energy Systems*, vol. 19, no. 5, pp. 287–292, 1997.

- [29] Y. del Valle, G. K. Venayagamoorthy, S. Mohagheghi, J.-C. Hernandez, and R. G. Harley, "Particle swarm optimization: Basic concepts, variants and applications in power systems," *IEEE Transactions on Evolutionary Computation*, vol. 12, no. 2, pp. 171–195, 2008.
- [30] C.-R. Wang, H.-J. Yuan, Z.-Q. Huang, J.-W. Zhang, and C.-J. Sun, "A modified particle swarm optimization algorithm and its application in optimal power flow problem," in *2005 International Conference on Machine Learning and Cybernetics*, vol. 5, pp. 2885–2889 Vol. 5, 2005.
- [31] A. Esmín, G. Lambert-Torres, and A. Zambroni de Souza, "A hybrid particle swarm optimization applied to loss power minimization," *IEEE Transactions on Power Systems*, vol. 20, no. 2, pp. 859–866, 2005.
- [32] R. Madani, S. Sojoudi, and J. Lavaei, "Convex relaxation for optimal power flow problem: Mesh networks," *IEEE Transactions on Power Systems*, vol. 30, no. 1, pp. 199–211, 2015.
- [33] B. C. Lesieutre, D. K. Molzahn, A. R. Borden, and C. L. DeMarco, "Examining the limits of the application of semidefinite programming to power flow problems," in *2011 49th Annual Allerton Conference on Communication, Control, and Computing (Allerton)*, pp. 1492–1499, 2011.
- [34] A. Castillo, P. Lipka, J.-P. Watson, S. S. Oren, and R. P. O'Neill, "A successive linear programming approach to solving the iv-acopf," *IEEE Transactions on Power Systems*, vol. 31, no. 4, pp. 2752–2763, 2016.
- [35] Z. Yang, H. Zhong, A. Bose, T. Zheng, Q. Xia, and C. Kang, "A linearized OPF model with reactive power and voltage magnitude: A pathway to improve the MW-only DC OPF," *IEEE Transactions on Power Systems*, vol. 33, no. 2, pp. 1734–1745, 2018.
- [36] R. Mota-Palomino and V. H. Quintana, "A penalty function-linear programming method for solving power system constrained economic operation problems," *IEEE Transactions on Power Apparatus and Systems*, vol. PAS-103, no. 6, pp. 1414–1422, 1984.

- [37] J. Momoh, M. El-Hawary, and R. Adapa, "A review of selected optimal power flow literature to 1993. ii. newton, linear programming and interior point methods," *IEEE Transactions on Power Systems*, vol. 14, no. 1, pp. 105–111, 1999.
- [38] M. A. El-Kady, B. D. Bell, V. F. Carvalho, R. C. Burchett, H. H. Happ, and D. R. Vierath, "Assessment of real-time optimal voltage control," *IEEE Transactions on Power Systems*, vol. 1, no. 2, pp. 98–105, 1986.
- [39] J. Momoh, M. El-Hawary, and R. Adapa, "A review of selected optimal power flow literature to 1993. II. Newton, linear programming and interior point methods," *IEEE Transactions on Power Systems*, vol. 14, no. 1, pp. 105–111, 1999.
- [40] S. N. Talukdar and T. C. Giras, "A fast and robust variable metric method for optimum power flows," *IEEE Transactions on Power Apparatus and Systems*, vol. PAS-101, no. 2, pp. 415–420, 1982.
- [41] R. S. Wibowo, R. Maulana, A. Taradini, F. A. Pamuji, A. Soeprijanto, and O. Penangsang, "Quadratic programming approach for security constrained optimal power flow," in *2015 7th International Conference on Information Technology and Electrical Engineering (ICITEE)*, pp. 200–203, 2015.
- [42] R. Burchett, H. Happ, and K. Wirgau, "Large scale optimal power flow," *IEEE Transactions on Power Apparatus and Systems*, vol. PAS-101, no. 10, pp. 3722–3732, 1982.
- [43] Y. Tao and A. P. S. Meliopoulos, "A sequential linear programming algorithm for security-constrained optimal power flow," in *41st North American Power Symposium*, pp. 1–6, 2009.
- [44] S. A. Sadat and M. Sahraei-Ardakani, "Customized sequential quadratic programming for solving large-scale AC optimal power flow," in *2021 North American Power Symposium (NAPS)*, pp. 1–6, 2021.
- [45] M. Farivar and S. H. Low, "Branch flow model: Relaxations and convexification—Part I," *IEEE Transactions on Power Systems*, vol. 28, no. 3, pp. 2554–2564, 2013.

- [46] S. H. Low, “Convex relaxation of optimal power flow—Part I: Formulations and equivalence,” *IEEE Transactions on Control of Network Systems*, vol. 1, no. 1, pp. 15–27, 2014.
- [47] S. Huang, K. Filonenko, and C. T. Veje, “A review of the convexification methods for AC optimal power flow,” in *2019 IEEE Electrical Power and Energy Conference (EPEC)*, pp. 1–6, 2019.
- [48] S. Moghadasi and S. Kamalasadani, “An architecture for voltage stability constrained optimal power flow using convex semi-definite programming,” in *2015 North American Power Symposium (NAPS)*, pp. 1–6, 2015.
- [49] A. R. Aldik and B. Venkatesh, “Fast SDP relaxation of the optimal power flow using the line-wise model for representing meshed transmission networks,” *IEEE Transactions on Power Systems*, vol. 38, no. 4, pp. 3814–3827, 2023.
- [50] M. Baradar, M. R. Hesamzadeh, and M. Ghandhari, “Second-order cone programming for optimal power flow in VSC-type AC-DC grids,” *IEEE Transactions on Power Systems*, vol. 28, no. 4, pp. 4282–4291, 2013.
- [51] M. M.-U.-T. Chowdhury, S. Kamalasadani, and S. Paudyal, “A second-order cone programming (SOCP) based optimal power flow (OPF) model with cyclic constraints for power transmission systems,” *IEEE Transactions on Power Systems*, vol. 39, no. 1, pp. 1032–1043, 2024.
- [52] S. Babaeinejadsarookolae, A. Birchfield, R. D. Christie, C. Coffrin, C. Demarco, R. Diao, M. Ferris, S. Fliscounakis, S. Greene, R. Huang, C. Jozs, R. Korab, B. Lesieutre, J. Maeght, T. W. K. Mak, D. K. Molzahn, T. J. Overbye, P. Panciatici, B. Park, J. Snodgrass, A. Tbaileh, P. V. Hentenryck, and R. Zimmerman, “The power grid library for benchmarking AC optimal power flow algorithms.” Data retrieved from GitHub, <https://github.com/power-grid-lib>, 2021.
- [53] EPDK, “Elektrik piyasaları dengeleme ve uzlaştırma yönetmeliği.” published in Official Journal of Republic of Türkiye, March 2015.
- [54] EPIAŞ, “Market clearing price (MCP),” 2025. Accessed: 2025-01-10.

APPENDICES

A Simulation Data

IEEE 30 Bus and IEEE 118 Bus test systems are used in simulations. The system data for IEEE 30 Bus test system used in Chapter 3 is given in Appendix A.1. The system data for IEEE 118 Bus test system used in Chapter 5 is given in the Appendix A.2.

A.1 IEEE 30 Bus Test System

The bus data for IEEE 30 Bus test system is given in Table A.1.

Table A.1: IEEE 30 Bus Test System

Id	Vnom	Type	P^L	Q^L	P^G	Q^G	V_{set}	Q_{max}^G	Q_{min}^G	B_s
1	132	Slack	0	0	260.2	-16.1	1.06	0	0	0
2	132	PV	21.7	12.7	40	50	1.045	50	-40	0
3	132	PQ	2.4	1.2	0	0	0	0	0	0
4	132	PQ	7.6	1.6	0	0	0	0	0	-0.3
5	132	PV	94.2	19	0	37	1.01	40	-40	0
6	132	PQ	0	0	0	0	0	0	0	0
7	132	PQ	22.8	10.9	0	0	0	0	0	0
8	132	PV	30	30	0	37.3	1.01	40	-10	0
9	1	PQ	0	0	0	0	0	0	0	0
10	33	PQ	5.8	2	0	0	0	0	0	0.19
11	11	PV	0	0	0	16.2	1.082	24	-6	0
12	33	PQ	11.2	7.5	0	0	0	0	0	0
13	11	PV	0	0	0	10.6	1.071	24	-6	0
14	33	PQ	6.2	1.6	0	0	0	0	0	0

Table A.1 – continued from previous page

Id	Vnom	Type	P^L	Q^L	P^G	Q^G	V_{set}	Q^G_{max}	Q^G_{min}	B_s
15	33	PQ	8.2	2.5	0	0	0	0	0	0
16	33	PQ	3.5	1.8	0	0	0	0	0	0
17	33	PQ	9	5.8	0	0	0	0	0	0
18	33	PQ	3.2	0.9	0	0	0	0	0	0
19	33	PQ	9.5	3.4	0	0	0	0	0	0
20	33	PQ	2.2	0.7	0	0	0	0	0	0
21	33	PQ	17.5	11.2	0	0	0	0	0	0
22	33	PQ	0	0	0	0	0	0	0	0
23	33	PQ	3.2	1.6	0	0	0	0	0	0
24	33	PQ	8.7	6.7	0	0	0	0	0	0.043
25	33	PQ	0	0	0	0	0	0	0	0
26	33	PQ	3.5	2.3	0	0	0	0	0	0
27	33	PQ	0	0	0	0	0	0	0	0
28	132	PQ	0	0	0	0	0	0	0	-0.1
29	33	PQ	2.4	0.9	0	0	0	0	0	0
30	33	PQ	10.6	1.9	0	0	0	0	0	0

A.2 IEEE 118 Bus Test System

The bus data for IEEE 30 Bus test system is given in Table A.2.

Table A.2: IEEE 118 Bus Test System

Id	Vnom	Type	P^L	Q^L	P^G	Q^G	V_{set}	Q^G_{max}	Q^G_{min}	B_s
1	138	PV	51	27	0	5	1	15	-5	0
2	138	PQ	20	9	0	0	0	0	0	0
3	138	PQ	39	10	0	0	0	0	0	0
4	138	PV	39	12	0	0	1	300	-300	0
5	138	PQ	0	0	0	0	0	0	0	-0.4
6	138	PV	52	22	0	18.5	1	50	-13	0

Table A.2 – continued from previous page

Id	V_{nom}	Type	P^L	Q^L	P^G	Q^G	V_{set}	Q^G_{max}	Q^G_{min}	B_s
7	138	PQ	19	2	0	0	0	0	0	0
8	345	PV	28	0	0	0	1	300	-300	0
9	345	PQ	0	0	0	0	0	0	0	0
10	345	PV	0	0	252.5	26.5	1	200	-147	0
11	138	PQ	70	23	0	0	0	0	0	0
12	138	PV	47	10	42.5	4	1	43	-35	0
13	138	PQ	34	16	0	0	0	0	0	0
14	138	PQ	14	1	0	0	0	0	0	0
15	138	PV	90	30	0	10	1	30	-10	0
16	138	PQ	25	10	0	0	0	0	0	0
17	138	PQ	11	3	0	0	0	0	0	0
18	138	PV	60	34	0	17	1	50	-16	0
19	138	PV	45	25	0	8	1	24	-8	0
20	138	PQ	18	3	0	0	0	0	0	0
21	138	PQ	14	8	0	0	0	0	0	0
22	138	PQ	10	5	0	0	0	0	0	0
23	138	PQ	7	3	0	0	0	0	0	0
24	138	PV	13	0	0	0	1	300	-300	0
25	138	PV	0	0	110.5	32	1	111	-47	0
26	345	PV	0	0	242.5	0	1	243	-243	0
27	138	PV	71	13	0	0	1	300	-300	0
28	138	PQ	17	7	0	0	0	0	0	0
29	138	PQ	24	4	0	0	0	0	0	0
30	345	PQ	0	0	0	0	0	0	0	0
31	138	PV	43	27	8.5	0	1	9	-9	0
32	138	PV	59	23	0	14	1	42	-14	0
33	138	PQ	23	9	0	0	0	0	0	0
34	138	PV	59	26	0	8	1	24	-8	0.14
35	138	PQ	33	9	0	0	0	0	0	0
36	138	PV	31	17	0	8	1	24	-8	0

Table A.2 – continued from previous page

Id	Vnom	Type	P ^L	Q ^L	P ^G	Q ^G	V _{set}	Q ^G _{max}	Q ^G _{min}	B _s
37	138	PQ	0	0	0	0	0	0	0	-0.25
38	345	PQ	0	0	0	0	0	0	0	0
39	138	PQ	27	11	0	0	0	0	0	0
40	138	PV	66	23	0	0	1	300	-300	0
41	138	PQ	37	10	0	0	0	0	0	0
42	138	PV	96	23	0	0	1	300	-300	0
43	138	PQ	18	7	0	0	0	0	0	0
44	138	PQ	16	8	0	0	0	0	0	0.1
45	138	PQ	53	22	0	0	0	0	0	0.1
46	138	PV	28	10	10	0	1	10	-10	0.1
47	138	PQ	34	0	0	0	0	0	0	0
48	138	PQ	20	11	0	0	0	0	0	0.15
49	138	PV	87	30	111.5	13.5	1	112	-85	0
50	138	PQ	17	4	0	0	0	0	0	0
51	138	PQ	17	8	0	0	0	0	0	0
52	138	PQ	18	5	0	0	0	0	0	0
53	138	PQ	23	11	0	0	0	0	0	0
54	138	PV	113	32	26.5	0	1	27	-27	0
55	138	PV	63	22	0	7.5	1	23	-8	0
56	138	PV	84	18	0	3.5	1	15	-8	0
57	138	PQ	12	3	0	0	0	0	0	0
58	138	PQ	12	3	0	0	0	0	0	0
59	138	PV	277	113	154	47	1	154	-60	0
60	138	PQ	78	3	0	0	0	0	0	0
61	138	PV	0	0	97.5	0	1	98	-98	0
62	138	PV	77	14	0	0	1	20	-20	0
63	345	PQ	0	0	0	0	0	0	0	0
64	345	PQ	0	0	0	0	0	0	0	0
65	345	PV	0	0	220.5	66.5	1	200	-67	0
66	138	PV	39	18	392	66.5	1	200	-67	0

Table A.2 – continued from previous page

Id	Vnom	Type	P^L	Q^L	P^G	Q^G	V_{set}	Q^G_{max}	Q^G_{min}	B_s
67	138	PQ	28	7	0	0	0	0	0	0
68	345	PQ	0	0	0	0	0	0	0	0
69	138	Slack	0	0	591	0	1	300	-300	0
70	138	PV	66	20	0	11	1	32	-10	0
71	138	PQ	0	0	0	0	0	0	0	0
72	138	PV	12	0	0	0	1	100	-100	0
73	138	PV	6	0	0	0	1	100	-100	0
74	138	PV	68	27	0	1.5	1	9	-6	0.12
75	138	PQ	47	11	0	0	0	0	0	0
76	138	PV	68	36	0	7.5	1	23	-8	0
77	138	PV	61	28	0	25	1	70	-20	0
78	138	PQ	71	26	0	0	0	0	0	0
79	138	PQ	39	32	0	0	0	0	0	0.2
80	138	PV	130	26	254.5	45	1	255	-165	0
81	345	PQ	0	0	0	0	0	0	0	0
82	138	PQ	54	27	0	0	0	0	0	0.2
83	138	PQ	20	10	0	0	0	0	0	0.1
84	138	PQ	11	7	0	0	0	0	0	0
85	138	PV	24	15	0	7.5	1	23	-8	0
86	138	PQ	21	10	0	0	0	0	0	0
87	138	PV	0	0	5	0	1	5	-5	0
88	138	PQ	48	10	0	0	0	0	0	0
89	138	PV	0	0	318.5	45	1	300	-210	0
90	138	PV	163	42	0	0	1	300	-300	0
91	138	PV	10	0	0	0	1	100	-100	0
92	138	PV	65	10	0	3	1	9	-3	0
93	138	PQ	12	7	0	0	0	0	0	0
94	138	PQ	30	16	0	0	0	0	0	0
95	138	PQ	42	31	0	0	0	0	0	0
96	138	PQ	38	15	0	0	0	0	0	0

Table A.2 – continued from previous page

Id	Vnom	Type	P^L	Q^L	P^G	Q^G	V_{set}	Q^G_{max}	Q^G_{min}	B_s
97	138	PQ	15	9	0	0	0	0	0	0
98	138	PQ	34	8	0	0	0	0	0	0
99	138	PV	42	0	0	0	1	100	-100	0
100	138	PV	37	18	326.5	52.5	1	155	-50	0
101	138	PQ	22	15	0	0	0	0	0	0
102	138	PQ	5	3	0	0	0	0	0	0
103	138	PV	23	16	54	12.5	1	40	-15	0
104	138	PV	38	25	0	7.5	1	23	-8	0
105	138	PV	31	26	0	7.5	1	23	-8	0.2
106	138	PQ	43	16	0	0	0	0	0	0
107	138	PV	50	12	0	0	1	200	-200	0.06
108	138	PQ	2	1	0	0	0	0	0	0
109	138	PQ	8	3	0	0	0	0	0	0
110	138	PV	39	30	0	7.5	1	23	-8	0.06
111	138	PV	0	0	39.5	0	1	40	-40	0
112	138	PV	68	13	0	450	1	1000	-100	0
113	138	PV	6	0	0	50	1	200	-100	0
114	138	PQ	8	3	0	0	0	0	0	0
115	138	PQ	22	7	0	0	0	0	0	0
116	345	PV	184	0	0	0	1	1000	-1000	0
117	138	PQ	20	8	0	0	0	0	0	0
118	138	PQ	33	15	0	0	0	0	0	0

CURRICULUM VITAE

PERSONAL INFORMATION

Surname, Name: ELMA, İsmail

Research Interests: Power system analysis, power system stability, ancillary services in power systems, power system optimization

EDUCATION

Degree	Institution	Year of Graduation
Ph.D.	METU Electrical and Electronics Engineering	2025
M.S.	METU Electrical and Electronics Engineering	2014
B.S.	METU Electrical and Electronics Engineering	2010
High School	Meram Anadolu High School, Konya	2004

Master Thesis Title: Determination of Optimum Values for Voltage Setpoints of Power Stations in Turkey

Supervisor: Prof. Dr. Ali Nezih Güven

FOREIGN LANGUAGES

Turkish (Native)

English (Advanced)

PROFESSIONAL EXPERIENCE

Year	Place	Enrollment
2010 - Present	TÜBİTAK MAM Energy Technologies	Senior Chief Researcher
2009 August	TÜBİTAK UZAY	Intern
2007 August	ASELSAN	Intern

PUBLICATIONS

1. I. Elma and A. N. Guven, "Multi-period Reactive Power Optimization for Determination of Switch Statuses of Shunt Elements and Voltage Setpoints of Power Plants," 13th International Conference on Electrical and Electronics Engineering (ELECO 2021), Bursa, Türkiye, 2021, pp. 6-10
2. S. Eren, D. Küçük, C. Ünlüer, M. Demircioğlu, Y. Yanık, Y. Arslan, B. Özsoy, A. H. Güverçinci, İ. Elma, Ö. Tanıdır, Y. C. Ölmez, S. Sönmez, "A ubiquitous Web-based dispatcher information system for effective monitoring and analysis of the electricity transmission grid", *International Journal of Electrical Power & Energy Systems*, Volume 86, March 2017, Pages 93-103.
3. I. Elma and O. Yılmaz, "Güneydoğu anadolu bölgesi gerilim çökme problemlerinin değerlendirilmesi," ELECO 2012 Electrical-Electronics and Computer Engineering Symposium, 2012, Bursa, Türkiye.
4. I. Elma and O. B. Tor, "Impact of wind penetration level on optimum transmission planning," IET Conference on Renewable Power Generation (RPG 2011), Edinburgh, 2011, pp. 1-5, doi: 10.1049/cp.2011.0187.

AWARDS - ACHIEVEMENTS

TÜBİTAK Marmara Research Center, Best Research Group Award of 2015